Universitat Ramon Llull

# TESIS DOCTORAL

| | |
|---|---|
| Título | Effect of the microenvironment in the *in vitro* chondrogenic and osteogenic differentiation of mouse embryonic fibroblasts |
| Realizada por | Maria Teresa Fernández Muiños |
| en el Centro | IQS School of Engineering |
| y en el Departamento | de Bioingeniería |
| Dirigida por | Dr. Carlos E. Semino |

*C. Claravall, 1-3*
*08022 Barcelona*
*Tel. 936 022 200*
*Fax 936 022 249*
*E-mail:* urlsc@sec.url.es
*www.url.es*

A mi querida familia

*“Imagination is more important than knowledge. For knowledge is limited, whereas imagination embraces the entire world”*

*Albert Einstein (1879-1955)*

*"La imaginación es más importante que el conocimiento. El conocimiento es limitado, la imaginación rodea el mundo."*

*Albert Einstein (1879-1955)*

# ACKNOWLEGMENTS

Empezar a escribir los agradecimientos significa que esto se acaba…Se acaba una etapa que empezó el día que me fui a hacer el trabajo final de carrera a Boston, lo que inicialmente sería un año se prolongó a 18 meses, a los cuales le siguieron unos meses en Leipzig y mi vuelta a Barcelona para continuar con el Máster en Bioingeniería y una vez finalizado, comenzar oficialmente con el doctorado en el IQS.

Se acaban los días en los que un buen resultado te alegran a ti y a la gente de tu alrededor, las ganas de seguir adelante, las largas horas de "brainstorming" en el laboratorio, las comidas en el bar, los cafés que nunca se acaban, las cervecitas después de un día largo y todos esos buenos momentos que pasé durante este tiempo y que echaré tanto de menos y serán irrepetibles. Pero también se acaban los largos días en el laboratorio en los que no sale nada de lo esperabas, los momentos de frustración, los fines de semana de cambios de medio de las células, los días de redacción… En definitiva, se acaba una etapa cargada de muy buenos y menos buenos momentos la cual termino con un sentimiento de tristeza pero a la vez con la ilusión de empezar una nueva etapa en mi vida.

Dicho esto, solo me queda dar las gracias a las personas que hicieron esto posible, y las que me han acompañado durante este camino. En primer lugar a Carlos, gracias por haberme dado la oportunidad de trabajar contigo a largo de todo este tiempo en tus diferentes laboratorios: primero en Boston, después en Alemania y finalmente en Barcelona. Gracias por contagiarme tu entusiasmo a la hora de hacer las cosas y sobre todo por la confianza que has puesto en mí todo este tiempo.

Durante estos años tuve la ocasión de conocer a muchas personas, entre ellas quiero destacar a mis compañeros en Boston: Elsa, Paco, Cris Cres, Carla, Claudia, Jordán, Nathan, Cherry, Núria, Alex, Alberto, Juan, Cris Purón, Laura, Nacho, Héctor, Marta...No me quiero olvidar de Mercedes Balcells y su ayuda en diferentes aspectos de mi etapa de TFC en Boston. Mis compañeras en Alemania Nerea y Rosita. Y finalmente mis compañeras del laboratorio de tejidos, en especial a las fundadoras del laboratorio: Cris, Nuria, Mire y Vero! Además de la gente que se fue incorporando con el paso del tiempo: Débora, Desi, Patri, Lourdes, Caterina, Javi, Alex, Raphaela, y como no, a mi gran estudiante de intercambio Melva. Ser 4 manos en la etapa final de la parte experimental fue de gran ayuda!

También quiero agradecer tanto a los compañeros de Biomateriales como a los de Bioquímica, que siempre que necesité su ayuda me la dieron sin dudar. Además, quiero agradecer a Salvador Borrós que nos dejase utilizar sus equipos siempre que los necesitamos.

A ti, Oscar, muchas gracias por acompañarme durante este camino. Por todo este tiempo que llevas a mi lado y por el que compartiremos en la siguiente etapa de nuestras vidas. Mil gracias por todo.

Y finalmente a mi familia, especialmente a mis padres y a mi hermano, gracias por vuestra confianza sin fin, por apoyarme de forma incondicional en los buenos y malos momentos, por vuestra paciencia, por vuestro cariño, por ser un ejemplo a seguir, porque sois lo mejor de mi vida y porque sin vosotros yo no sería la misma.

Esta tesis ha sido posible gracias a la beca pre-doctoral 2013FI_B2 00094 del SUR del ECO de la Generalitat de Catalunya, el proyecto europeo del 7º programa marco RECATABI y el presupuesto del IQS para el laboratorio de Ingeniería de Tejidos.

# ABSTRACT

Our group is focused on experimental models of cartilage and bone development in order to understand the biomechanical and biological parameters that regulate skeletal tissue formation. Previous results in our laboratory indicated that when mouse embryonic fibroblasts (MEFs) were cultured *in vitro* in three-dimensional (3D) scaffolds based on the self-assembling peptide RAD16-I, cells acquired multipotential capacity and engaged in a spontaneous process of chondrogenic differentiation. This thesis focuses on understanding the possible molecular mechanisms modulating the default cartilaginous commitment of these cells. Thus, the influence of matrix properties on the differentiation process was evaluated as well as the potential participation of genes involved in early tissue organization. Interestingly, cells only underwent chondrogenic differentiation under certain mechanical conditions, characterized by low stiffness (G' ~ 0.1 kPa). Similarly to *in vivo* processes, the mentioned differentiation appeared to be regulated by the balance on the expression of the chondrogenic inductor BMP4 and its antagonist Noggin.

Moreover, a novel and simple model was described in which the molecular events involved in bone formation through endochondral ossification could be studied *in vitro*. For this purpose, co-cultures of endothelial cells with 3D cultures of MEFs undergoing chondrogenesis were developed. Importantly, cells committed to osteogenic lineage under these new conditions. The osteogenic differentiation was evidenced by the expression of the hypertrophic marker collagen type X and the presence of calcium mineralized matrix at the interface between MEFs and endothelial cells, which suggested a cross-talk between both cell types.

Finally, a newly designed biomaterial for tissue engineering applications was developed by combining self-assembling peptide RAD16-I and polysaccharide heparin. Interestingly, this material exhibited sequential binding and delivery of the growth factor -containing heparin binding domain- $VEGF_{165}$. The new material supported the development of tubular-like structures in a 3D culture system of endothelial cells. These results suggested that this system could promote the development of a vascularized tissue and, as a consequence, promote tissue regeneration in an injured tissue. This platform could be used in other tissue engineering applications using heparin-binding affinity molecules such as TGFβ-1, which is a well-known chondrogenic inductor.

# RESUMEN

Nuestro grupo se ha centrado el en estudio de modelos experimentales de formación de cartílago y hueso con el objetivo de entender los parámetros biomecánicos y biológicos que regulan la formación de los tejidos que forman el esqueleto. En particular, resultados previos de nuestro laboratorio indican que cuando los fibroblastos embrionarios de ratón (del inglés, *mouse embryonic fibroblasts* , MEFs) se cultivaron *in vitro* en el péptido de auto-ensamblaje RAD16-I usando un sistema de cultivo tridimensional (3D), los MEFs adquirieron una capacidad de diferenciación multipotencial iniciando un proceso espontáneo de diferenciación condrogénica. En esta tesis, se estudió con más detalle el proceso con el objetivo de entender los posibles mecanismos moleculares que modulan el proceso de diferenciación condrogénica de estas células. Para ello se evaluó la influencia que las propiedades de la matriz ejercen en el proceso de diferenciación y la posible participación de genes involucrados en organización temprana de tejidos. De forma interesante, solamente bajo ciertas condiciones mecánicas, caracterizadas por la baja rigidez de la matriz (G' ~ 0.1 kPa), el sistema inició la diferenciación condrogénica, la cual pareció ser regulada por el balance entre el inductor condrogénico BMP4 y su antagonista Noggin en una forma similar a la que ocurre *in vivo.*

Además, en esta tesis se describió un nuevo y simple modelo en el cual se podrían estudiar *in vitro* los eventos moleculares involucrados en la formación de hueso a través del proceso de osificación endochondral. Para ello, cultivos 3D de MEFs experimentando condrogénesis fueron cocultivados con células endoteliales. De manera importante, en estas nuevas condiciones el sistema se redirigió hacia una diferenciación osteogénica. Dicha diferenciación fue probada por la expresión del marcador hipertrófico colágeno tipo X y la mineralización de la matriz en las zonas de interacción entre los MEFs y las células endoteliales, lo que sugiere un diálogo entre ambos tipos celulares.

Finalmente, se desarrolló un nuevo biomaterial para aplicaciones en ingeniería de tejidos formado por la simple combinación del péptido de auto-ensamblaje RAD16-I y el polisacárido heparina. De forma interesante, este material exhibió la unión y liberación secuencial del factor de crecimiento- con dominio de unión de la heparina- $VEGF_{165}$. Además, el nuevo material permitió la formación de estructuras tubulares en un cultivo 3D de células endoteliales. Estos resultados sugieren que este sistema podría promover el desarrollo de un tejido vascularizado y, como consecuencia, favorecer la regeneración en un tejido dañado. Esta plataforma podría ser usada en otras aplicaciones de ingeniería de tejidos usando moléculas con afinidad de unión de la heparina como el TGFβ-1, el cual es un conocido inductor condrogénico.

# RESUM

Durant els últims anys, el nostre grup s'ha centrat en l'estudi de models experimentals de formació de cartílag i ós amb l'objectiu d'entendre els paràmetres biomecànics i biològics que regulen la formació dels teixits que formen l'esquelet. En particular, resultats previs obtinguts en el nostre laboratori indiquen que quan els fibroblasts embrionaris de ratolí (de l'anglès, "*mouse embryonic fibroblasts*", MEFs) es cultiven *in vitro* en el pèptid auto-ensamblable RAD16-I, emprant un sistema de cultiu tridimensional (3D), els MEFs són capaços d'adquirir una capacitat de diferenciació multipotencial, iniciant un procés espontani de diferenciació condrogènica. En aquesta tesis, es va estudiar amb més detall el procés amb l'objectiu d'entendre els possibles mecanismes moleculars que modulen el procés de diferenciació condrogènica d'aquestes cèl·lules. Per a tal efecte es va avaluar l'influencia que les propietats de la matriu poden tenir en el procés de diferenciació i la possible participació de gens involucrats en l'organització primerenca de teixits. De manera interesant, es va veure que només sota certes condicions mecàniques caracteritzades per una rigidesa de la matriu baixa (G'=0,1KPa), el sistema va ser capaç d'iniciar la diferenciació condrogènica, cosa que va semblar venir regulada per la balança entre l'inductor condrogènic BMP4 i el seu antagonista Noggin, d'una manera similar al que succeeix *in vivo.*

Per una altra banda, en aquesta tesis es va descriure un model nou i simple en el qual es podrien estudiar *in vitro* els esdeveniments moleculars involucrats en la formació d'ós, a través del procés d'ossificació endocondral. Per a tal efecte, cultius tridimensionals de MEFs en procés de condrogènesis es van cocultivar amb cèl·lules endotelials. Aquestes noves condicions van permetre al sistema redirigir-se cap a una diferenciació osteogènica, provat per l'expressió del marcador hipertròfic col·lagen tipus X i la mineralització de la matriu en les zones d'interacció entre els MEFS i les cèl·lules endotelials. Tals resultat suggereixen un clar diàleg entre ambdós tipus cel·lulars.

Finalment també es va desenvolupar un nou material per a diferents aplicacions en l'àmbit de l'enginyeria de teixits, format per la simple combinació del pèptid d'auto-assemblatge RAD16-I i el polisacàrid heparina. Es va observar que aquest material exhibia la unió i alliberació seqüencial del factor de creixement – amb domini d'unió de l'heparina – $VEGF_{165}$. A part, el nou material va permetre la formació d'estructures tubulars en un cultiu 3D de cèl·lules endotelials. Aquests resultats suggereixen que aquest sistema podria promoure el desenvolupament d'un teixit vascularitzat i com a conseqüència, afavorir la regeneració d'un teixit fet malbé. Aquesta plataforma es podria emprar en diferents aplicacions de l'enginyeria de teixits fent servir molècules amb afinitat d'unió de l'heparina com el TGFβ-1, el qual és un conegut inductor condrogènic.

# TABLE OF CONTENTS

# LIST OF FIGURES

# LIST OF TABLES

# LIST OF ABBREVIATIONS

**2D:** Two-dimensional

**3D:** Three-dimensional

**ACI**: autologous chondrocyte implantation

**BMPs**: Bone Morphogenetic Proteins

**BMSC:** Bone Marrow Stromal Stem Cells

**Coll I:** Collagen type I

**Coll II:** Collagen type II

**DAPI**: 4',6-diamino-2-phenylindole,dihydrochloride

**DNA**: Deoxyribonucleic Acid

**DMA:** Dynamic Mechanical Analysis

**DMMB**: 1,9-dimethyl-dimethylene blue

**DPC:** days post coitum

**ECM**: Extracellular Matrix

**EBs:** Embryoid Bodies

**ECs** : Endothelial Cells

**EGF:** Epidermal Growth Factor

**ESCs**: Embryonic Stem Cells

**FBS**: Fetal Bovine Serum

**FDA:** Food and Drug Administration

**FGF:** Fibroblast Growth Factor

**FM**: Fibroblast Media

**GAGs**: Glycosaminoglycans

**GF:** Growth Factor

**GH:** Growth Hormone

**HDMECs**: Human Dermal Microvascular Endothelial Cells

**HGF:** Hepatocyte Growth Factor

**HNF**: Hepatic Nuclear Factor

**HRP**: Horse Radish Peroxidase

**HUVECs:** Human Umbilical Vein Endothelial Cells

**IGF:** Insulin- like Growth Factor

**iPSC**: induced Pluripotent Stem Cells.

**LIF**: Leukemia Inhibitory Factor

**MEFs**: Mouse Embryonic Fibroblasts

**MMP:** Metalloproteinase

**MSCs** Mesenchymal Stem Cells

**mRNA**: messenger Ribonucleic Acid

**N-CAM:** Neural Cell Adhesion Molecule

**OBs**: Osteoblasts

**PBS**: Phosphate Buffered Saline

**PCR**: Polymerase Chain Reaction

**PDGF:** Platelet Derived Growth Factor

**PFA**: Paraformaldehyde

**PGs**: Proteoglycans

**PLA:** Polylactic Acid

**PVDF:** Polyvinylidene fluoride

**RT-PCR**: Reverse Transcriptase PCR

**qPCR.:** Quantitative Reverse Transcriptase PCR

**SEM** Scanning electron microscopy

**TGF-β**: Transforming Growth Factor Beta

**VEGF:** Vascular Endothelial Growth Factor

**WB:** Western Blot

# <u>Chapter 1</u>: Introduction to tissue engineering and strategies for cartilage repair

## 1.1 Background

### 1.1.1 Overview

Even more than 250 years ago, William Hunter wrote "we shall find that an ulcerated cartilage is universally allowed to be a very troublesome disease...and that, when destroyed, it is never recovered" [1]. This is due to poor intrinsic healing ability of adult articular cartilage, and thus even minor injuries or lesions may lead to progressive damage and osteoarthritic joint degeneration resulting in significant pain and disability. Nowadays, after decades of research, there still remain significant challenges in the clinical application of cell-based therapies for cartilage repair. Although numerous strategies have been developed to address this issue, unfortunately, none of these approaches has provided a complete and reproducible solution to the problem.

### 1.1.2 Tissue Engineering

Advances in medicine over the past several decades have led to significant improvements in the quality of life. Despite these advances, alternative therapies must be developed to treat patients who suffer from loss or failure of organs and tissues [2]. Besides, organ transplantation is severely limited by a critical donor shortage. Consequently, in the last decade, the tissue engineering field emerged attempting to address tissue recovery of this significant number of patients who need a new or improved organ or tissue.

Tissue engineering was defined by Vacanti and Langer in 1993 as an interdisciplinary field that applies the principles of engineering and the life sciences toward the development of biological substitutes that restore, maintain, or improve tissue function [3]. Nevertheless, their work started in the mid-1980s when it was postulated that living organs might be designed and built based on the principles of biologic science and technologic advances in the engineering disciplines. Their first published data dates from 1988 [4]. In the following decade, many other laboratories worldwide demonstrated the fundamental principles to a successful tissue creation and their practical application in many systems eventually applied to human therapy [5]. The potential impact of this field includes the development of engineered tissues that could reduce the need of organ replacement and ease the study of physiology and pathophysiology *in vitro.* These studies could greatly accelerate the development of new drugs that may cure patients, eliminating the need for organ transplants altogether [6].

The basic principle of tissue engineering could be simplified as cells can be isolated, expanded *in vitro* and seeded onto scaffolds. In this scaffold, a variety of factors can be modulated (such as biological, biomechanical or biophysical factors) to obtain specific cell differentiation and further re-implantation of the engineered tissue into the patient (Figure 1.1.1). As it can be

observed in the general scheme, tissue engineering involves three main players: cells, biomolecules and scaffolds.

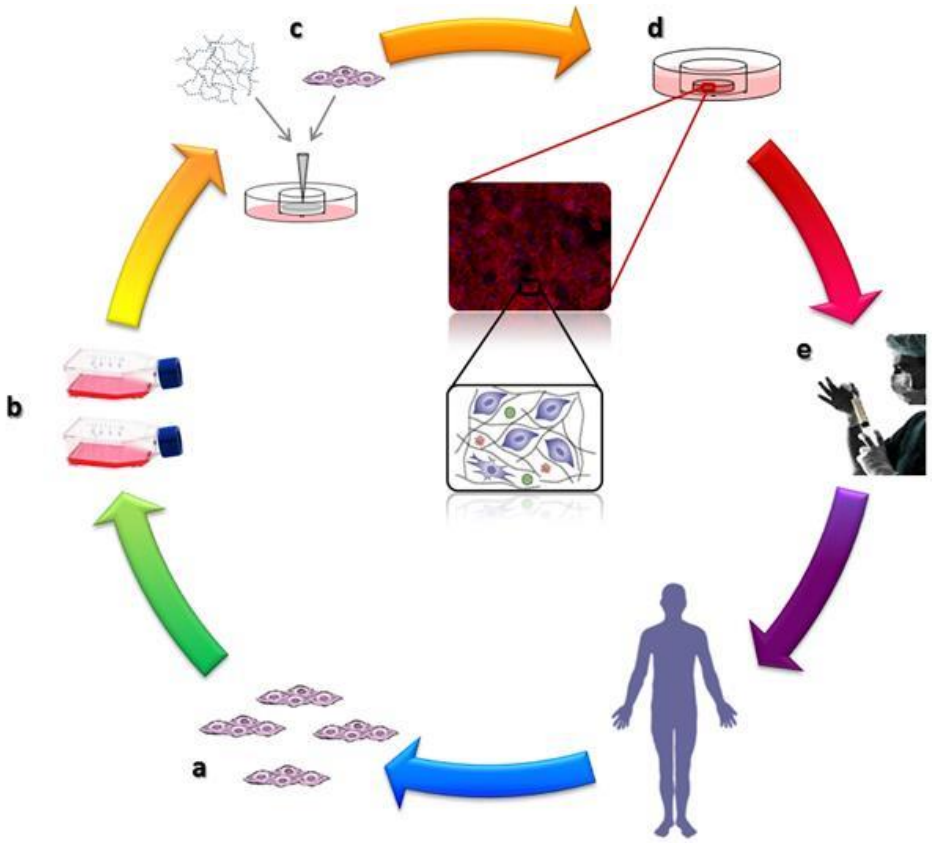


**Figure 1.1.1. Basic principle of Tissue Engineering.** First, cells are isolated from the patient or a donor (a), to be expanded *in vitro* (b). Then, cells are cultured in a scaffold (c) to obtain a 3D engineered scaffold (d), at this point a variety of factors can be modulated to obtain specific cell differentiation and be finally implanted in the patient (e).

Due to the promising applications of tissue engineering, several strategies have been designed during the last years aiming to obtain cartilage tissue substitutes. For this purpose, different cells, biomaterials and stimulating factors have been used, as it will be discussed in the next sections.

### 1.1.3 Cells

The optimal cell source for cartilage tissue engineering is still being identified. The goal is to find an ideal cell source that can be easily isolated, expanded and cultured to express and synthesize cartilage-specific molecules (Table 1.1.1) [7]. While chondrocytes should be the first choice, since they are found in cartilage, having the role of producing, maintaining, and remodeling the cartilage extracellular matrix (ECM), the main challenge is to obtain a sufficient cell number. Unfortunately, monolayer expansion causes their dedifferentiation, which is characterized by decreased production of cartilage specific ECM (mainly proteoglycans (PGs) and type II collagen) [7]. However, autologous chondrocyte implantation (ACI) is a common

strategy used in clinical practice since 1987 [8]. Briefly, cells from a biopsy are isolated and expanded *in vitro*. Then, they are re-implanted in the cartilage defect in a second surgical procedure usually under a membrane, which is often made of collagen type I/III or seeded onto a scaffold matrix [9]. ACI is one of the first developed FDA approved cell-therapies for articular cartilage repair (1997, Carticel™, Genzyme). Nowadays, some companies such as TETEC are currently developing similar therapeutic platforms (Novocart, Phase III clinical trials, TETEC, AG, Germany). Indeed, chondrocytes are the only source of cells currently approved for clinical use [10].

Mesenchymal stem cells (MSCs) represent a viable alternative to chondrocytes as a cell source for cartilage tissue engineering. Their main advantages are: ease of availability, high capacity of *in vitro* expansion in undifferentiated state, while retaining the ability to differentiate into mesodermal lineages after exposure to suitable stimuli [11,12]. *In vitro* chondrogenesis of different MSCs-derived sources has been described, however bone marrow and adipose derived stem cells are the most widely used [7]. Their extraction techniques are less invasive than other surgical procedures, but still uncomfortable and painful for the patients. Furthermore, isolation of MSCs typically yields very low amount of cells. Hence, the search for alternative cell sources is still ongoing.

**Table 1.1.1. Cell sources for cartilage tissue engineering and their advantages and disadvantages.**

| Cell Type | Advantages | Disadvantages |
|---|---|---|
| Autologous Chondrocyte | Native Phenotype<br>Minimal risk of immunological problem | Small cell number<br>De-differentiation on expansion |
| Adult Mesenchymal Stem Cells | Potential to obtain large cell numbers<br>Capacity to differentiate into mesodermal lineages | Potential for hypertrophy<br>Differentiation unstable and non-reproducible |
| Embryonic Stem Cells | Multiple cell types can be obtained | Potential tumorigenic<br>Ethical considerations<br>Differentiation unstable and non-reproducible |
| Induced Pluripotent Stem Cells(iPSCs) | Source of patient specific cells<br>Multiple cell types can be obtained | Potential tumorigenic<br>Differentiation unstable and non-reproducible |
| Fibroblasts | Source of patient specific cells<br>Multiple harvest sites | Low differentiation capacity |

Chondrogenic differentiation of embryonic stem cells (ESCs) has also been reported due to their pluripotency and self-renewal capacity. They can be expanded unlimitedly in vitro and generate cells of all three germ layers (endoderm, mesoderm and ectoderm) that can further differentiate into specific cell lineages [13–15]. However, the main disadvantage of ESCs is that they may be tumorigenic due to their highly proliferative ability when undifferentiated. Hence, even a single one cell that is not appropriately differentiated could lead to disastrous consequences if it initiates a different or undesired differentiation response upon implantation [10]. In addition, they

are surrounded by ethical concerns due to the need of embryo extraction. Therefore, their use has been limited mainly to better understand fundamental biological questions rather than study clinically applicable strategies.

In addition to ESCs, few studies reported the use of induced pluripotent stem cells (iPSCs) for cartilage tissue engineering strategies [16,17]. iPSCs are "embryonic-like" stem cells generated from fibroblasts by retrovirus mediated transfection of four transcription factors: Oct3/4, Klf4, Sox2 and c-Myc. iPSCs are indistinguishable from ESCs in morphology, proliferation, gene expression, and teratoma formation. This kind of cells bypasses the need for embryo extraction to generate pluripotent stem cell phenotypes from autologous sources [18]. The interest on this cell type is increasing as they have high differentiation capacity, but they also can be derived from the patient's own cells. Although it seems to be the ideal source of cells, this approach currently has serious limitations for its use in regenerative medicine due to the risks of tumor formation and function disruption of many endogenous genes by retroviral insertion. Therefore, the main drawbacks concerning the use of iPSCs are: low efficiency, questionable reproducibility, difficult standardization and control of differentiation. Hence, their clinical application will require a few years of safety trials before their clinical use becomes a reality [10].

Finally, in addition to chondrocytes and stem cells, fibroblasts have been widely used during the last years for tissue engineering applications. Different studies showed the ability of fibroblasts to redirect their fate towards mesodermal lineages (including adipocytes, osteoblasts and chondrocytes) when cultured under the appropriate conditions [19–22]. Dermal fibroblasts represent an easily accessible and abundant cell source, as a substantial cell yield can be obtained from a relatively small biopsy following minimally invasive procedures and routine cell-expansion techniques as compared to MSCs. However, their main limitation is the low differentiation capacity compared to the other cell types.

### 1.1.4 Stimulating chondrogenic factors

Stimulatory factors are required to induce or enhance cartilage formation and can be divided into: biophysical stimuli, which include oxygen tension and matrix deformation by mechanical loading; and biological, such as growth factors and cytokines. Cartilage is an avascular tissue and, consequently, chondrocytes naturally experience low oxygen tension. Indeed, the oxygen concentration varies from 1 to 7%. It was found that low oxygen tension is a key regulatory factor of proliferation, differentiation and activity of chondrogenic cells since chondrocytes and MSCs cultured in hypoxic conditions *in vitro* increased the synthesis of cartilage specific ECM proteins [23,24]. In addition, under physiological conditions, articular cartilage is subjected to various mechanical stimuli. Different studies showed that dynamic compressive loading has a chondrogenic stimulatory effect on cartilage, chondrocytes, and stem cells [20]. Therefore,

mechanical stimuli are important factors to take into account in the development of cartilage engineering products. Besides, matrix elasticity is also an important factor to consider as cells can "sense" and respond to the elasticity of their substrate. Moreover, compliant substrates appear to maintain the chondrogenic phenotype, which is indicated by round cellular morphology, diminished actin stress fiber formation, and chondrogenic ECM production, while stiffer substrates have a negative impact [25]. These results emphasize how important it is to control scaffold mechanical properties to engage a cellular system to undergo chondrogenic differentiation. Accordingly, a variety of bioreactor systems have been applied, determined to reproduce the mechanical stimuli experienced *in vivo* [26].

Similarly to most of tissue engineering applications, growth factors and other chemical additives may be added into the culture medium to control tissue formation *in vitro*. Some growth factors that have been widely described are TGF-β superfamily, several BMPs, insulin- like growth factor (IGF)-1, fibroblast growth factors (FGFs), and epidermal growth factor (EGF). Among them, members of the TGF-β family have been shown to play a key role on cartilage development [7,12].

### 1.1.5 Scaffolds

#### *2D versus 3D cultures*

Nowadays, it has been well established that traditional 2 dimensional (2D) cultures do not recreate *in vivo* conditions where cells are embedded in a natural 3 dimensional (3D) extracellular matrix (ECM) interacting with their neighboring cells and with the ECM through biochemical and mechanical cues (Figure 1.1.2) [27]. These cell–cell and cell–ECM interactions are essential to establish a 3D communication network to maintain the specificity and homeostasis of the tissue. However, cells cultured in 2D grow in physiological constrained conditions because they are unnaturally polarized: cells have the bottom surface attached to a rigid and flat substrate and, the upper surface exposed to culture media. As a consequence, *in vivo* conditions are not recreated in terms of cellular communication, gene and protein expression pattern and diffusion of soluble molecules such as oxygen, nutrients or growth factors [28–30]. Thus, the third dimension is required in order to capture the physiological cell responses and bridge the gap between simplistic 2D cultures and extremely complex animal models [31]. Altogether it motivates the use of 3D cultures as cellular models that mimic better the functions of living tissues.

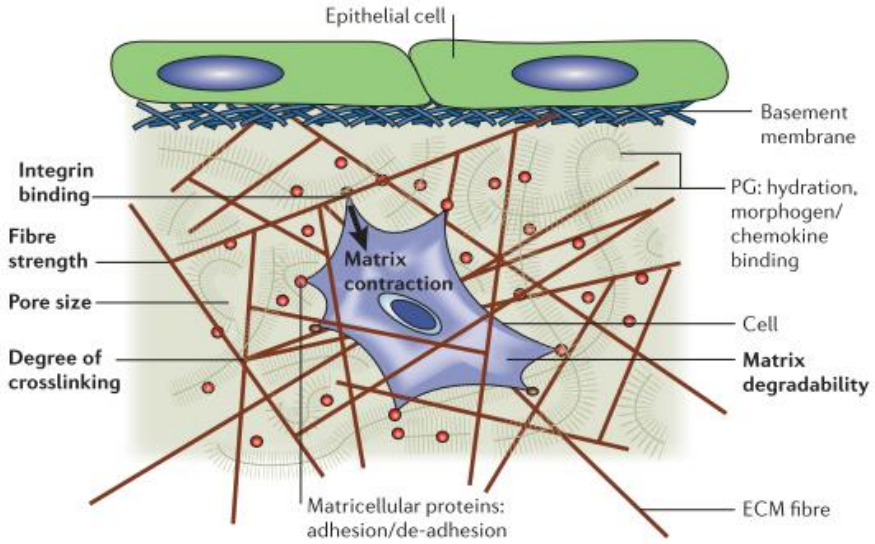


**Figure 1.1.2. Importance of the 3D environment for engineering cell function (Griffith et al 2006 [32])**

### *Ideal Scaffolds*

Currently, one major goal of tissue engineering is to develop new biomaterials similar structurally and mechanically to ECMs to mimic *in vivo* conditions (biomimetic). The ECM is the natural environment of cells and it is composed by a variety of proteins and polysaccharides assembled into an organized network in close association with the cellular surface [32]. It serves as a scaffold to maintain tissue and organ structure and also regulates many aspects of cell behavior, including cell proliferation and growth, survival, change in cell shape, migration, differentiation and function [33–35]. Variations in the relative amounts of the different types of matrix macromolecules and their organization in the ECM give rise to the functional requirements of particular tissues [36].

The ideal biologically compatible scaffold to support cell attachment and growth should be biomimetic among several other criteria [37]. First of all, it must be biocompatible to prevent an adverse tissue reaction of the immune system. Moreover, the scaffold should exhibit a controlled rate of degradation; ideally it should degrade and resorb at a rate that matches the formation of new tissue. Besides, the resulting degradation products should be non-toxic and, therefore, should not induce an inflammatory response. Lastly, in terms of material production, purification, and processing, it should be easy, cheap and scalable [37].

### *Scaffolds for cartilage tissue engineering*

It is well known that chondrocytes reside within a complex 3D environment, which is composed by a highly hydrated complex network of molecules. In contrast, as detailed in the previous section, isolated chondrocytes lose their differentiated phenotype in two-dimensional (2D) culture. Pellet and micromass culture systems have traditionally been used to re-differentiate chondrocytes or differentiate adult chondroprogenitors *in vitro* [38]. However, biomaterial-free

cultures present several disadvantages, such as the limited size, uncontrolled construct geometry and the poor mechanical properties. Therefore, 3D environments have been used to either culture chondrocytes or to promote the chondrogenic differentiation of chondroprogenitors [12].

Different types of biomaterials have been used for cartilage tissue engineering which can be classified into natural and synthetic biomaterials. Natural biomaterials exhibit complex structures and a variety of properties, such as water binding capacity, biodegradability and biocompatibility, among many others. However, another important aspect to consider when using natural materials is that they can induce an undesirable immune response due to the presence of impurities and endotoxins, and their variability from batch to batch due to the inability to accurately control the processing techniques [39]. Moreover, natural materials possess weak mechanical properties and the possible modifications to improve them are limited. Some examples that have been explored for cartilage engineering include: collagen [40], fibrin[41], alginate [42], agarose [43], gelatin [44], chondroitin sulfate [45], chitosan[46] or hyaluronic acid [47] (Table 1.1.2).

Alternatively, the use of synthetic polymers enables the design of scaffolds with specific mechanical and biological properties, and degradation rates. Moreover, this type of materials can be produced cheaply and reproducibly. However, their potential limitations include toxicity and restricted cellular interactions, unless they are modified with adhesion peptides or designed to release biological molecules [48]. Synthetic biomaterials currently used for cartilage repair include among others: poly (α-hydroxy esters) [49,50], poly(ethylene glycol) [51], poly(NiPAAm) [52], polyurethanes[53] or self-assembling peptides [54,55] (Table 1.1.2). Although hydrogels show weak mechanical properties, they are widely used due to their similarities to native cartilage tissue and the potentially to be injected transcutaneously into the cartilage defects. Among synthetic materials, self-assembling peptides are gaining scientific interest in tissue engineering due to the specific properties mentioned in the next section.

**Table 1.1.2. Examples of biomaterials used in cartilage tissue engineering applications**

| **Biomaterials used in in cartilage engineering applications** | |
|---|---|
| Naturally derived | Synthetically derived |
| Collagen [40] | Poly(glycolic acid) (PGA),[50,56] |
| Fibrin [41] | Poly(lactic acid) (PLA) [50] |
| Alginate [42] | Self-assembling peptides [54,55] |
| Agarose [43] | Poly(ethylene glycol) [51] |
| Gelatin [44] | Poly(NiPAAm) [52] |
| Chondroitin Sulphate [45] | Polyurethanes [53] |
| Hyaluronic Acid [47] | Poly(lactic-co-glycolic acid) (PLGA) [57] |

### 1.1.6 Self-assembling peptides

#### *Self-assembling concept*

Self-assembling is defined as the autonomous organization of components into patterns or structures without external instruction [58]. Self-assembling of biomolecules is a phenomenon commonly observed in biology, from DNA self-complementary double helix annealing, to protein aggregation or lipid membrane formation. It consists of the spontaneous organization of molecules under thermodynamic equilibrium conditions into structurally stable arrangements by the driving force of non-covalent interactions like hydrogen bonds, ionic bonds, electrostatic bonds, van der Waals interactions, etc. Although these interactions are rather weak by themselves, when in concert they govern the self-assembling process of biomolecules [33,59]. The consequence of this process is the formation of highly organized and stable macromolecular entities with specific functions. Among them are included the proteins forming the ECM of connective tissues, such as collagens, laminins and fibronectins. Some of these molecules are commonly used as natural biomaterials that mimic ECM milieu for the study of mammalian cells behavior *in vitro* [33].

#### *Peptide design*

First molecular self-assembling studies are dated on the seventies, when different chemical approaches showed that copolypeptides with alternating hydrophilic and hydrophobic residues formed water-soluble β-sheet structures by self-assembling in the presence of salts (high ionic strength) [60,61]. Later, in the nineties, new studies were carried out in this area with the aim of developing new materials. Scientists identified the key parts of proteins responsible for the self-assembling process and used them to develop simpler systems *in vitro*. The design of new self-assembling materials for future applications in biomedicine has been focused on the development of scaffolds that can self-assemble in water. Lysβ-21, one of the first examples of this class of self-assembling peptides, corresponds to residues 41-61 of the egg white lysozyme and forms a triple-stranded β-sheet in the β-domain of the native protein [62]. This peptide presents β-sheet configuration in water and forms insoluble macroscopic membranes depending on pH and ionic strength [63].

Several self-assembling peptides have been molecular designed, among them, the RAD16-I is used in this chapter to illustrate the self-assembling process since it is the gold standard scaffold used in this thesis (Figure 1.1.3). RAD16-I is composed by repeating units of hydrophilic-hydrophobic aminoacids, in which the charged residues include alternating positive and negative charges (with sequence: AcN-RADARADARADARADA-CONH2; where R = Arginine, A = Alanine and D= Aspartic acid). This peptide self-assembles under physiological conditions into a network of interweaving nanofibers of around 10 nm diameter, forming a hydrogel scaffold with pores size ranging from 50 to 200 nm and over 99% water content. The

size of animal cells varies from 20 to 50 μm and therefore, cells would experience a truly 3D environment when cultured within this scaffold.

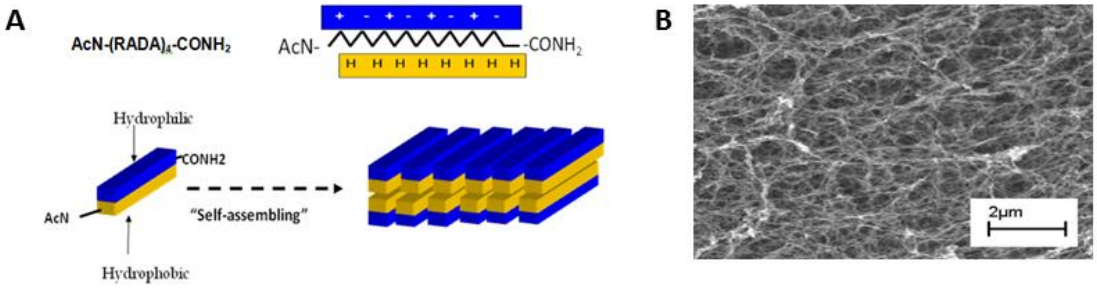


**Figure 1.1.3. Peptide RAD16-I self-assembles into a nanofiber network.** (A) Schematic model of the nanofiber developed by self-assembling RAD16-I molecules. Note: The nanofiber is formed by a double tape of assembled RAD16-I molecules in antiparallel β-sheet configuration (top tape in blue and bottom tape in yellow). (B) RAD16-I nanofiber network viewed by SEM (Genové et al. 2005 [64]). (Scale bar = 1 μm)

Self-assembling peptides of this class are good candidates to create artificial cellular niches, because their nanoscale network and biomechanical properties are similar to those of natural ECMs. Moreover, mechanical properties can be modulated by changing peptide concentration [65,66], and can be defined as "non-instructive" from the point of view of cell receptor recognition/activation [33]. Finally, RAD16-I peptide is easy to synthesize by solid phase synthesis, easy to purify and its degradation products are natural aminoacids. Several *in vitro* studies showed its ability to support cell attachment, growth, maintenance and differentiation of a variety of primary and cultured mammalian cells [37,54,64,67–71].

In addition to this class of self-assembling peptides, Stupp and coworkers also used rational molecular design for the development of new peptides that self-assemble into nanoscale fibers in water solutions. However, the peptide structure and its self-assembling are different from those of the β-sheet previously described (such as RAD16-I) [33]. This kind of amphiphilic molecules are composed by a peptide segment containing 6-12 amino acids, forming the hydrophilic region of the peptide, coupled via an amide bond to a fatty acid chain that varies in length from 10 to 22 carbon atoms, which confers the hydrophobic characteristics to drive the self-assembling. At concentrations as low as 0.25%, these molecules self-assemble into self-supporting gels via pH controlled and reversible mechanism. These gels are formed by a network of cylindrical nanofibers, ranging from 5 to 8 nm in diameter depending on the length of the self-assembling molecules forming them. The core of the nanofiber is formed by the hydrophobic alkyl tails and the outer surface is formed by the hydrophilic peptide segments (Figure 1.1.4) [72].

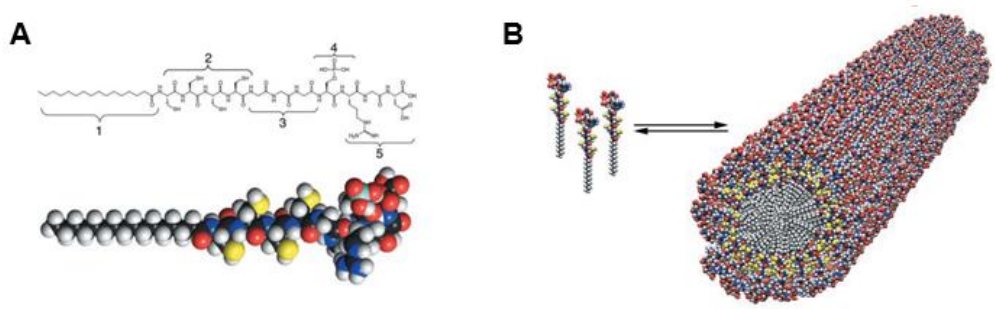


**Figure 1.1.4. Self-assembling peptides developed by Stupp and coworkers. (**A) Chemical structure and molecular model of the self-assembling peptide. Color scheme: C, black; H, white; O, red; N, blue; P, cyan; S, yellow. (B) Schematic showing the self-assembly into a cylindrical micelle. (Image adapted from Hartgerink et al 2001[72])

### *Application in cartilage tissue engineering*

Several studies reported the use of self-assembling peptides as scaffolds for cartilage tissue engineering applications where a major challenge is the identification of a material that can stimulate high rates of cell division as well as high rates of synthesis of phenotypically specific ECM macromolecules. The aforementioned RAD16-I was used in *in vitro* studies where rabbit chondrocytes and bone marrow mesenchymal stem cells (BMSCs) showed higher cellular proliferation and a better ability to synthesize cartilage-like ECM than control cultures in agarose [55,73]. Moreover, the self-assembling peptide KLD-12 has been widely used for cartilage tissue engineering purposes. The encapsulation of bovine chondrocytes in this peptide suggested its potential to maintain differentiated chondrocytes for four weeks while stimulating some cell division and maintaining the synthesis and accumulation of a mechanically functional cartilage-like ECM [74]. Moreover, the maturation of ECM was accelerated and characterized by the enrichment in PGs when long-term alternate day dynamic compression loading was applied to the bovine encapsulations [75]. Remarkably, an *in vivo* study showed that the injection of KLD in a full-thickness, critically-sized, rabbit cartilage defect model, markedly improved cartilage regeneration. Besides, the injection of combined chondrogenic growth factors and BMSCs did not result in any additional beneficial or deleterious effect compared to KLD alone [76].

Finally, Stupp and coworkers designed self-assembling peptides for their specific use in articular cartilage regeneration. One of them contained a terminal biosignaling peptide domain (a TGF-β1 binding domain), which became highly exposed on the surface of the nanofibers after self-assembling. In this case, they used mesenchymal stem cells (MSCs) and their *in vitro* studies showed that this material maintained the cellular viability and chondrogenic differentiation of the cells. Moreover, *in vivo* studies showed that the peptide containing the binding sequence for TGF-β1 enhanced the regenerative potential of micro-fracture chondral defects performed in rabbits without adding any external growth factor [77]. Altogether, it was

evidenced the potential use of self-assembling peptides as scaffolds for cartilage tissue engineering and regenerative medicine purposes.

## 1.2 Motivations and general aims

Our research group has been actively studying cellular *in vitro* models in a way to understand natural processes of regeneration. Thus, our general working hypothesis is based on the *in vitro* recreation of key biological, biophysical and biomechanical parameters of a tissue undergoing regeneration on a damaged tissue, which would promote healing and function recovery. In particular, during the last years, we have been involved in projects that aimed to develop new strategies to study *in vitro* cartilage formation using mouse and human fibroblasts cultured in the self-assembling peptide RAD16-I [45,67]. Besides, due to our expertise in the field of cartilage tissue engineering and in the development of biomaterials for tissue engineering applications, we are part of the project BIOCART, which consists of the development of potentially injectable scaffolds that mimic the natural extracellular matrix of cartilage. Remarkably, *in vivo* cartilage formation is in close interaction with bone formation since most of the bones in the human body are formed via a cartilage intermediate through the process of endochondral ossification. In fact, we have also expertise in models of *in vitro* osteogenesis using mouse embryonic stem cells, mouse fibroblasts and preosteoblastic cells [59,68]. However, the molecular mechanisms involved in the differentiation processes studied remain unclear.

Altogether this motivated us to study in detail the chondrogenic model described in our laboratory using mouse fibroblasts and, once obtained the cartilage-like tissues, develop a model for osteogenic differentiation in order to recreate most aspects of *in vivo* bone formation through the process of endochondral ossification. As part of this thesis, a new material for tissue engineering applications was also developed with biologically active motifs, which could be used, among others, for cartilage tissue engineering strategies. Thus, the general objectives of the present thesis are the following:

- To develop tissue engineering strategies for cartilage tissue repair using the self-assembling peptide RAD16-I (Chapter 2).
- To evaluate the biologically induced osteogenic differentiation of MEFs in the self-assembling peptide RAD16-I (Chapter 3).
- To develop a new biomaterial for tissue engineering applications based on the self-assembling peptide RAD16-I (Chapter 4).

## 1.3 References


1. Hunter, W. Of the structure and disease of articulating cartilages. 1743. *Clin Orthop Relat Res.* **317,** 3–6 (1995).

2. Silva, E. A. & Mooney, D. J. in **64,** 181–205 (2004).

3. Langer, R. & Vacanti, J. P. Tissue Engineering. *Science (80-. ).* **260,** 920–926 (1993).

4. Vacanti, J. *et al.* Selective cell transplantation using bioabsorbable artificial polymers as matrices. *J Pediatr Surg* **23,** 3–9 (1988).

5. Vacanti, J. Tissue engineering and regenerative medicine: from first principles to state of the art. *J. Pediatr. Surg.* **45,** 291–4 (2010).

6. Griffith, L. G. & Naughton, G. Tissue engineering--current challenges and expanding opportunities. *Science* **295,** 1009–14 (2002).

7. Chung, C. & Burdick, J. A. Engineering cartilage tissue. *Adv. Drug Deliv. Rev.* **60,** 243–62 (2008).

8. Lin, Z., Willers, C., Xu, J. & Zheng, M.-H. The chondrocyte: biology and clinical application. *Tissue Eng.* **12,** 1971–84 (2006).

9. Coates, E. E. & Fisher, J. P. in *Biomater. Tissue Eng. Appl.* (Burdick, J. A. & Mauck, R. L.) 279–306 (Springer Vienna, 2011). doi:10.1007/978-3-7091-0385-2

10. Johnstone, B. *et al.* Tissue engineering for articular cartilage repair--the state of the art. *Eur. Cell. Mater.* **25,** 248–67 (2013).

11. Guo, Q. & Elisseeff, J. H. in *Princ. Regen. Med.* 981–995 (Elsevier Inc., 2011). doi:10.1016/B978-0-12-381422-7.10053-7

12. Vinatier, C., Mrugala, D., Jorgensen, C., Guicheux, J. & Noël, D. Cartilage engineering: a crucial combination of cells, biomaterials and biofactors. *Trends Biotechnol.* **27,** 307–14 (2009).

13. Craft, A. M. *et al.* Specification of chondrocytes and cartilage tissues from embryonic stem cells. *Development* **140,** 2597–610 (2013).

14. Cheng, A., Hardingham, T. E. & Kimber, S. J. Generating Cartilage Repair from Pluripotent Stem Cells. **00,** (2013).

15. Beane, O. & Darling, E. M. Isolation, Characterization, and Differentiation of Stem Cells for Cartilage Regeneration. *Ann Biomed Eng* **40,** 2079–2097 (2013).

16. Wei, Y. *et al.* Chondrogenic Differentiation Of Induced Pluripotent Stem Cells. **23,** 1–12 (2012).

17. Diekman, B. O. *et al.* Cartilage tissue engineering using differentiated and purified induced pluripotent stem cells. *Proc. Natl. Acad. Sci. U. S. A.* **109,** 19172–7 (2012).

18. Takahashi, K. & Yamanaka, S. Induction of pluripotent stem cells from mouse embryonic and adult fibroblast cultures by defined factors. *Cell* **126,** 663–76 (2006).

19. Rakar, J., Lönnqvist, S., Sommar, P., Junker, J. & Kratz, G. Interpreted gene expression of human dermal fibroblasts after adipo-, chondro- and osteogenic phenotype shifts. *Differentiation.* **84,** 305–13 (2012).

20. Singh, M., Pierpoint, M., Mikos, A. G. & Kasper, F. K. Chondrogenic differentiation of neonatal human dermal fibroblasts encapsulated in alginate beads with hydrostatic compression under hypoxic conditions in the presence of bone morphogenetic protein-2. *J. Biomed. Mater. Res. A* **98,** 412–24 (2011).

21. Junker, J., Sommar, P., Skog, M., Johnson, H. & Kratz, G. Adipogenic, chondrogenic and osteogenic differentiation of clonally derived human dermal fibroblasts. *Cells. Tissues. Organs* **191,** 105–118 (2010).

22. Sommar, P. *et al.* Engineering three-dimensional cartilage- and bone-like tissues using human dermal fibroblasts and macroporous gelatine microcarriers. *J. Plast. Reconstr. Aesthet. Surg.* **63,** 1036–46 (2010).

23. Babur, B. K. *et al.* The interplay between chondrocyte redifferentiation pellet size and oxygen concentration. *PLoS One* **8,** e58865 (2013).

24. Koay, E. J. & Athanasiou, K. a. Hypoxic chondrogenic differentiation of human embryonic stem cells enhances cartilage protein synthesis and biomechanical functionality. *Osteoarthritis Cartilage* **16,** 1450–6 (2008).

25. Schuh, E. *et al.* Chondrocyte redifferentiation in 3D: The effect of adhesion site density and substrate elasticity. *J. Biomed. Mater. Res. Part A* **100A,** 38–47 (2012).

26. Egli, R. J., Wernike, E., Grad, S. & Luginbühl, R. *Physiological cartilage tissue engineering effect of oxygen and biomechanics. Int. Rev. Cell Mol. Biol.* **289,** 37–87 (2011).

27. Pampaloni, F., Reynaud, E. G. & Stelzer, E. H. K. The third dimension bridges the gap between cell culture and live tissue. *Nat. Rev. Mol. Cell Biol.* **8,** 839–45 (2007).

28. Dutta, R. C. & Dutta, A. K. Cell-interactive 3D-scaffold; advances and applications. *Biotechnol. Adv.* **27,** 334–339 (2009).

29. Santos, E., Hernández, R. M., Pedraz, J. L. & Orive, G. Novel advances in the design of three-dimensional bio-scaffolds to control cell fate: translation from 2D to 3D. *Trends Biotechnol.* **30,** 331–41 (2012).

30. Rice, J. J. *et al.* Engineering the regenerative microenvironment with biomaterials. *Adv. Healthc. Mater.* **2,** 57–71 (2013).

31. Yamada, K. M. & Cukierman, E. Modeling tissue morphogenesis and cancer in 3D. *Cell* **130,** 601–10 (2007).

32. Griffith, L. G. & Swartz, M. A. Capturing complex 3D tissue physiology in vitro. *Nat. Rev. Mol. Cell Biol.* **7,** 211–24 (2006).

33. Semino, C. E. Self-assembling Peptides: From Bio-inspired Materials to Bone Regeneration. *J. Dent. Res.* **87,** 606–616 (2008).

34. Burdick, J. a & Vunjak-Novakovic, G. Engineered microenvironments for controlled stem cell differentiation. *Tissue Eng. Part A* **15,** 205–19 (2009).

35. Kelleher, C. M. & Vacanti, J. P. Engineering extracellular matrix through nanotechnology. *J. R. Soc. Interface* **7 Suppl 6,** S717–29 (2010).

36. Kleinman, H. K., Philp, D. & Hoffman, M. P. Role of the extracellular matrix in morphogenesis. *Curr. Opin. Biotechnol.* **14,** 526–532 (2003).

37. Holmes, T. C. *et al.* Extensive neurite outgrowth and active synapse formation on self-assembling peptide scaffolds. *Proc. Natl. Acad. Sci. U. S. A.* **97,** 6728–33 (2000).

38. Nicoll, S., Wedrychowska, A., Smith, N. & Bhatnagar, R. Modulation of proteoglycan and collagen profiles in human dermal fibroblasts by high density micromass culture and treatment with lactic acid suggests change to a chondrogenic phenotype. *Connect Tissue Res.* **42,** 59–69 (2001).

39. Gomes, M. *et al.* in *Tissue Eng.* (Blitterswijk, C. van *et al.*) 145–192 (Elsevier, 2008).

40. De Franceschi, L. *et al.* Transplantation of chondrocytes seeded on collagen-based scaffold in cartilage defects in rabbits. *J. Biomed. Mater. Res. A* **75,** 612–22 (2005).

41. Choi, J. W. *et al.* Mechanical stimulation by ultrasound enhances chondrogenic differentiation of mesenchymal stem cells in a fibrin-hyaluronic Acid hydrogel. *Artif. Organs* **37,** 648–55 (2013).

42. Häuselmann, H. J. *et al.* Phenotypic stability of bovine articular chondrocytes after long-term culture in alginate beads. *J. Cell Sci.* **107,** 17–27 (1994).

43. Mauck, R. L., Yuan, X. & Tuan, R. S. Chondrogenic differentiation and functional maturation of bovine mesenchymal stem cells in long-term agarose culture. *Osteoarthritis Cartilage* **14,** 179–89 (2006).

44. Hoshikawa, A. *et al.* Encapsulation of chondrocytes in photopolymerizable styrenated gelatin for cartilage tissue engineering. *Tissue Eng.* **12,** 2333–41 (2006).

45. Coburn, J. M., Gibson, M., Monagle, S., Patterson, Z. & Elisseeff, J. H. Bioinspired nano fi bers support chondrogenesis for articular cartilage repair. *Proc. Natl. Acad. Sci. U.S.A* **109,** 10012–10017 (2012).

46. Nettles, D. L., Elder, S. H. & Gilbert, J. a. Potential use of chitosan as a cell scaffold material for cartilage tissue engineering. *Tissue Eng.* **8,** 1009–16 (2002).

47. Kim, I. L., Khetan, S., Baker, B. M., Chen, C. S. & Burdick, J. a. Fibrous hyaluronic acid hydrogels that direct MSC chondrogenesis through mechanical and adhesive cues. *Biomaterials* **34,** 5571–80 (2013).

48. Dijkhuizen-radersma, R. Van, Moroni, L., Apeldoorn, A. Van, Zhang, Z. & Grijpma, D. in *Tissue Eng.* (Blitterswijk, C. van *et al.*) 193–221 (Elsevier, 2008).

49. Uematsu, K. *et al.* Cartilage regeneration using mesenchymal stem cells and a three-dimensional poly-lactic-glycolic acid (PLGA) scaffold. *Biomaterials* **26,** 4273–9 (2005).

50. Ishaug-Riley, S. L., Okun, L. E., Prado, G., Applegate, M. a & Ratcliffe, a. Human articular chondrocyte adhesion and proliferation on synthetic biodegradable polymer films. *Biomaterials* **20,** 2245–56 (1999).

51. Bryant, S. J., Bender, R. J., Durand, K. L. & Anseth, K. S. Encapsulating chondrocytes in degrading PEG hydrogels with high modulus: engineering gel structural changes to facilitate cartilaginous tissue production. *Biotechnol. Bioeng.* **86,** 747–55 (2004).

52. An, Y. H., Webb, D., Gutowska, A., Mironov, V. A. & Friedman, R. J. Regaining Chondrocyte Phenotype in Thermosensitive Gel Culture. *Anat. Rec.* **341,** 336–341 (2001).

53. Chia, S.-L., Gorna, K., Gogolewski, S. & Alini, M. Biodegradable elastomeric polyurethane membranes as chondrocyte carriers for cartilage repair. *Tissue Eng.* **12,** 1945–53 (2006).

54. Quintana, L. *et al.* Early tissue patterning recreated by mouse embryonic fibroblasts in a three-dimensional environment. *Tissue Eng Part A* **15,** 45–54 (2009).

55. Kopesky, P., Vanderploeg, E., Kurz, B. & Grodzinsky, A. J. Self-assembling peptide hydrogels modulate in vitro chondrogenesis of bovine bone marrow stromal cells. *Tissue Eng Part A* **16,** (2009).

56. Zhu, L. *et al.* Engineered cartilage with internal porous high-density polyethylene support from bone marrow stromal cells: A preliminary study in nude mice. *Br. J. Oral Maxillofac. Surg.* **48,** 462–5 (2010).

57. Mercier, N. R., Constantino, H. R., Tracy, M. A. & Bonassar, L. J. Poly(lactide-co-glycolide) microspheres as a moldable scaffold for cartilage tissue engineering. *Biomaterials* **25,** 1945–52 (2005).

58. Whitesides, G. M. & Grzybowski, B. Self-assembly at all scales. *Science* **295,** 2418–21 (2002).

59. Ma, P. X. Biomimetic Materials for Tissue Engineering Peter. *Adv. Drug Deliv. Rev.* **60,** 184–198 (2008).

60. Peggion, E., Cosani, A., Terbojevich, M. & Borin, G. Conformational studies on polypeptides. The effect of sodium perchlorate on the conformation of poly-L-lysine and of radom copolymers of L-lysine and L-phenylalanine in aqueous solution. *Biopolymers* **11,** 633–643 (1972).

61. Rippon, W., Chen, H. & Walton, A. Spectroscopic characterization of poly (Glu-Ala). *J Mol Biol* **75,** 369–375 (1973).

62. Aggeli, A. *et al.* Responsive gels formed by the spontaneous self-assembly of peptides into polymeric beta-sheet tapes. *Nature* **386,** 259–262 (1997).

63. Zhang, S., Holmes, T., Lockshin, C. & Rich, a. Spontaneous assembly of a self-complementary oligopeptide to form a stable macroscopic membrane. *Proc. Natl. Acad. Sci. U. S. A.* **90,** 3334–8 (1993).

64. Genové, E., Shen, C., Zhang, S. & Semino, C. E. The effect of functionalized self-assembling peptide scaffolds on human aortic endothelial cell function. *Biomaterials* **26,** 3341–51 (2005).

65. Zhang, S. & Semino, C. E. Design peptide scaffolds for regenerative medicine. *Adv. Exp. Med. Biol.* **534,** 147–63 (2003).

66. Sieminski, a. L., Was, a. S., Kim, G., Gong, H. & Kamm, R. D. The Stiffness of Three-dimensional Ionic Self-assembling Peptide Gels Affects the Extent of Capillary-like Network Formation. *Cell Biochem. Biophys.* **49,** 73–83 (2007).

67. Zhang, S. *et al.* Self-complementary oligopeptide matrices support mammalian cell attachment. *Biomaterials* **16,** 1385–93 (1995).

68. Kisiday, J. *et al.* Self-assembling peptide hydrogel fosters chondrocyte extracellular matrix production and cell division : (2002).

69. Scaffold, T. P. N., Semino, C. E., Kasahara, J. & Hayashi, Y. Entrapment of Migrating Hippocampal Neural Cells in. *Tissue Eng Part* **10,** (2004).

70. Garreta, E., Genové, E., Borrós, S. & Semino, C. E. Osteogenic Differentiation of Mouse Embryonic Stem Cells and Mouse Embryonic Fibroblasts in a Three-Dimensional. *Tissue Eng Part A* **12,** 2215–2227 (2006).

71. Semino, C. E. Can We Build Artificial Stem Cell Compartments? *J. Biomed. Biotechnol.* **2003,** 164–169 (2003).

72. Hartgerink, J. D., Beniash, E. & Stupp, S. I. Self-assembly and mineralization of peptide-amphiphile nanofibers. *Science* **294,** 1684–8 (2001).

73. Liu, J., Song, H., Zhang, L., Xu, H. & Zhao, X. Self-assembly-peptide hydrogels as tissue-engineering scaffolds for three-dimensional culture of chondrocytes in vitro. *Macromol. Biosci.* **10,** 1164–70 (2010).

74. Kisiday, J. *et al.* Self-assembling peptide hydrogel fosters chondrocyte extracellular matrix production and cell division : Implications for cartilage tissue repair. *Proc. Natl. Acad. Sci. U.S.A* **99,** 9996–10001 (2002).

75. Kisiday, J. D., Jin, M., DiMicco, M. a, Kurz, B. & Grodzinsky, A. J. Effects of dynamic compressive loading on chondrocyte biosynthesis in self-assembling peptide scaffolds. *J. Biomech.* **37,** 595–604 (2004).

76. Miller, R. E. *et al.* Effecr of Self-assembling Peptide, Chondrogenic Factors, and Bone Marrow Derived Stromal Cells on Osteochondral Repair. *Osteoarthr. Cartil.* **18,** 1608–1619 (2010).

77. Shah, R. N. *et al.* Supramolecular design of self-assembling nanofibers for cartilage regeneration. *Proc. Natl. Acad. Sci. U. S. A.* **107,** 3293–8 (2010).

78. Bussmann, B. M. *et al.* Chondrogenic potential of human dermal fibroblasts in a contractile soft self-assembling peptide hydrogel. *J Tissue Eng Regen Med* (2013).

79. Marí-Buyé, N., Luque, T., Navajas, D. & Semino, C. Development of a three-dimensional bone-like construct in a soft self-assembling peptide matrix. *Tissue Eng Part A* **19,** 870–881 (2013).

# **Chapter 2: Development of tissue engineering strategies for cartilage tissue repair using the self-assembling peptide RAD16-I**

# 2.1 Introduction

## 2.1.1 Overview

As introduced in Chapter 1, different strategies have been designed to restore the damaged cartilage whereas significant challenges still remain in the clinical application of cell-based therapies for cartilage repair. Novel approaches should envisage adequate cell culture models involving different cell sources, stimulatory factors and biomaterials, which could offer healthy cartilage-like tissue that would restore the functionality of the damaged cartilage.

## 2.1.2 Cartilage formation *in vivo*

The design of new strategies to regenerate cartilage tissue requires preliminary identification of key factors that regulate and control in vivo processes. Cartilage is an avascular tissue formed by chondrocytes embedded in a specialized extracellular matrix composed by a highly complex network of collagen fibrils and proteoglycans. Chondrocytes form three different types of cartilage characterized by a unique molecular composition and extracellular matrix (ECM) organization: hyaline, fibrous and elastic cartilage (Table 2.1.1). Hyaline cartilage is the most abundant and it constitutes the articular cartilage. It is also present in costal cartilage, nose, trachea, larynx and embryonic skeleton. Moreover, it is involved in skeletal development through the process of endochondral ossification (reviewed in Chapter 3). Instead, fibrocartilage is typically found in the intervertebral discs, meniscus and it is also temporarily formed at fracture sites. Finally, elastic cartilage is present in the outer ear, larynx and epiglottis [1]. Independently of the type of cartilage, its formation is a stepwise process: first, determination of cells and their aggregation into pre-chondrogenic condensations; second, differentiation into chondrocytes; and third, maturation (Figure 2.1.1).

**Table 2.1.1. Types of cartilage, location and function.**

| Cartilage Type | Location | Function |
|---|---|---|
| Hyaline Cartilage | Articular Cartilage<br>Costal cartilage<br>Nose<br>Trachea<br>Larynx<br>Embryonic skeleton | Supports and reinforces<br>Resilient cushioning properties<br>Resists compressive stress |
| Fibrous Cartilage | Intervertebral discs<br>Meniscus<br>Temporarily formed at fracture sites | Resists compression and tension |
| Elastic Cartilage | Outer ear<br>Larynx<br>Epiglottis | Maintains the shape<br>Great flexibility |

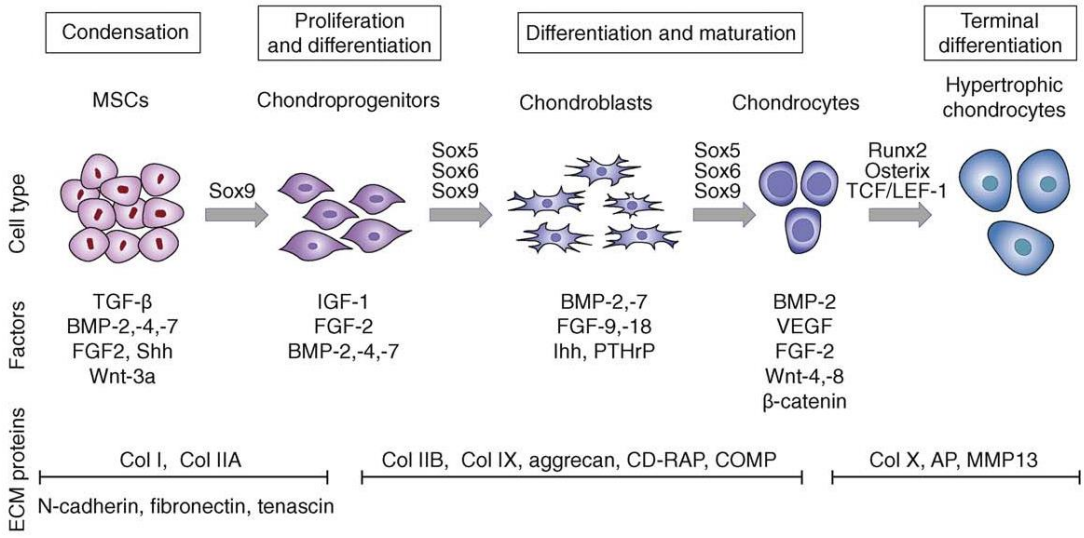


**Figure 2.1.1 Sequence of events leading to the differentiation of mesenchymal stem cells (MSCs) towards chondrocytes.** The scheme illustrates the temporal expression profiles of the different growth and differentiation factors and proteins characteristic of the extracellular matrix (ECM). Abbreviations: AP, alkaline phosphatase; CD-RAP, cartilage-derived retinoic acid-sensitive protein; Col, collagen; COMP, cartilage oligomeric protein; MMP, matrix metalloprotease; VEGF, vascular endothelial growth factor. (Image from Vinatier et al 2009 [2])

Mesenchymal condensation is the first step in chondrogenic differentiation, which consists of physical compaction of resident mesenchymal cells driven by proper cell signaling. Cellular interactions increase; mostly N-cadherin and neural cell adhesion molecule (N-CAM) mediate cell–cell interactions[3]. At the same time, these cells synthesize new matrix that is mainly composed by collagen type I, fibronectin, and distinct proteoglycans, such as versican or syndecan[4]. After the condensation, mesenchymal cells express transcription factor Sox9 that controls downstream genes involved in chondrogenesis and promotes these progenitor cells to secrete cartilage-specific ECM molecules and differentiate to chondroblasts. The expression of Sox9 is regulated by members of the families of fibroblast growth factor (FGF), transforming growth factor-β (TGF-β), bone morphogenetic protein (BMP) and Wnt. All these molecules are essential for the formation of chondrogenic mesenchymal condensation[3]. The next stage is characterized by the deposition of cartilage specific collagen types II, IX and XI, and proteoglycans, while the expression of collagen type I is turned off [5]. Therefore, cells exchange their elongated fibroblastic-like shape (typical of mesenchymal progenitors) for new round chondroblastic morphology and finally become mature chondrocytes that are sparsely distributed within the matrix.

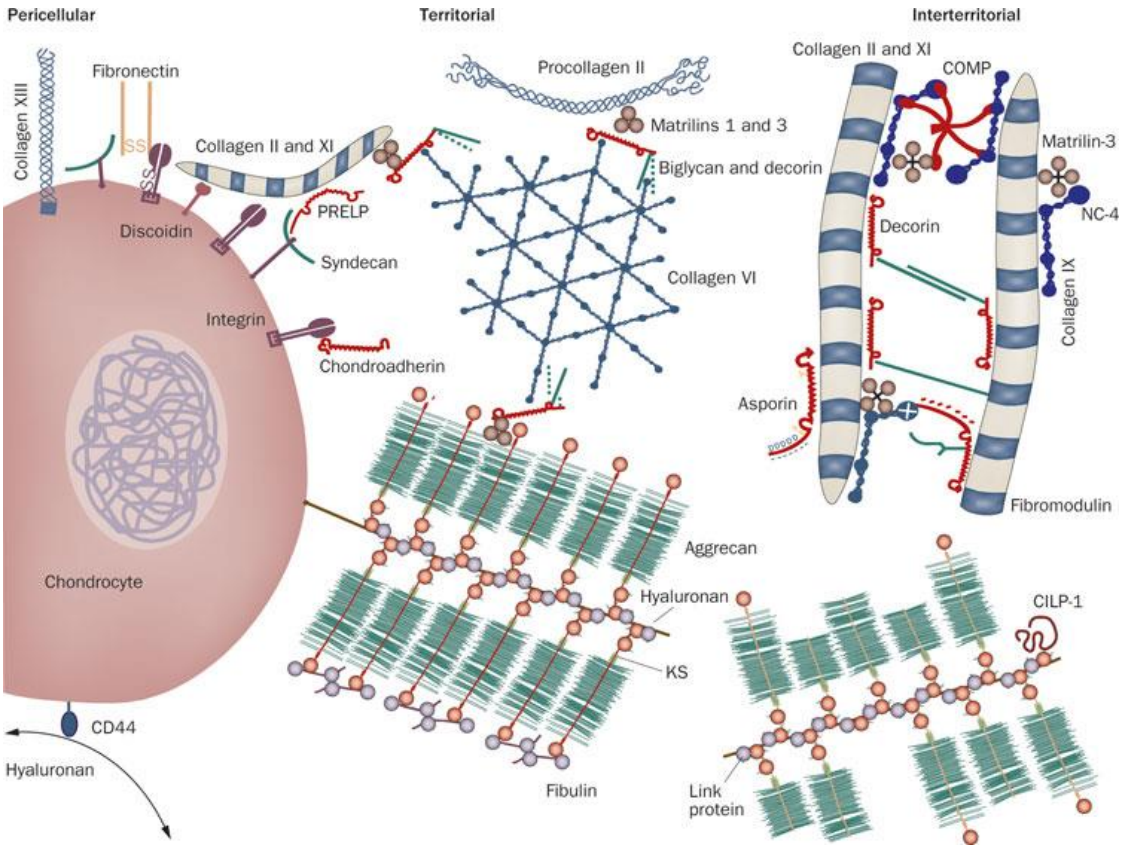


**Figure 2.1.2 Molecular organization of normal articular chondrocytes.** (Image adapted from Heinegård, D. & Saxne, T. 2010 [6])

Mature cartilage is a tissue with an ECM composed of collagenous and noncollagenous elements which together form an interconnected elastic network surrounding chondrocytes providing its unique mechanical properties (Figure 2.1.2). Independently of the type of cartilage, the primary collageneous component is collagen II (about 90% of the collagenous fraction), however, collagens I, VI, IX, X, and XI are also present in the collagen fibrils with different percentages depending on the particular cartilage. Altogether, collagens form the fibrillar network that confers strength to the chondrogenic ECM. The noncollagenous fraction of cartilage is basically composed of proteoglycans, hyaluronan, link protein, and interfibrillar proteins like COMP or decorin [3]. Regarding the proteoglycans, the short proteoglycans that are present in the mesenchymal condensation (versican and syndecan) are gradually substituted by larger and more complex proteoglycans, mainly aggrecan which accounts for about 90% of the proteoglycan content. The structural features of proteoglycans, which consist of a core protein and one or more covalently attached negatively charged glycosaminoglycan chains (GAGs), provide biomechanical properties that allow resistance to compressive loading *in vivo*.

### 2.1.3 Role of BMPs and their antagonist Noggin in chondrogenesis

As mentioned before, cartilage formation is regulated by a complex and orchestrated secretion of biological factors. Among them, Bone Morphogenetic Proteins (BMPs), are present in the hole process having an essential role in the formation of chondrogenic mesenchymal condensation [7]. BMPs were originally isolated from mammalian bone and they were characterized by their ability to induce ectopic bone formation. Further *in vitro* and *in vivo* studies have shown that BMP signaling not only is required for the formation of pre-cartilaginous condensations and the differentiation of precursors into chondrocytes, but it also regulates the later stages of chondrocyte maturation and terminal differentiation to the hypertrophic phenotype. Regulation of BMP activity occurs in several different ways including the direct inhibition of BMP signaling by secreted antagonists such as Noggin and Chordin [8].

Noggin was first identified in *Xenopus* as a dorsalizing signal playing a crucial role in neural development [9,10]. Nevertheless, Noggin is also expressed in condensing cartilage and immature chondrocytes, like many BMPs, having an important role in the regulation of chondrocyte proliferation and differentiation [11–14]. It is known that mutant mice lacking Noggin show excessive cartilage formation due to the enhanced BMP activity in the absence of Noggin antagonism (Figure 2.1.3) [13]. In addition, these mutants failed to initiate joint formation which proves that Noggin is not required for cartilage initiation but is involved in regulating chondrocyte proliferation and differentiation [12,13]. Moreover, misexpression of Noggin in an embryonic chick limb model prior to the onset of chondrogenesis leads to the total absence of skeletal elements [15]. Finally, *in vitro* studies also showed the inhibition of chondrogenic but not osteogenic differentiation of a mesodermal stem cell line due to the recombinant overexpression of Noggin. [16].

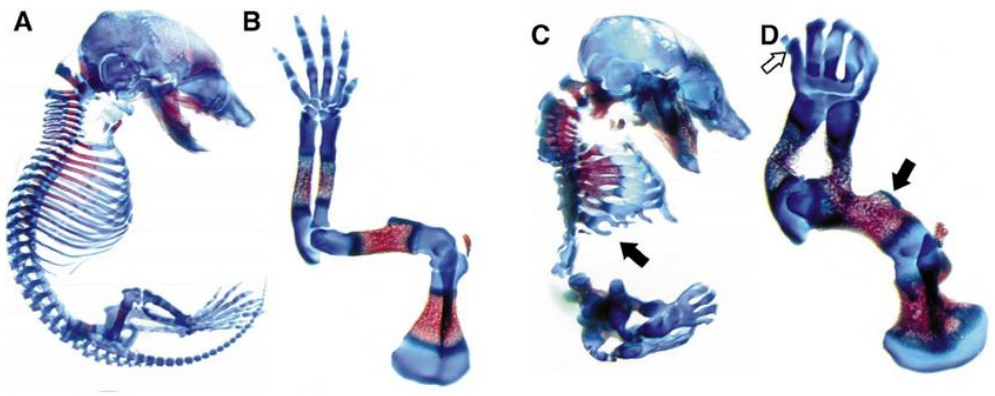


**Figure 2.1.3. Noggin mice knockout phenotype** Skeletal abnormalities in *Noggin* homozygous mutants. Skeletons, with forelimbs removed, from (A) wild-type and (C) mutant and Forelimbs of (B) wild type and (D) mutant 18.5- dpc (days post coitum) embryos were stained with alcian blue for nonmineralized cartilage and alizarin red for mineralized cartilage and bone. (Image adapted from Brunet et al 1998 [13])

Similarly, mutations of Noggin in humans cause two autosomal dominant disorders: proximal symphalangism and multiple synostosis syndrome, both characterized by multiple joint fusions [17,18]. Altogether, these features emphasize how important the balance BMP/Noggin is for the correct development of chondral and skeletal elements during embryogenesis. Thus, it seems to be a crucial factor to take into account in the development of strategies for cartilage tissue engineering.

It is important to mention that Noggin is also a soluble factor secreted during the embryogenesis by the *organizer*, a signaling center which provides spatial pattern information to its microenvironment during gastrulation [19]. The molecular exploration of the *organizer* (the node in mouse) showed that it is a source of nuclear transcription factors and secreted factors that mediate the inducing activities of the organizer. Mostly, these secreted factors are antagonists of growth factors, which they bind in the extracellular space, and they can act as inhibitors that prevent binding to the growth factor receptors [20]. In the embryonic development, Noggin also acts as an antagonist of BMPs, which can modulate the formation of the three germ layers: mesoderm, endoderm and ectoderm [21]. Among the transcription factors secreted by the organizer are included the Hepatic Nuclear Factor 3-β (HNF-3β or Foxa2) and goosecoid. Foxa2 has also been shown to be expressed with a dual role during early embryogenesis: as an organizer when expressed in the early mouse embryo, and as an endodermal marker when expressed in the visceral and definitive endoderm later in embryogenesis [22]. Interestingly, it was recently reported to be a crucial regulator in the hypertrophic chondrocyte differentiation program in combination with Foxa3 [23]. Instead, *goosecoid* was the first organizer gene isolated from the Spemann organizer in *Xenopus* and it determines the mesodermal fates of those cells expressing it. It is related to the transcription factor *Brachury*, since they are both expressed in the same population of cells when the first mesodermal cells come up and as a consequence are some of the first mesodermal markers [24].

### 2.1.4 Scaffold design for cartilage tissue engineering: influence of stiffness.

Once understood the process of cartilage formation *in vivo* and identified the main factors involved in the commitment to chondrogenic differentiation, the next step is to identify scaffolds to design tissue engineering strategies for cartilage repair.

Nowadays, several groups are focused on designing new biomaterials for cartilage tissue engineering trying to mimic the *in vivo* microenvironment. Although most studies are centered in scaffold properties such as composition, porosity, degradation or the influence of biochemical cues on cell behavior [25], an increasingly number of studies is now focusing on the influence of mechanical properties on cell behavior and differentiation [26–29].

It is known that cell morphology and functions can depend strongly on substrate stiffness under conditions where chemical signals are constant. In the body, the range of ECM stiffness is immense, from soft brain tissue with an elastic modulus over 1 kilopascal (kPa) to hard bones with hundreds of megapascals (MPa) [30]. These tissues contain cells that are tuned to the specific mechanical environments in which they reside. In accordance to this, recent studies have demonstrated that the biomechanical properties of the substrate itself, specifically stiffness, directly influence the differentiation of the attached cells [31]. As an example, it was reported that materials with similar mechanical attributes to those of native tissues associated with a cell type are most relevant for stem cell differentiation towards the corresponding phenotype than chemical signals. Thus, it was demonstrated that ECM guides MSC differentiation into osteoblastic, skeletal muscular and neural lineages in a dependent manner on ECM stiffness [27].

In terms of chondrogenic differentiation, it has been recently found that MSCs commit to chondrogenic lineage when cultured in more compliant scaffolds rather than stiff ones [25,32,33]. The stiffness range associated with driving mesenchymal cell fate has generally been in the kPa – Mpa range, which is biologically relevant for cartilage and bone [31]. Although mature cartilage may not be as soft as 1 kPa, this stiffness could be the reminiscent of the stiffness during cartilage development [30]. Altogether, these results show how important it is to control scaffold mechanical properties to engage a cellular system to undergo chondrogenic differentiation.

### 2.1.5 Mouse embryonic fibroblasts (MEFs) as a model of spontaneous chondrogenic differentiation in the self-assembling peptide RAD16-I

As it has been introduced in Chapter 1, the optimal cell source for cartilage tissue engineering is still unclear. During the last years, cell types other than chondrocytes and MSCs have been widely used, such as fibroblasts, for tissue engineering applications. Different studies showed the ability of fibroblasts to redirect their fate towards mesodermal lineages (including adipocytes, osteoblasts and chondrocytes) when cultured under the appropriate conditions [34–39]. In fact, clonal analysis determined that dermal fibroblasts were constituted by a heterogeneous population containing progenitors with different levels of differentiation [40]. Hence, different studies report that dermal progenitors show a profile of cell surface markers very similar to that of mesenchymal stem cells [38,40]. Remarkably, it was reported that mouse embryonic fibroblasts (MEFs) were not distinguishable from Bone Marrow Stem Cells (BMSCs) based on typical BMSCs CD surface marker expression. However, *in vitro* differentiation assays suggested that, although osteogenic, adipogenic and chondrogenic differentiations were obtained under specific induction using MEFs, there were differences in their cellular response to differentiation signals [41].

MEFs are derived from 13.5-day old embryos after removing head and viscera, thus mesodermal tissues are their major contributors. They have been mainly used as feeder layers to culture embryonic stem cells (ESCs). Moreover, fibroblasts have triggered studies of fibroblast biology, cancer and aging [41,42].Moreover, they have been the first cells reported in the generation of induced pluripotent stem cells (iPSCs); briefly, MEFs were reprogramed to a pluripotent state by the introduction the four transcription factors Oct3/4, Sox2, c-Myc and Klf4, under ESCs culture conditions [43].

Thus, MEFs may represent a good alternative to BMSCs to study molecular mechanisms in the commitment to osteoblasts, adipocytes and chondrocytes [41]. Taking this into account, MEFs have been widely used in our laboratory to study chondrogenic, osteogenic and adipogenic differentiation using a 3D culture system based on the self-assembling peptide RAD16-I. Interestingly, it was found that MEFs 3D cultures underwent dramatic morphological changes mainly caused by an organized cell contraction and migration that ended, after 7-10 days in culture, with the formation of a highly condense 3D construct. During this process the system was found to spontaneously up-regulate the expression of a subset of chondrogenic genes including the transcription factor Sox9 and two main components of the chondrocytes extracellular matrix, collagen type II and proteoglycans. Remarkably, the default chondrogenic differentiation was not observed when using collagen type I or agarose as scaffolds for the 3D culture. These results suggested that the biomechanical and non-instructive properties of the self-assembling peptide environment might have a key role in the process (Figure 2.1.4) [44].

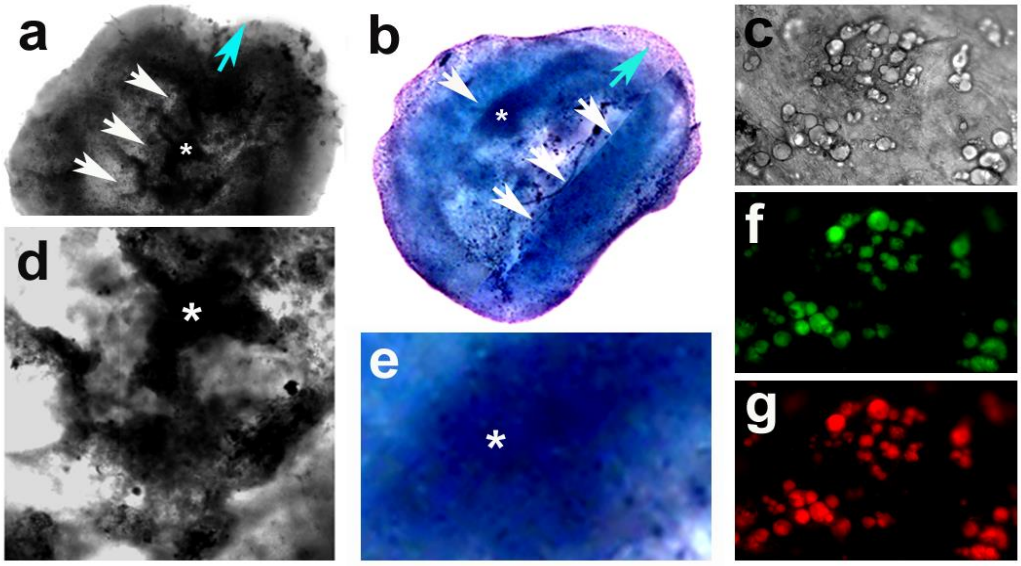


**Figure 2.1.4. Multipotential capacity of MEFs.** Phenotype of MEFs cultured in three- dimensional (3D) self-assembling peptide hydrogel RAD16-I was assessed under different culture conditions. (A, D) Only after osteogenic induction, von Kossa staining showed calcium deposition. (B, E) Toluidine Blue staining showed default chodrogenic differentiation without need of supplements. (C) Adipocytes in non-supplemented cell cultures were detectable by visual inspection, and (F,G) Neutral lipids present in the adipocytes were stained using Nile Red. (Image adapted from Quintana et al 2009 [44])

In addition, Nile Red staining showed some spontaneous adipogenic differentiation restricted to isolated cells. Regarding the osteogenic differentiation, MEFs 3D-cultures only exhibited matrix mineralization (characteristic of osteogenic phenotype) after the addition of specific induction media. Hence, it was hypothesized that during this process MEFs could be acquiring a multipotent state, from which they could give rise to most of the cell types of mesodermal germ lineages [44,45].

## 2.2 Hypothesis and specific aims

In view of the multipotential capacity acquired by MEFs when embedded in the self-assembling peptide RAD16-I, this chapter aims to study the possible mechanisms that modulate the spontaneous multipotent commitment of these cells. We hypothesized that early organizer genes may be involved in the initial steps of the chondrogenic process and their expression could be regulated by the mechanical properties of the scaffold matrix. In addition, it was hypothesized that the scaffold RAD16-I could support the chondrogenic differentiation of other cell types. Therefore, the aims for this chapter are the following:

(1) To evaluate the influence of matrix properties in the spontaneous chondrogenic differentiation that MEFs suffer in the self-assembling peptide RAD16-I.
(2) To analyze the isolated adipogenic differentiation also observed in the 3D cultures of MEFs.
(3) To characterize the molecular mechanisms regulating the multipotent commitment of MEFs in the self-assembling peptide RAD16-I.
(4) To evaluate the self-assembling peptide RAD16-I as a support scaffold for chondrogenic differentiation using dedifferentiated bovine chondrocytes.

## 2.3 Materials and Methods

### 2.3.1 Culture of mouse embryonic fibroblasts (MEFs)

MEFs isolated from C57BL=6 embryos at day 14 were purchased from the American Type Culture Collection (scrc-1008; ATCC). The use of these cells has been approved by the Ramon Llull University Ethics Committee (CER URL 2013-001). MEFs (<10th passage) were cultured in 25 and 75-cm2 flasks in fibroblast medium (FM), which contains high-glucose Dulbecco's modified Eagle medium (DMEM; D5671, Sigma) supplemented with 15% (v/v) Fetal Bovine Serum (FBS) (DE14-801F, Lot: 1SB003, Lonza), 100 U/mL Penicillin / 0.1 mg/mL Streptomycin (P11-010, PAA), 2mM L-Glutamine (M11-004, PAA), 1mM Sodium Piruvate (11360-039, Gibco) and 100µM Minimum Essential Medium Non-essential Amino Acid solution (M7145, Sigma). Cultures were maintained in the incubator in humidified atmosphere at 37ºC and 5% $CO_2$.

### 2.3.2 Chondrocyte isolation

Saddle sections (7-14 kg) of 1-2 week old calves were obtained from a local abattoir (Arena, Hopkinton, MA) directly after slaughter. The intact femoropatellar joint was isolated by transecting the femur and mounting the distal segment in a drilling apparatus. The femoropatellar articular cartilage was then exposed by opening the joint capsule, severing the medial, lateral, and cruciate ligaments, and removing the tibia, patella, and surrounding tissue. During this entire process, the cartilage was kept moist and free of blood by frequent rinsing with sterile PBS supplemented with antibiotics (100 U/ml penicillin and 0.1 mg/ml streptomycin). Full-thickness cartilage pieces were shaved off using a sterile surgical blade. Care was taken not to include the underlying subchondral bone. Chondrocytes were isolated from whole cartilage using sequential digestions of 0.4% (w/v) pronase (P6911,Sigma) for 1 hour at 37ºC, and 0.08% (w/v) collagenase (C5894, Sigma) overnight at 37ºC. After digestions, cell solution was filtered using 70µm cell strainer, centrifuged for 8 min at 1900g and resuspended in sterile PBS. Total cell number was determined using a hemocytometer and viability was assessed using Trypan Blue (T8154, Sigma). Cultures were maintained in FM in the incubator at 37ºC and 5% $CO_2$.

### 2.3.3 Cell harvesting and subculture from tissue culture flasks

Tissue culture flasks were washed with 1mL Trypsin-EDTA (0.05% Trypsin, 0.02% EDTA, L11-004, PAA) and treated again with 2mL or 4mL Trypsin–EDTA (for T25 and T75 flasks, respectively) for 5 minutes at 37°C, or until cells started to detach from the flask. Trypsin's activity was inhibited adding serum containing medium, then cells were disrupted mechanically with a micropipette until single cells were obtained as observed using phase microscopy. Released cells were washed with complete culture medium, counted, resuspended as needed and then seeded in other plaque or used for cell encapsulation in hydrogels.

### 2.3.4 3D culture technique using the self-assembling peptide RAD16-I

To obtain a 3D culture, a solution of commercial 1% (w/v) RAD16-I (PuraMatrix™,354250, Beckton Dickinson) was diluted in sucrose 10% (w/v) (S1888, Sigma), to obtain a concentration of 0.5 % or 0.14% (w/v) (depending on the final concentration wanted). This solution was mixed with an equal volume of a cell suspension (4 x $10^6$ cells/mL) in sucrose 10% (w/v), to obtain a final concentration of 2 x $10^6$ cells/mL in 0.25% or 0.07% (w/v), respectively, of RAD16-I in sucrose 10% (w/v). 80µL of this mix was loaded into 9mm diameter cell culture inserts (PICM01250, Millipore), previously placed into a 6-well culture plate and equilibrated with culture media. Immediately, cell-peptide cultures were placed for 30 minutes in the incubator at 37°C and 5% $CO_2$, to allow the formation of the hydrogel by the action of the high ionic strength and the neutral pH of the medium. Elapsed this time, when working at low peptide concentrations (0.07% (w/v)) and to dilute the content of sucrose, subsequent washing steps were performed by aspiration of the culture media in the well (outside of the insert), and the addition of the same amount (500µL) of fresh medium (Figure 2.3.1). The plate was placed again in the incubator for 10 minutes and this step was repeated 3 times, after which 2.5mL of fresh medium were added outside the insert and the plate placed in the incubator for 30 more minutes, to finally allow the construct to form, preventing its rupture. At this point, the addition of medium over the cell culture began, by adding 10µL in the inner wall of the insert letting it slowly slide to the gel, until a volume of 40µL is reached. The plate was placed once again in the incubator for 15 minutes and then the addition of fresh medium over the cell construct continued, by addition of 20µL inside the insert, until a final volume of 200µL. Instead, when working at higher peptide concentrations (0.25% (w/v)), washing steps were performed by adding 60 µL directly on top of the hydrogel (Figure 2.3.1). Lastly, after the 10 minutes washing steps, 250 µL of medium were loaded inside the insert and 2.5mL in the well outside the insert. In both cases, the 3D cell cultures were maintained in the incubator at 37°C and 5% $CO_2$, for 5, 14 or 28 days. The medium was changed every second day by removing 500µL of medium from the well and the addition of 500µL of fresh medium inside the insert.

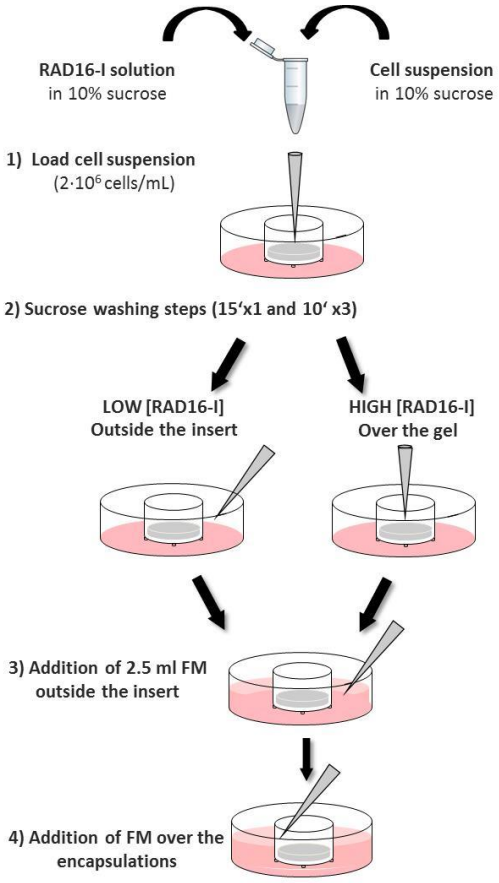


**Figure 2.3.1. Schematic process of the 3D encapsulation protocol in RAD16-I**

### 2.3.5 3D culture technique using collagen type I

Cells were harvested and re-suspended in PBS (H15-002, PAA), to obtain a final concentration of 4 x $10^6$ cells/mL. Aside, a solution of Phenol Red was prepared, mixing 1µL of phenol red (P0290, Sigma) with 99µL of PBS 10X. This solution was added to a determined volume of Collagen Type I (from rat tail, initial concentration: 3.81mg/mL, 354236, Lot: 2152614, BD) in PBS, to obtain a final concentration of 0.28% (w/v) Collagen Type I in 1ml of 1X PBS. The solution was stored on ice, to prevent the gelation of the Collagen. The volume was adjusted to 1mL with tissue culture water (521-012, PAA) and the pH was raised to 8-9 by adding NaOH 1M (tissue culture grade, S2770, Sigma), until change in the color of the pH indicator solution from yellow to pink, checked with pH test paper. Equal volumes of cell suspension and Collagen type I solution were mixed to obtain a suspension of 2 x $10^6$ cells/mL in 0.14% Collagen type I in PBS. 80µL of this suspension were loaded in wells of a 48-well culture plate (PAA30024X, PAA), previously coated with agarose 10 mg/mL (A9045-5G, Sigma). The culture plate was placed for 30 minutes in the incubator at 37°C and 5% $CO_2$, to induce the gelation of the construct, which takes place by changes in the pH and temperature. After this time, 0.7mL of FM were carefully added to the well. The culture was maintained for 5, 14 or 28

days, at 37°C and 5% $CO_2$, and the medium was changed every second day by removing 0.5mL of medium and the addition of 0.5mL of fresh medium (Figure 2.3.2).

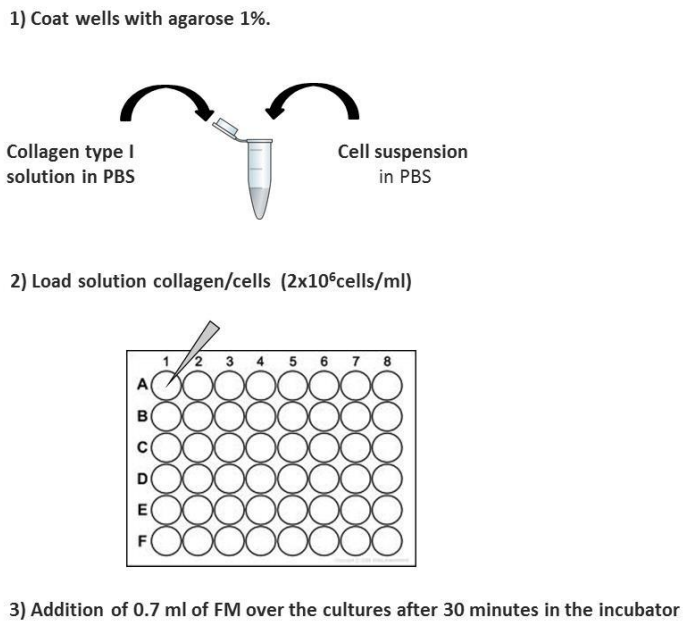


**Figure 2.3.2 Schematic process of the 3D encapsulation protocol in collagen type I**

### 2.3.6 Cell lysis from 3D cultures

After the specific cultivation time has elapsed, 3D cultures were lysed with a specific buffer depending on the subsequent analysis. For protein extraction, a solution of RIPA buffer (R0278, Sigma), with protease inhibitor cocktail (11836153001, Roche) was used. In the case of RNA extraction, RNA lysis buffer (12-TRK-02, PeqLab) was used. In both cases, the medium was carefully removed from the insert and the well, and the cell culture was washed twice with PBS. A volume of 250µL of lysis buffer was added, and the complete lysis of the construct was reached by pipetting up and down the cells several times. The samples obtained were stored at -80°C until their posterior analysis.

### 2.3.7 Reverse transcriptase polymerase chain reaction

The RNA was extracted from the samples using peqGOLD total RNA kit (12-6834-02, PeqLab). After the removal of the genomic DNA, cDNA was synthesized using QuantiTect Reverse Transcription kit (205311, Qiagen). The cDNA obtained was analyzed by RT-PCR using, using either Deep Vent DNA Polymerase (M0258S, New England Biolabs) or Taq DNA Polymerase master mix (D1806, Sigma) and primers designed for each gene of interest (Table 2.3.1). In both cases, 50ng of cDNA sample were used for the analysis, dNTPs at a final concentration of 200µM and primers at a final concentration of 0.3µM. The amplification reaction was performed according the following parameters: Stage 1: 5 min at 95°C, Stage 2: 40 cycles of 30s at 95°C, 15s at Tm (depending on the primers used) and 20s at 72°, Stage 3: 1 min

at 72°C. DNA fragments were visualized under UV light in a 2% (w/v) agarose gel to estimate their size, which allows the identification of the aforementioned fragments.

**Table 2.3.1. Designed primers used for RT-PCR**

| Gene | F/R | Sequence (5' - 3') | Length |
|---|---|---|---|
| **18S** | F | GCTACCACATCCAAGGAAGGCAG | 234bp |
| | R | CGCTCCCAAGATCCAACTACGAG | |
| **BMP4** | F | TGATACCTGAGACCGGGAAG | 190bp |
| | R | AGCCGGTAAAGATCCCTCAT | |
| **Coll I** | F | TGACTGGAAGAGCGGAGAGT | 151bp |
| | R | GTTCGGGCTGATGTACCAGT | |
| **Coll X** | F | CAAGCCAGGCTATGGAAGTC | 154bp |
| | R | AGCTGGGCCAATATCTCCTT | |
| **Noggin** | F | GCAAGAAGCTGAGGAGGAAGTTACAGA | 184bp |
| | R | TGCACAGACTTGGATGGCTTACACA | |
| **PPAR** | F | AGGCCGAGAAGGAGAAGCTGTTG | 276bp |
| | R | TGGCCACCTCTTTGCTCTGCTC | |
| **Runx2** | F | GCCGGGAATGATGAGAACTA | 180bp |
| | R | GGACCGTCCACTGTCACTTT | |
| **Sox9** | F | AAACTTCTGTGGGAGCGACA | 155bp |
| | R | TCAGCTGCCGGCTCTAAAC | |

### 2.3.8 Agarose gel for DNA visualization

DNA amplified fragments were run in a 2%(w/v) agarose gel used to estimate their size. To prepare the gel, 1g or 3g agarose (depending on the gel size) (A9539, Sigma) were dissolved in 50mL or 150mL TAE buffer 1X (from a stock solution TAE 50X: 252g Tris-Base, 57,1mL AcOH glacial, 100mL 18,5g solid EDTA and deionized $H_2O$ up to 1L), by heating until complete dissolution. Then, 4µL or 12µL of EtBr (10µg/mL) were added to the agarose solution. 16µL of the DNA sample were mixed with 4µL loading buffer 5X (G2526, Sigma), and these 20µL were loaded into the agarose gel-wells. DNA ladder was also run to estimate DNA fragments size (10821705001or 11062590001, Roche). The gel was run at 90V or 150V during 1h. Finally, the gel was observed using a UV lamp.

### 2.3.9 Real-time reverse transcriptase polymerase chain reaction (qPCR)

Real-time reverse transcriptase polymerase chain reactions were performed in SYBR green PCR master mix (204141, Qiagen). Commercial primers were used for mouse expression analysis of: 18S (QT01036875, Qiagen), Sox9 (QT00163765), Aggrecan (QT00175364, Qiagen), Perlecan (QT01534141, Quiagen), Syndecan (QT01751029, Quiagen) and Versican (QT00143220, Qiagen). Designed primers used for mouse and bovine expression analysis are listed in Table 2.3.2. The real-time polymerase chain reaction was carried out under the following conditions: 2 min at 50 ºC, 10 min at 95ºC followed by 45 cycles of 15 s at 94ºC, 30 s at 60º C and 30 s at 72 ºC. Finally it was performed a melting step from 62 to 95 ºC to obtain the melting curve.

Relative gene fold variations were all determined according to the $2^{-\Delta\Delta Ct}$ method using the ribosomal unit 18S as a housekeeping gene.

**Table 2.3.2. Primers for bovine analysis**

| Gene | Molecular Weight | Catalog # |
|---|---|---|
| **18S** | F | TCGAGGCCCTGTAATTGGAA |
| | R | GCTATTGGAGCTGGAATTACCG |
| **Aggrecan** | F | CCTGAACGACAAGACCATCGA |
| | R | TGGCAAAGAAGTTGTCAGGCT |
| **Coll I** | F | AATTCCAAGGCCAAGAAGCATG |
| | R | GGTAGCCATTTCCTTGGTGGTT |
| **Coll II** | F | AAGAAGGCTCTGCTCATCCAGG |
| | R | TAGTCTTGCCCCACTTACCGGT |
| **Sox9** | F | TGGAGACTGCTGAACGAGAG |
| | R | GTACTTGTAGTCCGGGTGGTC |
| **Versican** | F | AGCTGCATGCCGCCTATG |
| | R | ATCCGTAGGTCCGGACTCCTT |

### 2.3.10 Western Blot (WB)

After the lysis of the samples with buffer for protein extraction, a quantification step was performed to determine total protein content using BCA Protein Assay kit (23225, Pierce). Acrylamide gels were prepared according to the size of the proteins, generally in concentrations of 7 or 12% (w/v). Cell lysates (5µg of each sample) were mixed with protein loading buffer containing 5% (v/v) β-mercaptoethanol, and this mix was heated at 95°C for 10 minutes. Samples and protein ladder (161-0374, Bio Rad) were run applying 150V during 1h in electrophoresis buffer (30g Tris-base (154563, Sigma), 144g Glycine (0167, Amresco) and 10g SDS (L5750, Sigma) in 1L $H_2O$). After the run, proteins were transferred to a PVDF membrane (LC 2005, Invitrogen) applying 40V during 2h at RT using transfer buffer (3.03g Tris-base, 36g Glycine, 200mL Methanol and $H_2O$ up to 1L). Then, the membrane was incubated at RT for 2h in blocking buffer (4% (w/v) non-fat powered milk in PBST). Membranes were incubated for 1h at RT with primary antibodies at a final concentration of 1µg/mL in PBST (Table 2.3.3). Then a secondary antibody IgG-HRP was added at a concentration of 1µg/mL, and incubated at RT for 1h (Table 2.3.4). Finally, the membrane was revealed for HRP detection (34080, Pierce). Chemiluminescent images were taken in the ImageQuant™ LAS 4000 mini (GE HealthCare). Images were analyzed with *ImageQuant™ Image Analysis Software 7.0*. Actin was used as an internal protein standard.

**Table 2.3.3. Primary Antibodies used for Western Blot**

| Primary Antibodies | Molecular Weight | Catalog # | Lot | Brand |
|---|---|---|---|---|
| **Actin** | 43kDa | sc-1615 | K0612 | Santa Cruz |
| **BMP4** | 50kDa (precursor)<br>23kDa (mature) | sc-6896 | B1412 | Santa Cruz |
| **Collagen 1A1** | 140-210kDa (prec)<br>70-90kDa (mature) | sc-8784 | B1211 | Santa Cruz |
| **Collagen 2A1** | 190kDa | sc-7764 | F2912 | Santa Cruz |
| **Collagen 10A1** | 66kDa | sc-323750 | K1011 | Santa Cruz |
| **Foxa2** | 52kDa | sc-6554 | | Santa Cruz |
| **Noggin** | 55kDa | sc-25656 | B2409 | Santa Cruz |
| **Runx2** | 55kDa | sc-10758 | D1411 | Santa Cruz |
| **Sox9** | 65kDa | sc-17340 | K0411 | Santa Cruz |

**Table 2.3.4. HRP-Labeled Secondary Antibodies used for Western Blot**

| Secondary Antibodies | Catalog # | Lot | Brand |
|---|---|---|---|
| **Donkey anti-Goat** | sc-2020 | F1212 | Santa Cruz |
| **Donkey anti-Rabbit** | sc-2317 | F2212 | Santa Cruz |

### 2.3.11 Glycoproteins separation using lectins

For each protein sample, 10 µl of saline solution of lectins conjugated to agarose beads (L1394, Sigma) were centrifuged for 30 seconds at 1,000*g* to pellet. Then, the supernatant was discarded and replaced by binding buffer (Tris-HCl 20mM). After that, 10 µg of each protein sample were incubated with the lectins at room temperature and agitation for 3 hours. Samples were centrifuged and the supernatant was discarded. Then samples were resuspended in protein charge buffer and boiled for 10 minutes before loading in the polyacrylamide gels.

### 2.3.12 Immunofluorescence

Cell constructs were washed with PBS and then fixed with paraformaldehyde (PFA) 1% (w/v) for 1h at RT. Samples were incubated for 2 hours in blocking buffer (BB) (20% (v/v) FBS, 0.1% (v/v) Triton x-100 solution and 1% (v/v) DMSO in PBS, filtered through 0.45µm filter). The primary antibody anti-BMP4 (sc-6896, SCBT) was prepared in BB at 1µg/mL, added to the cell construct and incubated for 1.5 hours. Subsequently, samples were washed 3 times with BB for 30 minutes and a final wash overnight at 4°C. Secondary antibody (A21084, Invitrogen) was prepared in BB at 1µg/mL, was added to the sample and incubated for 1.5 hours in dark chamber. Samples were washed 3 times with BB for 30 minutes and a final wash overnight at 4°C. Finally, samples were counterstained with DAPI to determine the location of nuclei and analyzed under fluorescence microscope (Zeiss Axiovert 200M inverted microscope with coupled ApoTome system).

### 2.3.13 Cell viability

The live/dead staining was performed to qualitatively determine proportion of live and dead cells. Cell cultures were washed 3 times with PBS and then covered with a solution 2µM of EthD-1 and Calcein AM in PBS (L3224, Invitrogen). After 15 minutes of incubation at RT in dark chamber, the solution was removed and samples were washed 3 times with PBS, after which they were analyzed under fluorescence microscope (Zeiss Axiovert 200M inverted microscope with coupled ApoTome system).

### 2.3.14 sGAG quantification

***DMMB (1,9-dimethyl-dimethylene blue) assay for sGAG quantification***

Samples were digested overnight at 60ºC with a solution of 250 ng/ml Proteinase K (03115887 001, Roche). DMMB working solution which was composed of 0.16% (w/v) DMMB (341088, Sigma), 0.24% (w/v) NaCl, 0.30% (w/v) Glycine and 10 mM HCl was prepared. Standards for chondroitin-6-sulfate from shark cartilage (27043, Sigma) with concentrations between 0 and 100 µg/ml were also prepared to get the calibration curve. In a 96-well plate, 20 µl of standards and sample supernatants, obtained as previously described, were incubated with 200 µl of DMMB working solution. Absorbance was read at 520 nm in a spectrophotometer. The calibration curve was used to calculate the amount of chondroitin-6-sulfate in each sample, and results were normalized by the total amount of DNA obtained with Hoescht dye for each sample as described below.

***Hoescht assay for DNA quantification***

Hoescht working solution was prepared from the dilution 1:1000 of a 10 mg/ml Hoescht **(861405, Sigma)** stock solution with TNE buffer (50 mM Tris–HCl (pH 7.4), 100 mM NaCl and 0.1 mM EDTA). Standards for DNA with concentrations between 0 and 10 ng/ml were prepared to get the calibration curve. In a fluorescence 96-well plate, 20 µl of standards and sample supernatants were incubated with 20 µl of Hoescht working solution. Samples were excited at 352 nm and the emission was read at 461 nm in a fluorimeter (VICTOR, Perkin Elmer). The obtained calibration curve was used to calculate the amount of DNA in each sample.

### 2.3.15 Toluidine Blue staining

Toluidine blue staining was performed to detect GAGs in the 3D cultures. Samples were washed with PBS and fixed with 2% (w/v) PFA (P6148, Sigma) in PBS for 1 hour at RT. Fixed samples were incubated with 0.05% (w/v) Toluidine Blue (T3260, Sigma) in water during 20 minutes and then washed several times with distilled water. Finally the samples were analyzed under a stereoscopic microscope (Nikon SMZ660).

### 2.3.16 Nile Red

Nile red staining was performed in order to detect intracellular lipid droplets. Cell cultures were washed with PBS, fixed with PFA 2% (w/v) for 2h. Then, samples were covered with a solution of 0.01% (w/v) Nile Red (72485, Sigma) in Dimethyl Sulfoxide (DMSO) (D5879, Sigma), and incubated for 5 minutes at RT in dark chamber. The solution was removed and the culture washed 3 times with PBS to finally observe the sample under fluorescence microscope (Zeiss Axiovert 200M inverted microscope with coupled ApoTome system).

### 2.3.17 DAPI-Phallodin staining

This staining allows the observation of the cell nuclei and cytoskeletons, thanks to the selective binding of the 4',6-Diamidino-2-phenylindole (DAPI) to the minor groove of double stranded DNA, and of phalloidin–tetramethylrhodamine B isothiocyanate to the F-actin of the cytoskeleton of cells. Cell cultures were fixed with 2%(w/v) PFA for 1h at RT, and then washed 3 times with PBS. After this, and to permeabilize the cell membrane, the cultures were incubated for 30 minutes in Triton x-100 0.1% (v/v) (X100, Sigma). Then, cell cultures were incubated in a dark chamber with 0.1% (w/v) Phalloidin (P1951, Sigma) for 25 minutes. After this, phalloidine solution was removed and 1µg/mL DAPI solution (D9542, Sigma) was added and samples were incubated for 5 minutes. Cultures were washed 3 times with PBS and then observed under fluorescence microscope (Zeiss Axiovert 200M inverted microscope with coupled ApoTome system).

### 2.3.18 Embryoid Bodies (EBs) preparation

Mouse Embryonic Stem Cells (mESCs) were cultured in 75-cm2 cell culture flasks, previously coated with 0.1% gelatin (G9391, Sigma), in Mouse Embryonic Stem Cells medium (ESCM). ESCM contained high-glucose Dulbecco's modified Eagle medium (DMEM; D5671, Sigma) supplemented with 15% (v/v) Fetal Bovine Serum (FBS) (DE14-801F, Lot: 1SB003, Lonza), 100 U/mL Penicillin / 0.1 mg/mL Streptomycin (P11-010, PAA), 4mM L-Glutamine (M11-004, PAA), 1mM Sodium Piruvate (11360-039, Gibco), 100µM Minimum Essential Medium Non-essential Amino Acid solution (M7145, Sigma), 1500 U/ml Leukemia Inhibitory Factor (LIF) (ESG1106,Millipore), 100µM β-mercaptoethanol (M3148, Sigma) and 1% nucleosides (ES-008-D, Millipore). Once expanded the cells, embryoid bodies formation was performed. Briefly, a suspension of mESC in ESCM without LIF and β-mercaptoethanol at final concentration of 100.000 cells/ml was cultured in non-adherent dishes. Cultures were maintained in the incubator at 37ºC and 5% $CO_2$. Samples were taken at various time points for their analysis by PCR and WB.

### 2.3.19 Brachyury *In situ* hybridization

MEF cultures in RAD16-I were fixed at days 7, 11 and 15. *In situ* hybridization was performed whole mount and onto 14 µm slices of the tissue-like cell mass obtained after culturing. Slices were obtained by cryosectioning of the cell-mass with Leica CM 3050 S cryostat using OCT compound (Tissue-tek®, VWR) as freezing support. The DNA probe used for the *in situ* hybridization was synthesized with the PCR DIG Probe synthesis kit (11636090910, Roche) using primers kindly provided by D. Shaywitz (Forward: CATGTACTCTTTCTTGCTGG; Reverse: GGTCTCGGGAAAGCAGTGGC). The *in situ* hybridization was performed following the company's instructions for embryos and for tissue sections. After hybridization of the DIG labeled probe, samples were immunostained for digoxigenin using anti-DIG sheep antibody (11333089001, Roche) and anti-sheep HRP-conjugated antibody (sc2473, SCBT). Reaction with DAB substrate (1718906, Roche) showed the localization of Brachyury mRNA.

### 2.3.20 Mechanical characterization

MEFs constructs were fixed with 2% (w/v) PFA during 1 hour. A compression assay with *DMA Multi-Frequency-Strain* mode and a *frequency sweep* test was applied to each sample with a DMA Q800 (TA Instruments). The conditions of the assay were: Amplitude= 1µm, Preload force= 0.001 N and Frequency= 1 Hz. Construct diameter and thickness were measured for each sample. Results were obtained with *TA Instrument Explorer* software and analyzed with *TA Universal analysis* software.

### 2.3.21 Statistics

All values were expressed as mean ± SD. Statistical differences were analyzed with GraphPad Prism 6 when samples were prepared in triplicate for the condition analyzed. When comparing two groups, unpaired student's t test was used to test for the significance level. When comparing three or more groups statistical analysis was carried out by 1-way or 2-way ANOVA, as appropriate, followed by Tukey post analysis.

## 2.4 Results

### 2.4.1 Influence of matrix properties in the spontaneous differentiation that MEFs suffer into cartilage-like tissue in the self-assembling peptide RAD16-I

Previous results from our group indicate that when primary mouse embryonic fibroblasts (MEFs) were cultured *in vitro* in the self-assembling peptide scaffold RAD16-I using the three-dimensional (3D) culture system, they acquired multipotential capacity engaging into a spontaneous process of chondrogenic differentiation [44]. In this work, we studied in more detail the aforementioned process by evaluating the influence of matrix properties (including stiffness and instruction) on the spontaneous chondrogenic differentiation.

Aiming to study the influence of mechanical properties, cultures of MEFs were prepared using 0.07% (w/v) RAD16-I which corresponded to low matrix storage modulus (G' around 0.1kPa) and 0.25% (w/v) RAD16-I which corresponded to higher values (G' around 5 kPa) as it was obtained in the dynamic mechanical analysis (DMA) of the gels (Figure 2.4.1, A). Both types of cultures were maintained for 5, 14 and 28 days and analyzed for protein and gene expression of specific chondrogenic markers. Samples were prepared in triplicate for each condition and day of culture analyzed.

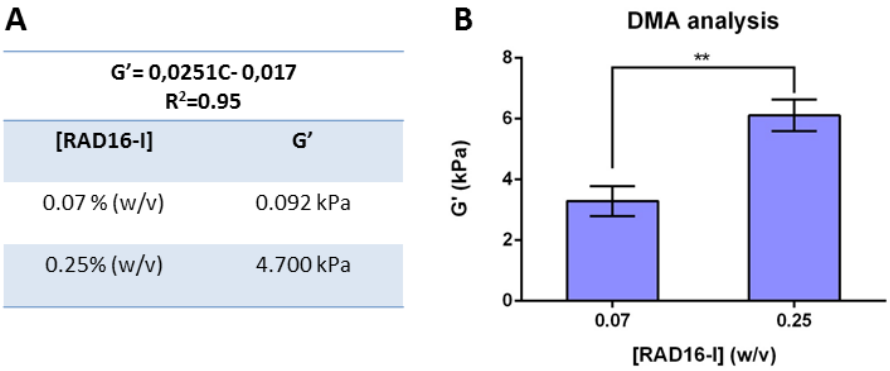


**Figure 2.4.1. DMA analysis of RAD16-I and MEFs 3D cultures.** DMA was used for the analysis of the: (A) Self-assembling peptide at different concentrations, G' was calculated as function of the peptide concentration (C, in w/v percentage) and (B) MEFs cultured for 28 days in 0.07 and 0.25% (w/v) RAD16-I. (Statistical differences are indicated as ** for $p<0.01$, Unpaired t-student, n=3)

First of all, it was observed that when MEFs were cultured at low peptide concentration (low G' values) the system underwent morphological changes caused mainly by a complex dynamical behavior including cell migration, proliferation and cell-cell network formation that ended, after a few days, with the formation of a highly contracted 3D-construct (Figure 2.4.2, A). This reduction of the construct size caused an increase in the G' as it was observed in the DMA analysis of the samples, from initial values at 0.07% (w/v) RAD16-I of 0.1 kPa to final values after 28 days of culture of around 3 kPa (30 fold increase) (Figure 2.4.1, B). Contrariwise, when MEFs were cultured at high peptide concentration (high matrix G' values) cells could not

migrate nor form cell network nor contract the construct (Figure 2.4.2, B). In this case, the initial G' value of 0.25% (w/v) RAD16-I of around 5kPa slightly increased to 6 kPa after 28 days (1.2 fold increase) (Figure 2.4.1, B).

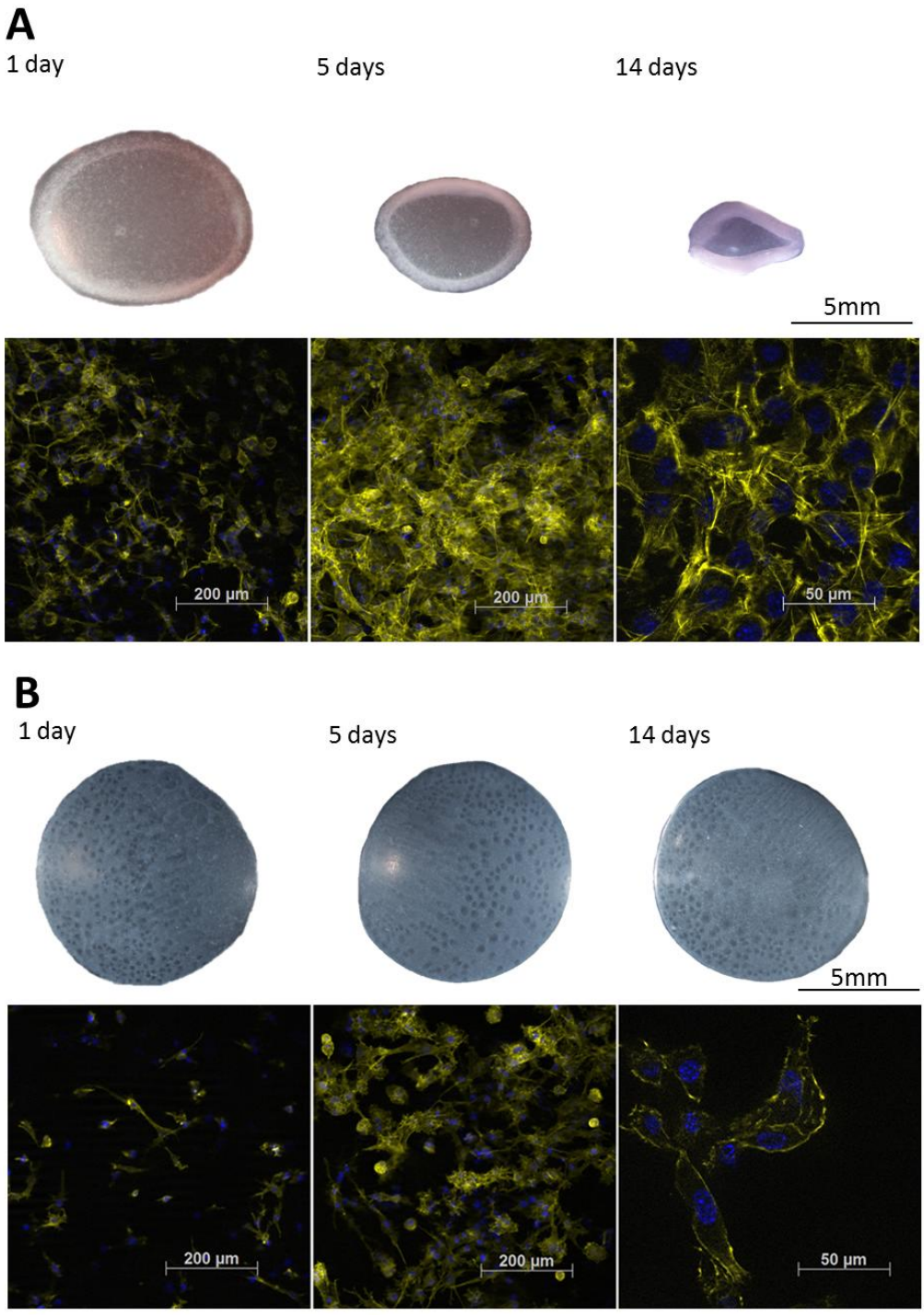


**Figure 2.4.2..MEFs cultured in self-assembling peptide scaffold RAD16-I at two peptide concentrations.** Evolution of the 3D constructs on time represented by phase contrast and DAPI-Phalloidine images at 1, 5 and 14 days of culture when MEFs were cultured in (A) 0.07% RAD16-I which corresponded to G' values around 0.1 kPa and (B) in 0.25% RAD16-I which corresponded to G' values around 5 kPa.

As expected, cell behavior radically changed depending on the initial peptide concentration (0.07 to 0.25% (w/v) RAD16-I or in other words, matrix storage modulus (G') values between 0.1 to 5 kPa. For instance, it was observed that the capacity of the cells to migrate and create cellular network was highly dependent on the initial G' value of the construct. Interestingly, the formation of the cellular network was associated with the process of a global 3D-construct contraction, which promoted the increase of several basic parameters including cell density, cell-cell contact and matrix mechanical properties.

Then, Live-Dead staining was performed to qualitatively determine the proportion of living and dead cells in the construct at both peptide concentrations. Even though some dead cells were observed, the number of living cells was much higher in both cases, which suggested that peptide concentration was not interfering in cell viability (Figure 2.4.3).

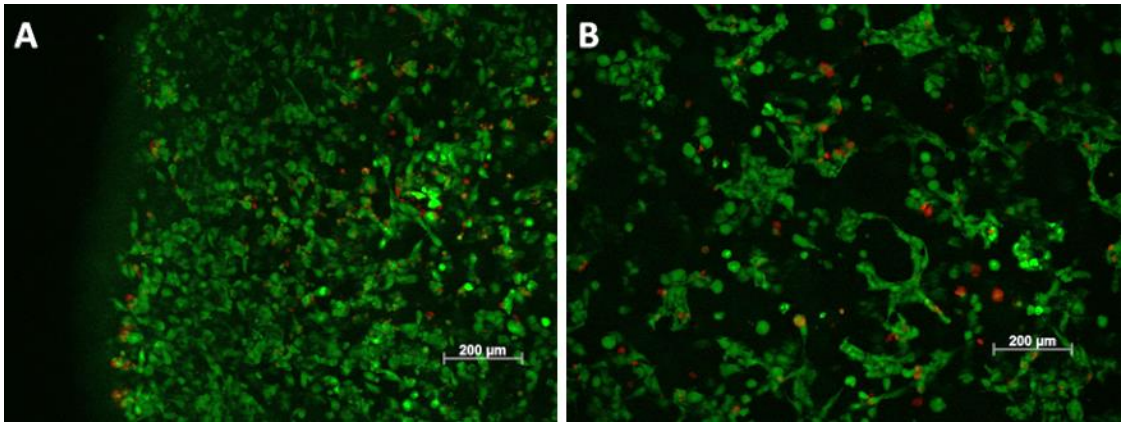


**Figure 2.4.3. Live and Dead staining of MEFs cultured in RAD16-I.** Cultures of MEFs were prepared in RAD16-I at (A) 0.07% and (B) 0.25%(w/v) RAD16-I and stained after 14 days of culture. In both cases most of the cells stained green -alive- and only few nuclei stained red –dead.

After that, the influence of matrix mechanical properties on the spontaneous chondrogenic differentiation was evaluated. Initially, the expression of Collagen type II (Coll II), one of the main components of the extracellular matrix of chondrocytes, and Collagen type I (Coll I), characteristic of MEFs extracellular matrix, was evaluated by western blot (WB) (Figure 2.4.4, A) [8]. Band quantification was performed using the software of the chemiluminescence equipment and the obtained values were first normalized to actin and then to 2D cultures used as control (Figure 2.4.4, B, C). Interestingly, when MEFs were cultured at low peptide concentration (0.07% (w/v) RAD16-I) Coll II was up-regulated over the time. However, Coll I was constantly expressed during the course of the experiment. Instead, at high peptide concentration (0.25% (w/v) RAD16-I) the trend of the expression of both collagens changed radically compared to low peptide concentration.

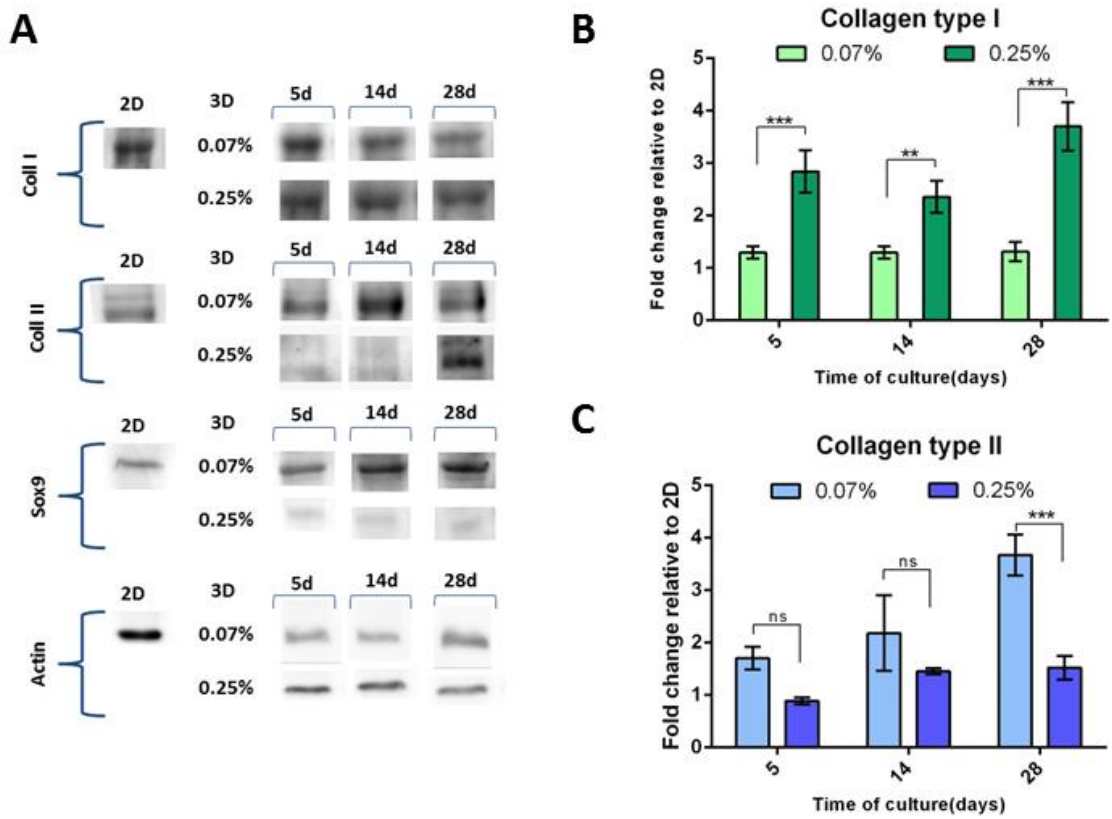


**Figure 2.4.4**. **Expression of chondrogenic markers depending on mechanical properties.** (A)WB results of chondrogenic markers when MEFs were cultured at two peptide concentrations for 5, 14 and 28 days. Actin was used as internal control. Samples were prepared in triplicate. (B) Band areas quantification from (A) normalized by Actin and relative to 2D of Collagen type I and (C) Collagen type II. (Statistical differences are indicated as:** for p<0.01, and *** for p<0.001, Two-way ANOVA, n=3).

These results could be better analyzed and interpreted after plotting the ratio Coll II/Coll I. The ratio increased over the time at low peptide concentration whereas it was very low and constant at high peptide concentration (Figure 2.4.5).

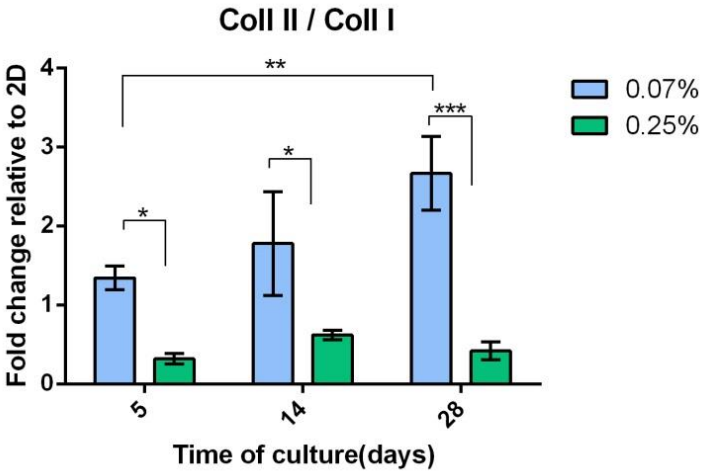


**Figure 2.4.5. Ratio Collagen type II / Collagen type I**. MEFs were cultured at two peptide concentrations for 5, 14 and 28 days and the Ratio Coll II/Coll I was calculated from western blot band areas normalized by Actin. (Statistical differences are indicated as:* for p<0.05, ** for p<0.01, and *** for p<0.001, Two-way ANOVA, n=3).

Moreover, the transcription factor Sox9, which is required for the expression of Collagen II was also analyzed by WB [8,46]. As it was expected, its expression was higher in 3D-cultures at low peptide concentration than in stiffer ones which correlated with the results obtained for Coll II (Figure 2.4.4).

In addition, the synthesis of proteoglycans (PGs) by the cells was analyzed qualitatively with Toluidine Blue staining of the constructs. This dye forms complexes with anionic glycoconjugates such as PGs [47]. Samples cultured at low peptide concentration that up-regulated the chondrogenic markers Sox9 and Coll II presented a stronger staining than the samples at high peptide concentration (Figure 2.4.6). These results clearly indicated that the initial mechanical properties of the system directly affected the chondrogenic differentiation of our system. Coincidently, our results agreed with the recently published studies where MSCs differentiate to chondrogenic lineage in two types of compliant scaffolds with similar mechanical properties as described in this work [25,32].

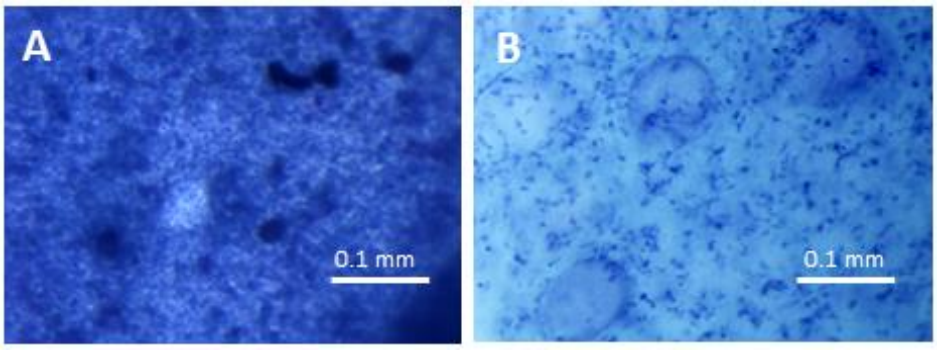


**Figure 2.4.6 Toluidine blue staining.** MEFs cultured in (A) 0.07% and (B) 0.25% RAD16-I for 28 days.

As a control, MEFs cultured in the commercial natural matrix Collagen type I were also stained with toluidine blue. Although they presented the similar cell behavior observed above for low peptide concentration cultures in RAD16-I (cell migration, dense cellular network formation and contracted structure), they stained negatively (Figure 2.4.7, A, B, C). It is important to mention that most of the cells were alive as observed in the live and dead staining (Figure 2.4.7, D).Since Collagen type I is the natural component of the skin it could indicate that this material is instructive in guiding MEFs into dermal lineages, preventing them from spontaneously undergo chondrogenesis. It is important to mention that although cell density strongly increased in both materials, it is not enough to drive the system towards a chondrogenic phenotype. This corroborates the hypothesis that only when MEFs were cultured in the self-assembling peptide scaffold RAD16-I (non-instructive scaffold) cells engaged in a default chondrogenic differentiation process, probably due by the presence of a special cell microenvironment.

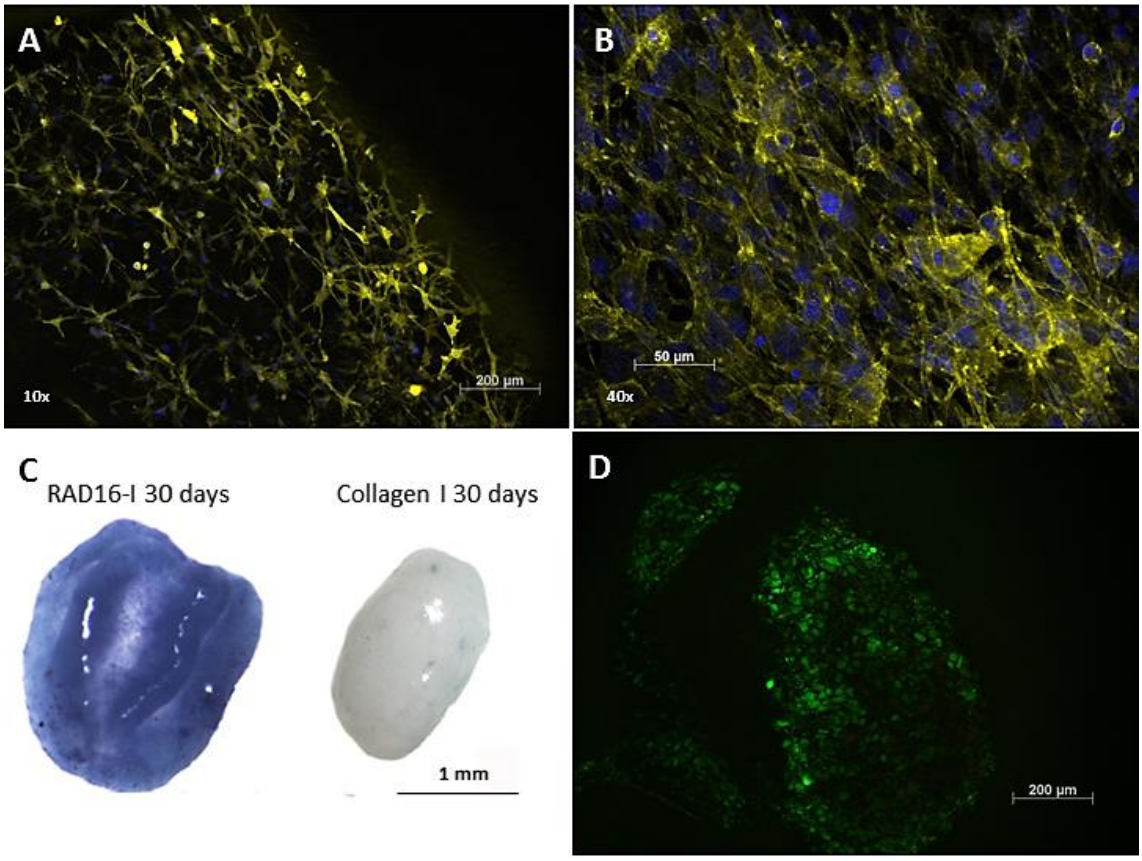


**Figure 2.4.7 MEFs cultured in collagen type I scaffold. . (**A,B)Development of celular network was observed after 1 day of culture by DAPI-Phalloidine staining.(C) Toluidine Blue staining after 30 days of culture showed a negative staining for sGAG, RAD16-I culture of MEFs was used as control. (D) Live and Dead after 28 days of culture showed the viability of the cells, almost of cells were alive (green staining).

Then, a quantitative characterization of PGs was performed with MEFs cultured in 3D at low peptide concentration due to the results obtained above for Sox9, Coll II and Toluidine Blue. Samples were cultured for 5, 10, 20, 25 and 30 days and analyzed using real time PCR for the expression of different proteoglycans (Aggrecan, Versican, Syndecan and Perlecan) and the transcription factor Sox9 [48]. It was found that the gene expression of *Aggrecan* and *Versican* was up-regulated from day 5 of culture onwards in the 3D scaffold. In contrast, *Syndecan* and *Perlecan*, which are characteristic of embryonic cartilage formation, were not expressed in the same conditions. Moreover, *Sox9* was up-regulated in the 3D cultures during the 30 days of culture as it was previously observed by WB (Figure 2.4.8, A). These results confirmed the presence of PGs as previously observed with Toluidine Blue staining. Furthermore, 1,9-dimethyl-dimethylene blue (DMMB) was used to quantify the synthesis of PGs. The technique is based on the ability of sGAG (mainly chondroitin-6-sulfate) to bind the cationic dye DMMB. Results obtained using this method were normalized with the total amount of DNA of each sample which was quantified using Hoechst 33258 [49]. As it can be observed, the total amount of sulfated GAGs was higher when MEFs were cultured in the peptide scaffold than in 2D cultures (Figure 2.4.8, B).

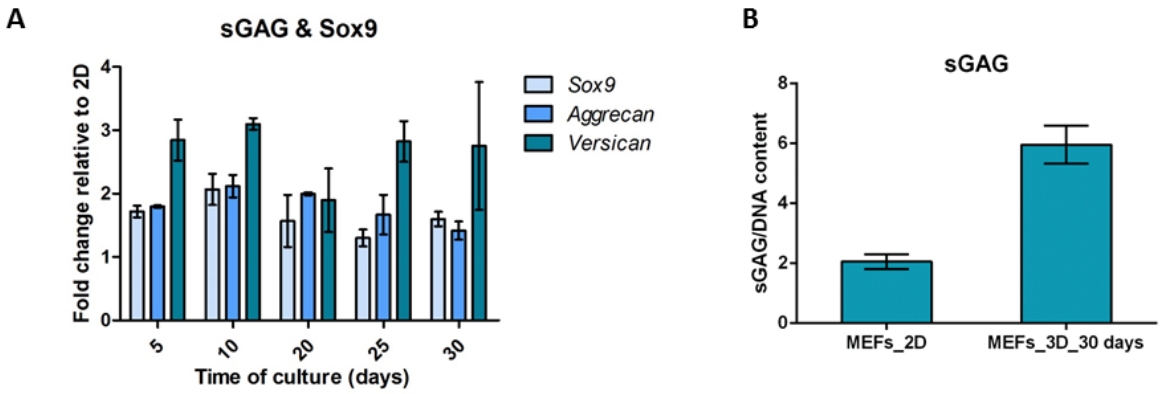


**Figure 2.4.8 . sGAG quantification in MEFs cultured at low peptide concentration**. (A) qPCR of Aggrecan, Versican and Sox9 when MEFs were cultured in 0.07% (w/v) RAD16-I scaffolds for 5, 10, 20, 25 and 30 days. Relative gene fold variations were all determined according to the $2^{-\Delta\Delta Ct}$ method using the ribosomal unit 18S as a housekeeping gene. (B) sGAG quantification using DMMB of MEFs in 2D cultures and MEFs cultured for 30 days in 0.07% (w/v) RAD16-I scaffold.

Finally, the influence of oxygen diffusion was evaluated in the described spontaneous chondrogenic differentiation. As previously mentioned, cartilage is an avascular tissue and as a consequence, oxygen concentration (ranging from 1 to 7%) is lower than in other vascularized tissues (below 20%). It has been widely described that oxygen diffusion plays an important role in chondrogenic differentiation using stem cells, where hypoxic conditions induced earlier differentiation as compared to the regular normoxic conditions [50–52]. Taking this into account, the influence of oxygen concentration was evaluated in the spontaneous chondrogenic differentiation observed in our system. The experiment designed to study this effect consisted of preparing samples of different volumes and same cell densities, and as a consequence, different oxygen requirements, which probably resulted in different oxygen concentrations (due to the mass transfer phenomena). Samples were fixed after 21 days of 3D culture and stained with toluidine blue to detect the presence of GAGs.

Interestingly, sample size had an important role in the chondrogenic differentiation: only the control samples with initial volumes of 80 µl (final diameters ~ 1,6 mm) stained positive for toluidine blue. Small samples with initial volumes of 20 and 40 µl (with final diameters ~ 0.5 and 1.0 mm), did not stain positive for toluidine blue (Figure 2.4.9). These results suggested that sample size and as a consequence, oxygen concentration played an important role in the observed spontaneous chondrogenic differentiation of MEFs in the self-assembling peptide.

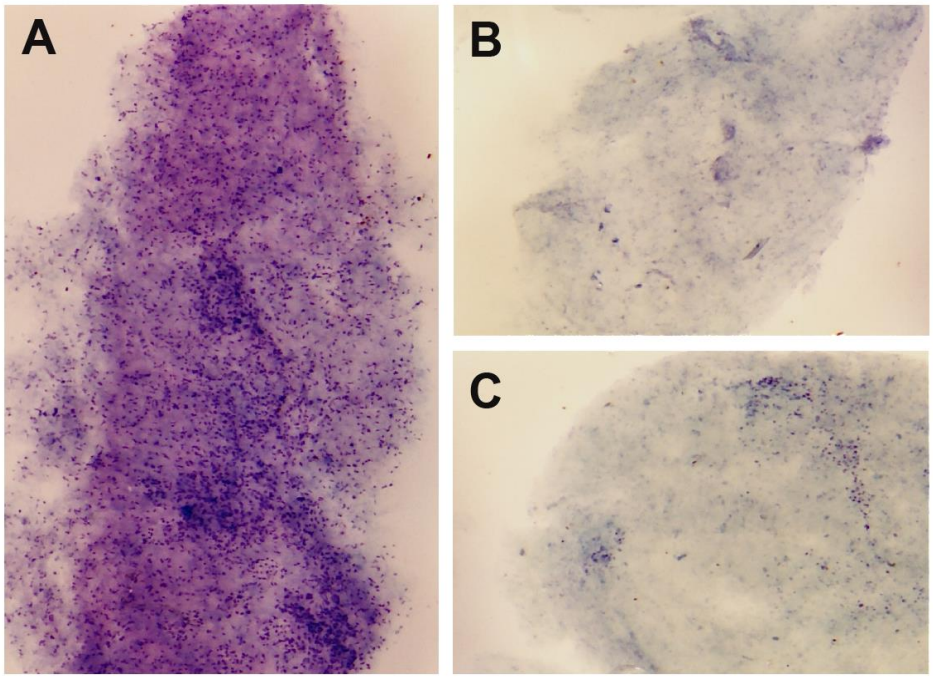


**Figure 2.4.9. Influence of contruct dimensions in chondrogenic commitment.** Toluidine Blue staining of MEFs samples with different initial volumes, (A) 80, (B) 40 and (C) 20 µl after 21 days of culture. Samples of 80 µl (regular volume) stained strongly positive as compared to the smaller volumes.

### 2.4.2 Analysis of the isolated adipogenic differentiation of MEFs in RAD16-I

As it was reported by Quintana et al., MEFs cultured in RAD16-I not only engaged spontaneously to chondrogenesis but also some cells acquired adipogenic phenotype. In order to better understand the spontaneous adipogenic differentiation of this few cells, we proceeded to study in more detail this associated process.

For this purpose, samples were prepared at the same peptide concentrations studied before (0.07 and 0.25% (w/v) RAD16-I) and analyzed for the expression of the adipogenic regulator PPARγ [53,54]. Interestingly, it was found that PPARγ was expressed in 2D cultures and the expression was maintained in the 3D cultures over the course of the experiment in both peptide concentrations (Figure 2.4.10). These results evidenced the adipogenic potential of these cells in the 2D cultures, which is maintained in the 3D constructs as well.

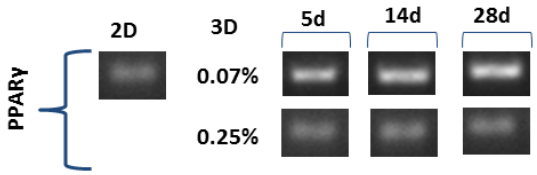


**Figure 2.4.10. Expression of the adipogenic marker PPARγ by MEFs analyzed by RT-PCR.**

Hence, the adipogenic differentiation was confirmed by staining with Nile Red, where some lipid droplets were observed occasionally at both peptide concentrations but was notable that the amount of these droplets was higher at 0.07% (w/v) RAD6-I (Figure 2.4.11).

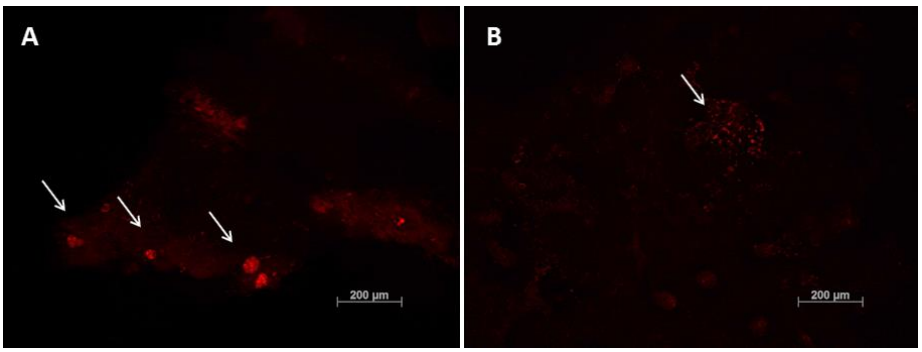


**Figure 2.4.11. Nile Red staining of MEFs cultured in in 0.07 and 0.25% (w/v) RAD16-I for 28 days.** MEFs cultured in (A) 0.07%(w/v) and (B) 0.25%(w/v) RAD16-I.

Then, the influence of the composition of the medium on the adipogenic differentiation was evaluated . For this purpose, cultures were prepared using the previously mentioned peptide concentrations (0.07% and 0.25% (w/v) RAD16-I) and cultures were maintained in culture media composed of MEM-Alpha Modification instead of DMEM, and supplemented with 2nM PDFG. The mitogenic activity of PDGF and the presence of nucleosides in the culture media promoted cell division and higher cell densities were obtained [55,56]. Surprisingly, the adipogenic commitment of these cells radically changed in the new culture conditions with much higher formation of lipid droplets in the cultures at low peptide concentrations (Figure 2.4.12, A,B) than at high ones. This is in agreement with the higher expression of PPARγ at low peptide concentration values (see Figure 2.4.10).

We speculate that, as observed in the chondrogenic differentiation, an intimate cell interaction is required to develop a tight cellular network that contracts the matrix and to start molecular events that end with differentiation processes. Although some adipogenic phenotype was observed using regular culture conditions, the differentiation was restricted to isolated cells as compared to the global spontaneous chondrogenic differentiation described in the previous section (2.4.1). However, the expression of the adipogenic regulator PPARγ in the 2D control cultures confirmed their adipogenic potential, which was evident when the culture media was supplemented with PDFG and as a consequence higher cell densities were obtained and a global adipogenic differentiation was observed. In addition, MEFs were cultured within the scaffold collage type I in order to study the influence of matrix instruction in the adipogenic commitment. Interestingly, MEFs did not commit to adipogenic lineage when cultured in collagen I (Figure 2.4.12, D). As observed in the previous section (2.4.1), this material is very instructive and could be guiding MEFs into dermal lineages, preventing them from spontaneously undergo adipogenesis.

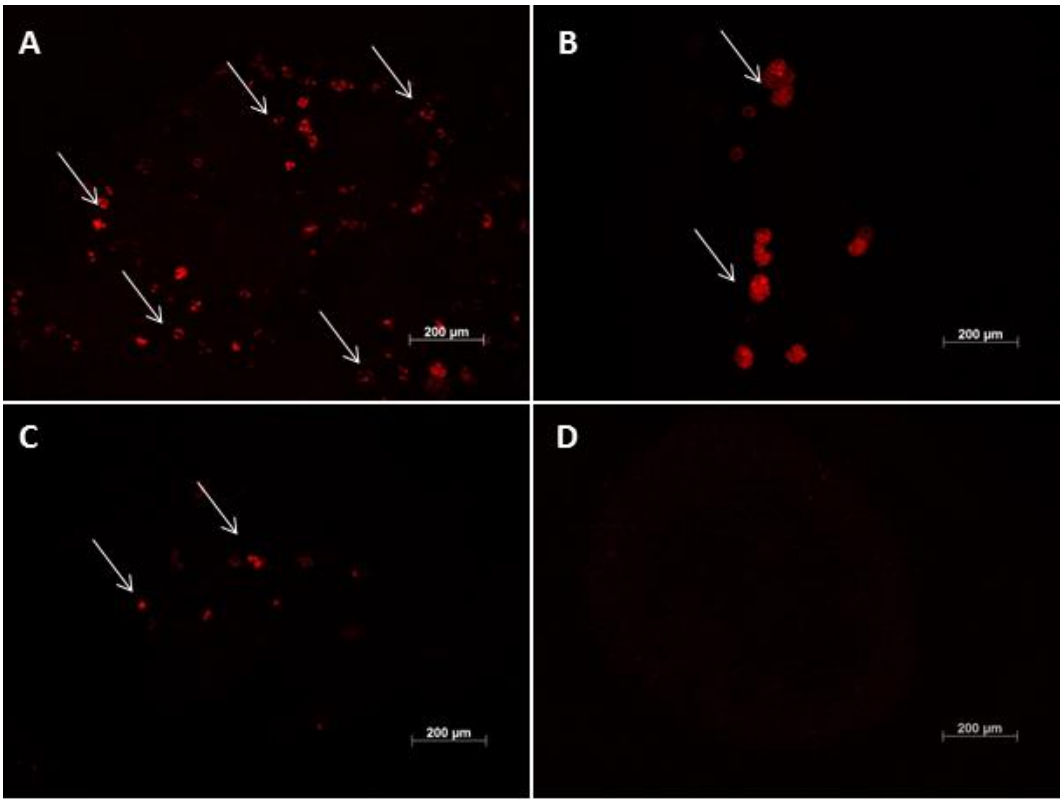


**Figure 2.4.12. Influece of media composition and matrix instruction in lipid droplets formation.** Nile red staining of MEFs cultured in (A, B) 0.07%(w/v) RAD16-I and (C) 0.25%(w/v) RAD16-I and maintained in culture media supplemented with PDGF for 28 days. (A) Represents the central part of the sample and (B) the edge of the sample were lipid droplets formation was exacerbated. (D) Nile red staining performed in MEFs cultured in collagen type I for 28 days and maintained in media supplemented with PDGF.

Remarkably, the analysis of the 2D cultures using both culture media revealed an increased formation of lipid droplets only in cultures supplemented with PDGF (Figure 2.4.13). Even though some studies report the differentiation of fibroblasts into adipogenic lineage using classical induction media, none of them used PDGF for the induction [34,38,57]. Taking this into account, this is the first description of adipogenic differentiation from MEFs with the addition of PDGF in 2D cultures, which is enhanced only under certain 3D culture conditions.

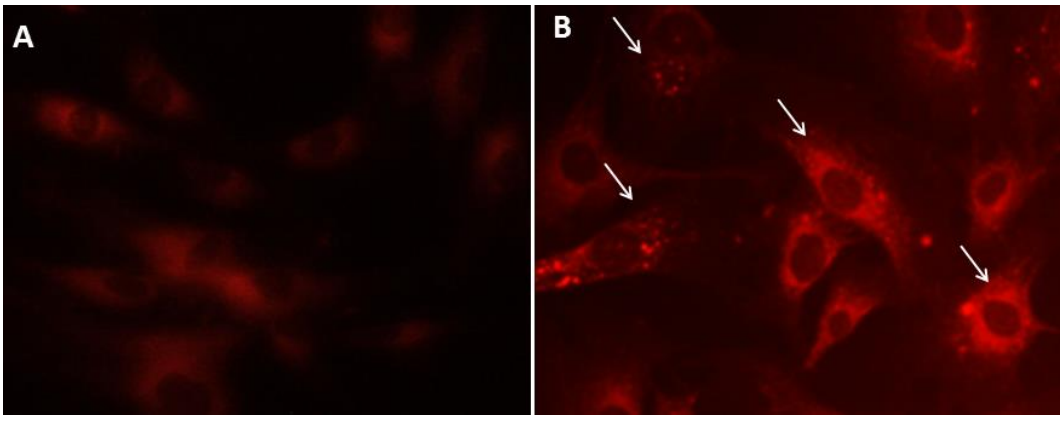


**Figure 2.4.13. Nile Red staining 2D cultures. (**A) MEFs cultured in regular FM media for 7 passages. (B) MEFs cultured in media supplemented with PFGD for 7 passages.

### 2.4.3 Characterization of the molecular mechanisms regulating the multipotential commitment of MEFs in RAD16-I

***Preparation of EBs as positive controls for genes involved in early tissue organization***

First of all, embryoid bodies (EBs) were prepared as positive controls for the genes that would be studied. ESCs were cultured onto non adherent dishes with embryonic media without Leukemia Inhibitory Factor (LIF) and then they aggregated forming EBs [58], which can differentiate into any type of cells and recapitulate some of the aspects of early embryogenesis [59]. Taking this into account, EBs were used as benchmark for the expression of genes involved in early cell differentiation (Figure 2.4.14).

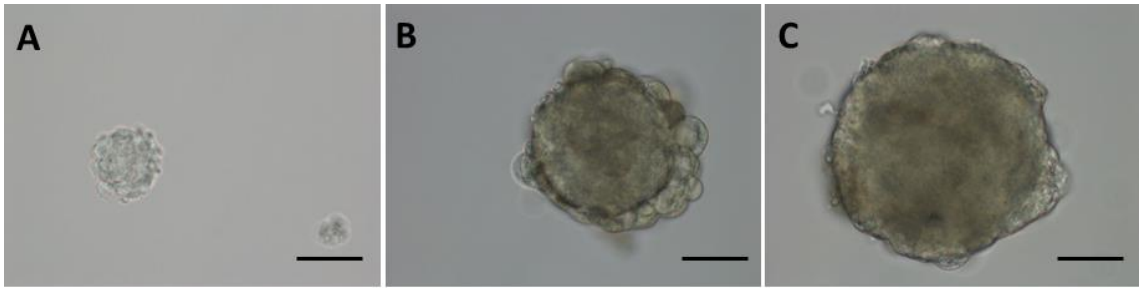


**Figure 2.4.14. Embryoid Bodies formation.** Evolution of embryoid bodies formation with the time of culture. Phase contrast image after (A)1 day, (B) 4 days and (C) 7 days of culture. (Scale bar: 100µm)

The expression of genes involved in early tissue organization was studied with PCR and WB (Figure 2.4.15). Moreover, in each WB or PCR performed, lysates of EBs were used as positive control to assure that the observed band was the correct.

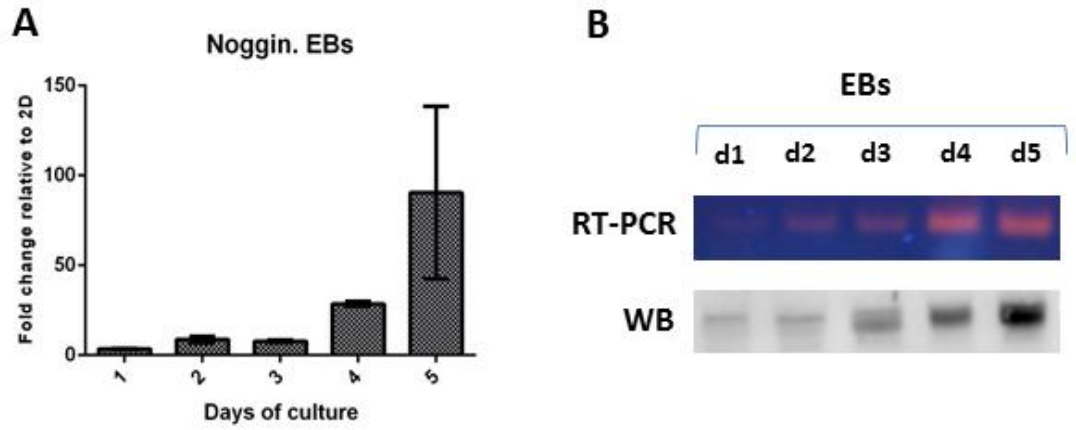


**Figure 2.4.15. Expression of early organizer genes by EBs.** EBs were prepared and cultured for 1,2,3,4 and 5 days. (A) Noggin expression quantified by qPCR. (B) Foxa2 expression qualitatively studied by RT-PCR and WB.

### *Noggin and BMP4*

In order to better understand the possible molecular mechanisms involved in the default cartilaginous commitment acquired by MEFs in the self-assembling peptide cultures, the expression of genes involved in the early events that take place in the chondrogenic process, such as *Noggin* and *BMP4*, was studied (8, 22). Cultures were prepared at 0.07 and 0.25 % (w/v) RAD16-I, maintained for 5, 14 and 28 days and analyzed for protein and gene expression. Remarkably, in the experimental system used in this work, both molecules were found in 2D cultures indicating the potentiality of these cells to differentiate into chondrogenic-like lineages. However, BMP4 expression was only maintained in 3D cultures at low peptide concentration and as a consequence low matrix G' values (~0.1 kPa) which correlated with the up-regulation of chondrogenic markers observed in section 2.4.1 (Figure 2.4.16).

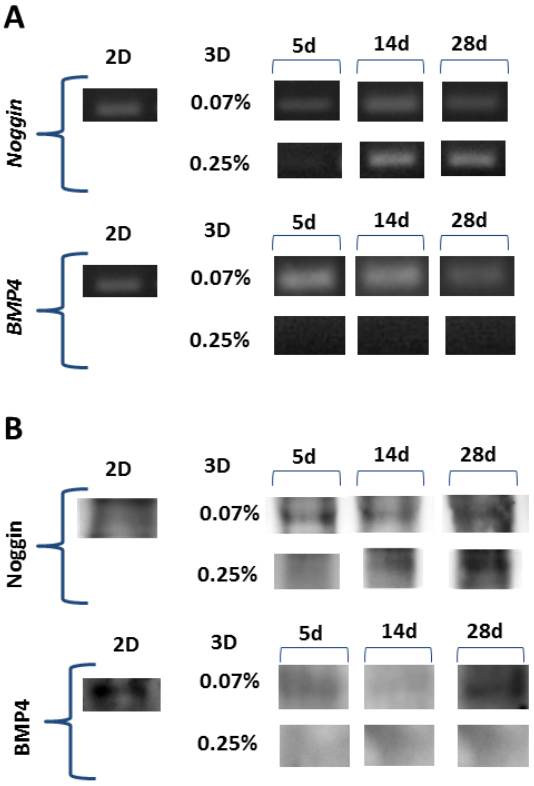


**Figure 2.4.16. Noggin and BMP4 expression by MEFs in 0.07 and 0.25% (w/v) RAD16-I scaffold.** **(**A) RT-PCR from samples cultured for 5, 14 and 28 days. (B) WB from samples cultured for 5, 14 and 28 days.

Then, Noggin expression was quantified by qPCR and it was found that at day 5 of culture, its expression was higher in cultures at low peptide concentrations than at high ones. This finding was in concordance with the results obtained with regular RT-PCR (Figure 2.4.17).

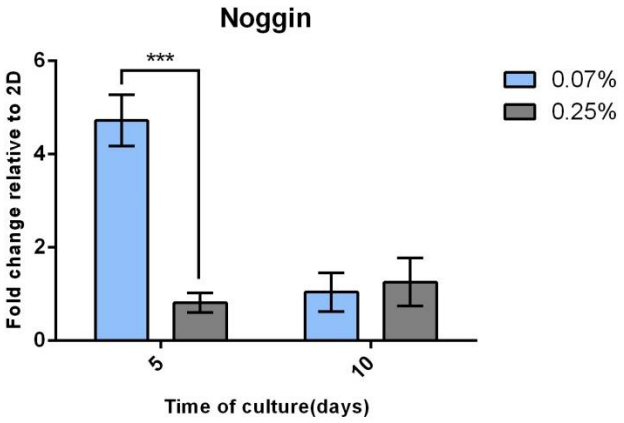


**Figure 2.4.17. *Noggin* qPCR results when MEFs were cultured in 0.07% and 0.25% (w/v) RAD16-I for 5 and 10 days.** (Statistical differences are indicated as *** for p<0.001, Two-way ANOVA, n=3)

It is important to mention, that due to the nature of BMP4 and Noggin, which are factors secreted in very low quantities, it was difficult to obtain clear WB results as compared to the results obtained with RT-PCR. In addition, the antibody anti-Noggin exhibited an unspecific binding to other proteins in the EBs lysates used as positive control and complicated the recognition of the correct WB band. Hence, taking into account that Noggin is a glycosylated protein and that lectins are capable to bind glycoproteins even in presence of various detergents, samples were treated with lectins conjugated to agarose beads in order to isolate them from the protein lysate (Figure 2.4.18, A, B). After that, samples were analyzed by WB with the purpose to elucidate the correct band. Remarkably, the results obtained when EB samples were treated with the lectins showed a unique band at 53 kDa as compared to the many bands obtained with the same sample without treatment (Figure 2.4.18, C). This test allowed us to identify the correct band for Noggin in the analysis of the MEFs 3D cultures lysates by WB.

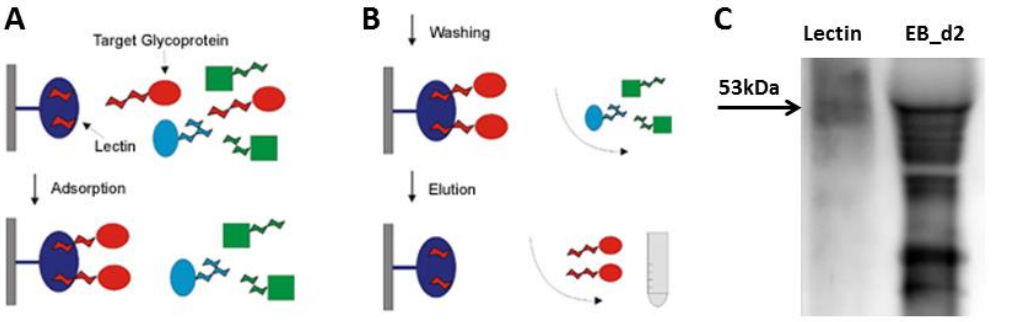


**Figure 2.4.18. EBs lysate treated with lectins for detection of Noggin by western blot**. (A,B) Schematic representation of glycoprotein purification using lectins in which is described (A) the adsorption to the lectin, (B) the washing and elution from the resin. (C) WB results of a lysate of EBs tretated with lectins (Lectin), and without treatment (EB_d2).

Surprisingly, when cultures were prepared using peptide concentrations lower than 0.07% (w/v) (0.05, 0.06% (w/v) RAD16-I) which corresponded to G' values lower than 0.1 kPa, cells presented rounded shape, developed weak cellular network and the aforementioned expression of Noggin and BMP4 was not observed (Figure 2.4.19).

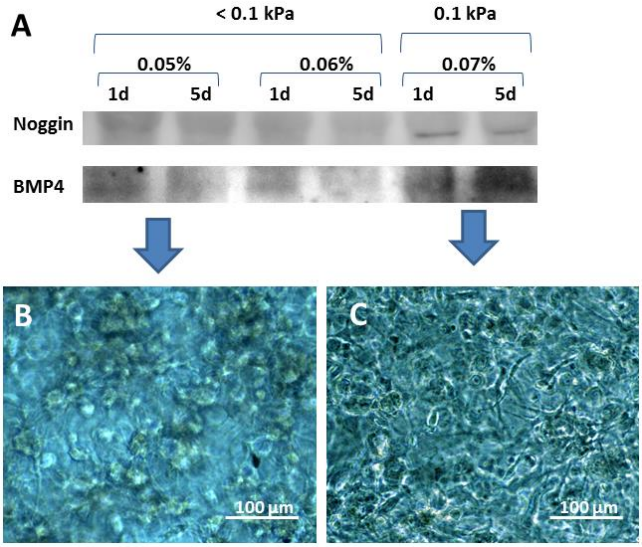


**Figure 2.4.19. Noggin and BMP4 expression when MEFs were cultured at peptide concentrations lower than 0.07% (w/v).** (A) WB results after 1 and 5 days of culture in RAD16-I. (B) Phase contrast image of the rounded cell morphology and cell network developed at 0.05% (w/v) and (C) the elongated cell morphology and denser cell network developed at 0.07% (w/v) RAD16-I.

In accordance to these results, the expression of BMP4 was confirmed by immunofluorescence staining only in cells cultured under confluent conditions in 2D. For this purpose, 2D cultures of MEFs were prepared at low cell seeding density (5.000 cells/cm$^2$) and regular cell seeding density (30.000 cells/cm$^2$), and immunostained after 2 days of culture (Figure 2.4.20). The expression of BMP4 was clearly observed only in cultures at regular seeding density and as a consequence increased cell-cell contacts.

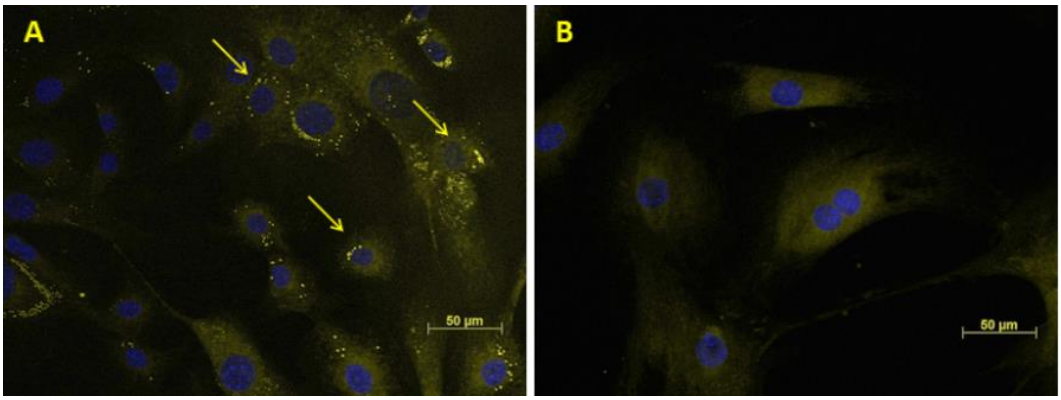


**Figure 2.4.20. BMP4 immunofluorescence of MEFs cultured in 2D cultures. (**A) High cell seeding density (30.000 cells/cm$^2$) and (B) Low cell seeding density (5.000 cells/cm$^2$).Arrows indicate BMP4 expression.

Then, immunofluorescence staining of 3D cultures showed clear localization of BMP4 only in cultures at low peptide concentrations (0.07% (w/v) RAD16-I), where it was previously described the formation of a tight cell-cell network, as compared to higher peptide concentrations (0.25% (w/v) RAD16-I) which stained negative (Figure 2.4.21).

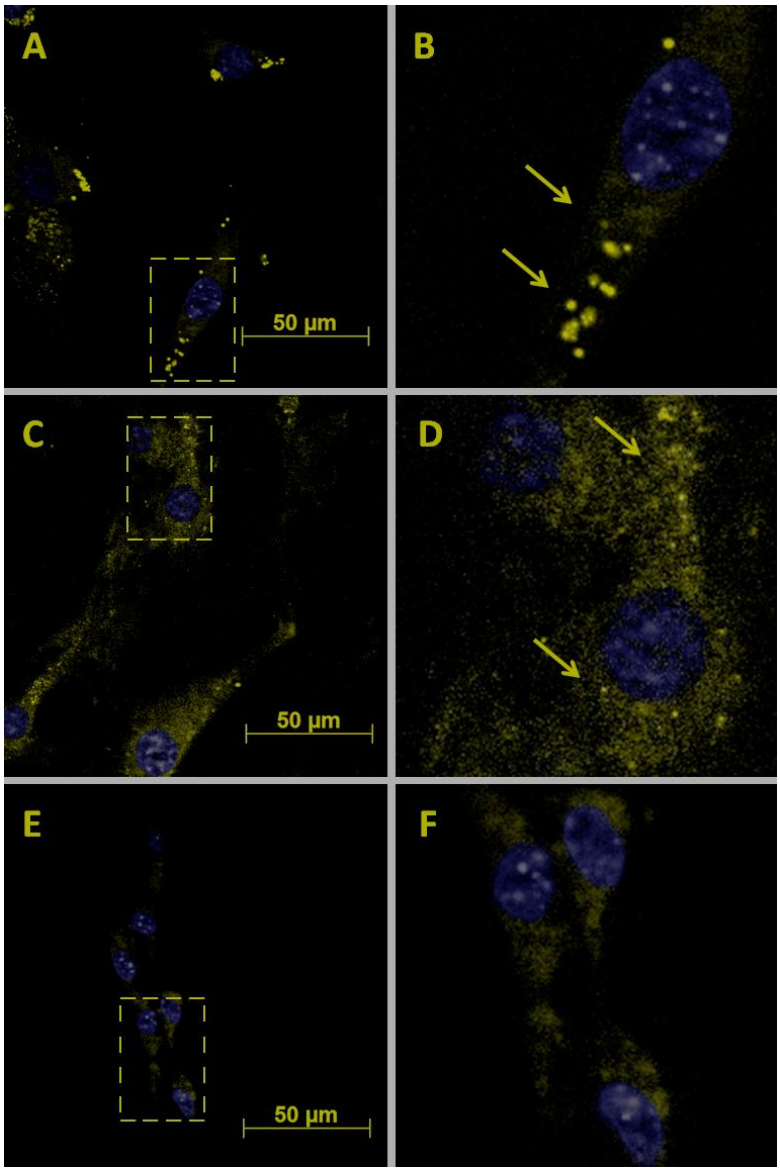


**Figure 2.4.21 BMP4 immunofluorescence of MEFs cultured in 2D- and 3D-system.** BMP4 protein was immunostained with an antibody anti-BMP4 developed with a secondary antibody Alexafluor680-congugated (yellow). Nuclei were stained with DAPI (blue). (A) MEFs cultured in 2D-sytem. (B) 3x close up of the dashed area from (A). (C) MEFs cultured at 0.07% (w/v) RAD16-I scaffold for 10 days. (D) 3x close up of the dashed area from (C). (E) MEFs cultured at 0.25% (w/v) RAD16-I scaffolds for 10 days. (F) 3x close up of the dashed area from (E).

Altogether, these results suggested that BMP4 was expressed only when cell-cell contact was present (confluent 2D cultures and low peptide concentration 3D-cultures). Thus, we speculate that intimate cell interaction is needed in order to up-regulate the expression of this chondrogenic inductor.

### *Organizers: Foxa2 and goosecoid*

In view of the results obtained with Noggin and BMP4, it was speculated that the system may be up-regulating the expression of other organizers such as Foxa2 and goosecoid.

*Foxa2* or *Hepatic Nuclear Factor 3-β (HNF-3β)* presents a dual role during embryogenesis, first as an organizer and then as an endodermal marker. Moreover, it has been recently found that its expression is induced during chondrogenesis and it is necessary for chondrocyte hypertrophy [7,23]**.** In the other hand, *goosecoid* is the first organizer gene isolated from the Spemann organizer in *Xenopus* and its expression has been detected in a wide variety of vertebrates. Both *goosecoid* and *Foxa2* are coexpressed in several regions of the early mouse embryo, suggesting the possibility of functional interactions between the two genes. Later in embryogenesis the patterns of the two genes become distinct and *goosecoid* and *HNF-3β* show complementary in the mesoderm and the endoderm respectively [22].

The expression of both organizers was analyzed by RT-PCR after 5 and 10 days of culture in 0.07% (w/v) RAD16-I. Interestingly, transcription factor Foxa2 was up-regulated only in cells cultured with media supplemented with PDGF. Instead, when cultures were maintained in regular FM its expression was not detected neither in the 2D nor 3D cultures (Figure 2.4.22). These results suggest that Foxa2 is not taking part in the regulation of the spontaneous chondrogenic differentiation process described in section 2.4.1 since PDFG was not added to the culture media. However, when the medium was supplemented with PDGF, its expression was observed in both 2D and 3D cultured of MEFs which correlates with the increase in the formation of lipid droplets observed in section 2.4.2. This relation between Foxa2 and adipogenesis is not described in the literature and as a consequence the role of the transcription factor is not clear in our system.

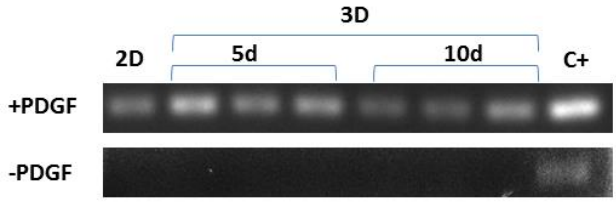


**Figure 2.4.22. Foxa2 gene expression in MEFs.** RT-PCR of MEFs cultured in 0.07%RAD16-I for 5 and 10 days. Cultures were maintained in regular FM (-PDGF) and culture media supplemented with PDFG. Embryoid bodies of 5 days were used as positive control.

Instead, the expression of goosecoid was not detected independently of the days of culture or the culture media used. These results suggested that the regulation of chondrogenesis in our system is not regulated by part of the organizers genes. Thus, Noggin and BMP4 may be acting as chondrogenic regulators and not as organizers.

### *Mesodermal marker: Brachyury*

To provide more insight into the possible patterned chondrogenesis, the expression of brachyury, one of the first mesodermal-specific transcription factors that are expressed in the early mesoderm, was also studied. Interestingly, *in situ* hybridization with a *Brachyury* probe showed that after seven days of culture, cells residing in the external layer of the 3D culture expressed the transcription factor. Then, the surface staining migrated inwards the structure during the next days (11 days. We speculate that cells originally labeled at the surface moved inwards leaving the surface with unlabeled cells (Figure 2.4.23). After the process (15 days), the structure ended with a surface layer negative for *Brachyury* and an internal mass of cells positively stained for *Brachyury*

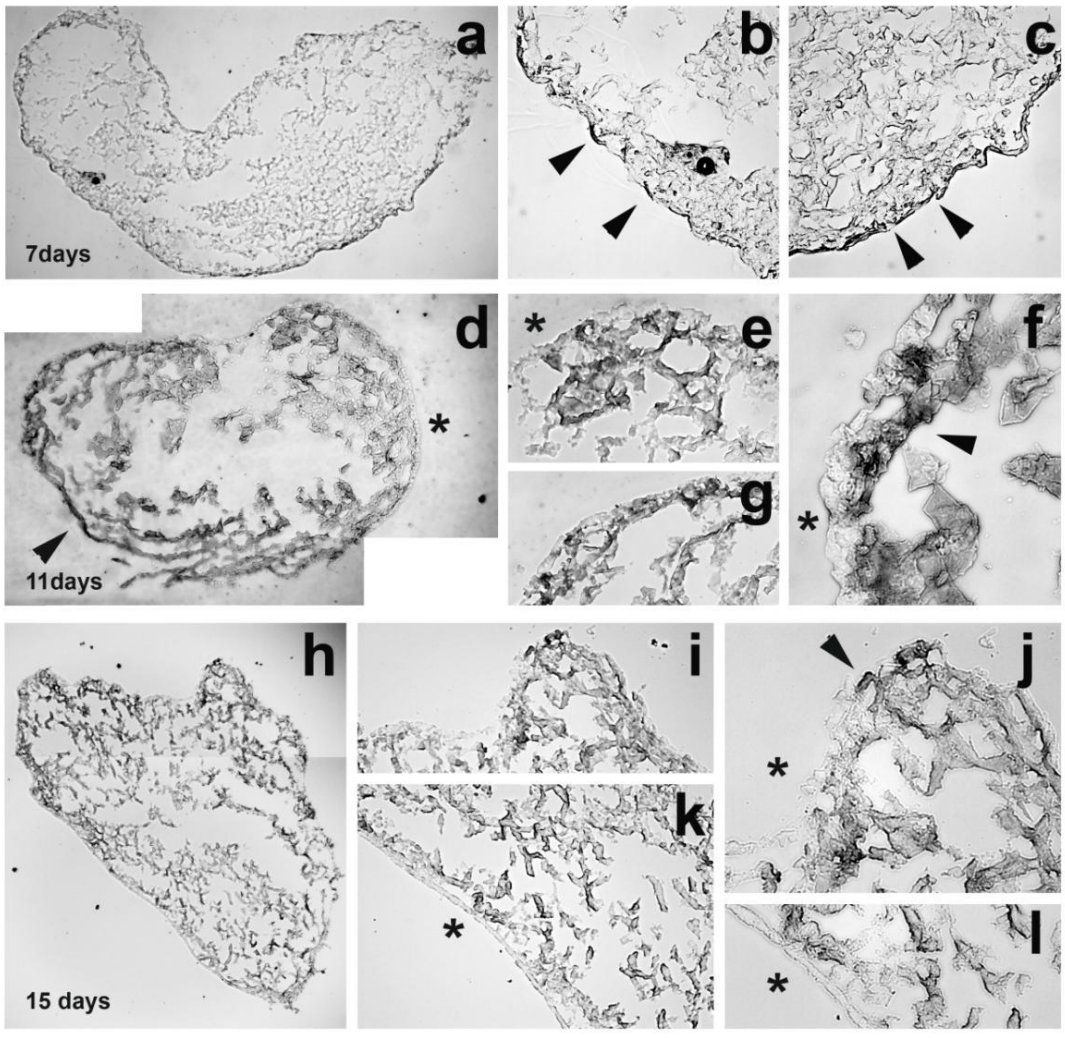


**Figure 2.4.23 *Brachyury in situ* hybridization of mouse embryonic fibroblasts (MEF) 3D structures of different culture times.** At seven days, positive staining is detected at the surface of the structure in (Panels a-c). At 11 days, positive stained cells are localized in a most internal position of the structure, suggesting that they have migrated inward, leaving behind negative cells at the surface (Panels d-g). Finally, at 15 days of culture, all positive stained cells are localized internally (Panels h-l). Black asterisks indicate the closing up regions. Black arrows indicate cells stained positive for *brachyury.*

These results are in concordance with the findings that Brachyury is required not only for patterning but also contributing to the determination of the chondrogenic lineage since forced expression of Brachyury in MSCs is sufficient to initiate chondrogenic development bot *in vitro* and *in vivo* [60].

### *iPSCs transcription factors*

Finally, in view of the results obtained for the spontaneous processes of chondrogenic and adipogenic differentiation, it was speculated that MEFs were undergoing early stage reprogramming in the self-assembling peptide RAD16-I. As it was described by Yamanaka, pluripotent stem cells can be directly generated from fibroblast cultures by the addition of only a few defined factors: c-Myc, Klf4, Oct3/4 and Sox2 [43]. We wondered whether MEFs in the 3D culture system in the self-assembling peptide expressed these factors. For this purpose, cultures were prepared at 0.07% (w/v) RAD16-I and samples were taken at different times of culture and analyzed for the expression of the four transcription factors to show at which specific multipotent state the cells were when cultured in 3D compared to designed iPSCs.

As it was described by Yamanaka, RT-PCR results showed a basal expression of c-Myc and Kfl4 in the 2D cultures of MEFs [43]. Interestingly, only the expression of c-Myc was maintained in 3D cultures. A weak expression of Klf4 was observed after 5 days of 3D culture but it was totally down-regulated over the time. However, the expression of the two factors, Oct3/4 and Sox2, mainly involved in maintenance of pluripotency was not detected (Figure 2.4.24, A). Then, qPCR was used to analyze the expression of the transcription factors during the first 48 hours of culture in the self-assembling peptide. Interestingly, the down-regulation of Kfl4 was observed from the first 6 hours in the 3D culture onwards (Figure 2.4.24, B).

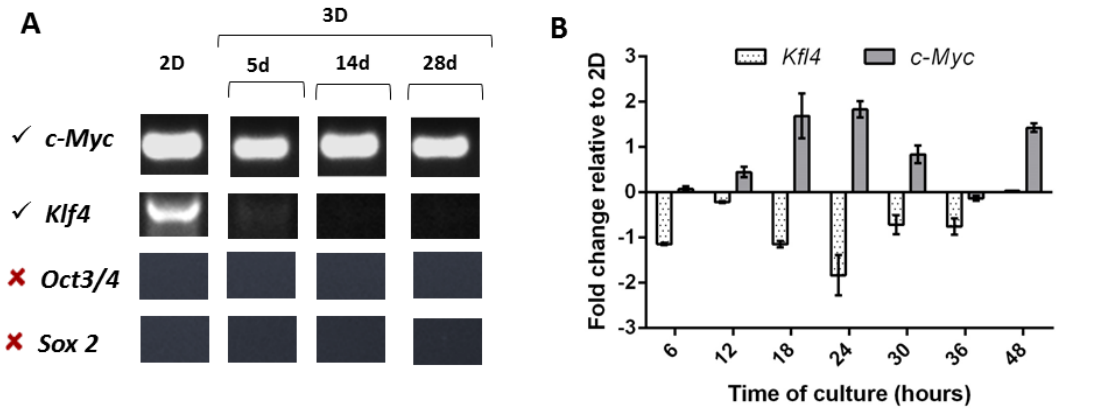


**Figure 2.4.24. Expression of transcription factors characteristics of iPSCs. (**A) RT-PCR of MEFs cultured for 5,14 and 28 days in 0.07% RAD16-I, MEFs 2D were used as control. (B) qPCR of *Kfl4* and *c-Myc* of MEFs cultured in 0.07% RAD16-I for hours, samples were taken every 6 hours. Relative gene fold variations were all determined according to the $2^{-\Delta\Delta Ct}$ method using the ribosomal unit 18S as a housekeeping gene.

### 2.4.4 Evaluation of the self-assembling peptide RAD16-I as a support scaffold for chondrogenic differentiation using dedifferentiated bovine chondrocytes.

Although chondrocytes should be the first choice when using cells for cartilage tissue engineering, their main drawback is the limited cell number obtained. As it was described in Chapter 1, expansion in cell monolayer causes their dedifferentiation, which is characterized by decreased production of cartilage specific ECM (mainly proteoglycans (PGs) and collagen type II) [61]. As chondrocytes attach to a flat surface, they spread and acquire fibroblast-like morphologies, which is accompanied by an increase in proliferation and an altered phenotype [62]. There are different ways to overcome this issue and slow the dedifferentiation: supplement culture media with growth factors [63,64] , vary cell seeding density or hypoxic conditions [65,66]. Remarkably, other studies reported the redifferentiation of dedifferentiated articular chondrocytes using high density 3D cultures in a variety of materials such as agarose [67], alginate beads [68–70], fibrin glue [71] or compressing cells into pellets [72,73].

According to what has been previously observed, MEFs spontaneously commit to chondrogenic lineage when cultured in the self-assembling peptide RAD16-I under certain mechanical conditions; together with the limited expansion of chondrocytes *in vitro* due to the loss of chondrogenic and acquirement of fibroblastic phenotype, it was hypothesized that the culture of dedifferentiated chondrocytes in the peptidic matrix could favor their redifferentiation to a chondrogenic phenotype.

For this purpose, fresh chondrocytes were extracted from femoral plates of 2 weeks old calves as described in Materials and Methods section 2.3.2 [74]. Then, chondrocytes were expanded and dedifferentiated using low density seeding of 8.000 cells/cm$^2$ for 5 passages as previously described [75]. In order to assess their dedifferentiation, cultures were analyzed after each passage using qPCR for the expression of the chondrogenic markers: Aggregan, Versican, Sox9 and Collagen type I and II. As expected, down-regulation of the proteoglycans Aggrecan and Versican was observed over the course of the experiment (Figure 2.4.25, A). Moreover, the expression of collagen types I and II, and Sox9 was also down-regulated, which evidenced the dedifferentiation of the chondrocytes during the *in vitro* expansion (Figure 2.4.25, B).

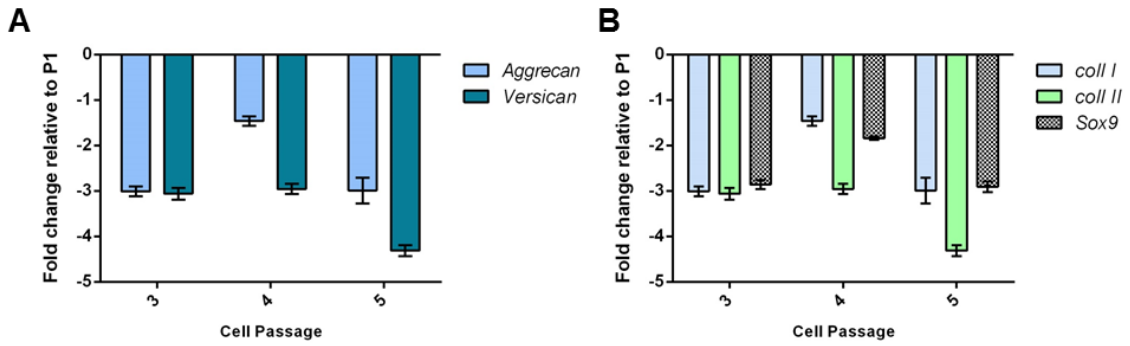


**Figure 2.4.25. Chondrocytes dediffentiation during expansion in 2D.** qPCR was performed to quantify the expression of chondrogenic markers by chondrocytes after each passage *in vitro*. (A) Proteoglycans quantification (Aggrecan and Versican), (B) collagen type I and II and Sox9. Relative gene fold variations were all determined according to the $2^{-\Delta\Delta Ct}$ method using the ribosomal unit 18S as a housekeeping gene. Results were relative to chondrocytes after passage 1 (P1).

Once dedifferentiation was reached, cells were encapsulated in the self-assembling peptide RAD16-I following the 3D culture technique previously performed with MEFs at a final peptide concentration of 0.10% (w/v). First of all, similar behavior to MEFs cultured at low peptide concentration was observed in terms of cell migration, cell network development and matrix contraction (Figure 2.4.26).

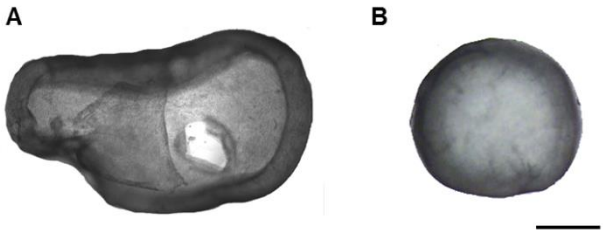


**Figure 2.4.26. Dedifferentiated chondrocytes behavior in RAD16-I 3D cultures.** Phase contrast image after (A) 5 days and (B) 30 days of culture. (Scale bar = 1mm)

Then, samples were cultured for 5, 10, 20, 25 and 30 days and analyzed using real time PCR for the expression of proteoglycans (Aggrecan and Versican), the transcription factor Sox9 and collagens type I and II [48]. Remarkably, a recovery in the expression of all the genes analyzed was found in 3D compared to control 2D cultures (cells harvested just before the encapsulation in the peptidic matrix) (Figure 2.4.27). However, if we look at the expression of collagen type I, characteristic of fibroblastic phenotype, a marked up-regulation was observed reaching levels of expression higher than collagen type II, characteristic of chondrogenic phenotype. It is important to mention that 3D cultures were maintained in FM, and as a consequence without chondrogenic inductors. Therefore, the expression of chondrogenic markers seemed to recover and it was only influenced by the 3D culture environment as it was previously observed with MEFs.

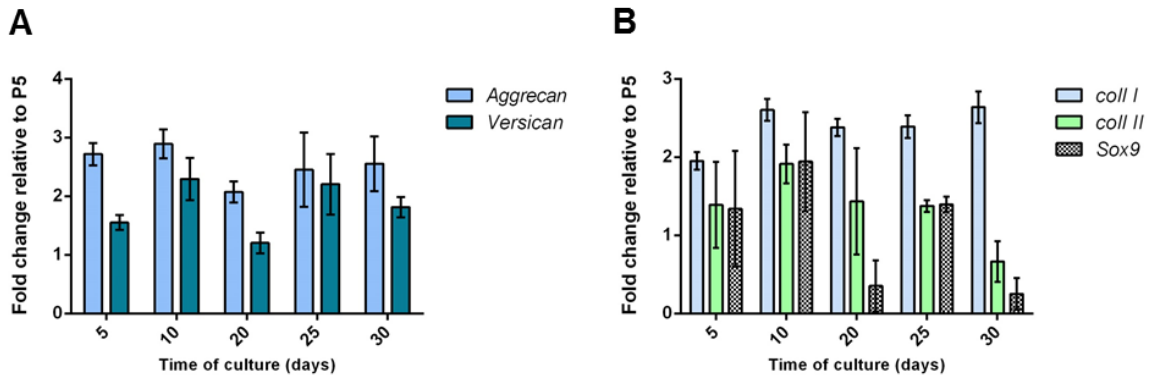


**Figure 2.4.27. Chondrocytes redifferentiation**. qPCR was performed to quantify the expression of chondrogenic markers by chondrocytes after each passage *in vitro*. (A) Proteoglycans quantification (Aggrecan and Versican), (B) collagen type I and II and Sox9. Relative gene fold variations were all determined according to the $2^{-\Delta\Delta Ct}$ method using the ribosomal unit 18S as a housekeeping gene. Results were relative to chondrocytes before encapsulation in RAD16-I (P5).

Finally, PGs synthesis was analyzed qualitatively by Toluidine Blue staining which showed the presence of proteoglycans after 30 days of culture in the peptidic matrix (Figure 2.4.28, A). However, the staining was weaker than MEFs in section 2.4.1. Then, PGs synthesis was analyzed quantitatively using DMMB and the obtained results were normalized with the total amount of DNA. Interestingly, a clear increase in the synthesis of proteoglycans was observed after 30 days of culture in the RAD16-I compared to control 2D cultures before the encapsulation in the peptidic matrix (Figure 2.4.28, B). These results corroborated the previous analysis of PGs expression obtained by qPCR.

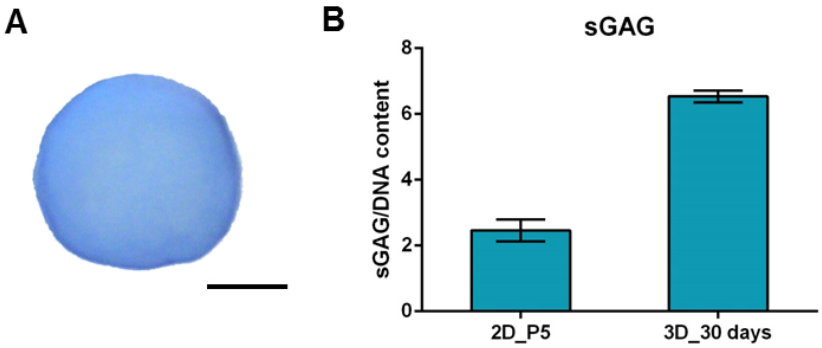


**Figure 2.4.28. sGAG characterization after 30 days of culture in RAD16-I.** (A) Toluidine Blue staining. Scale bar= 1mm; (B) sGAG quantification using DMMB of dedifferentiated chondrocytes in 2D cultures before encapsulation in RAD16-I and after 30 days of culture in RAD16-I.

## 2.5 Discussion

In view of the multipotential capacity that MEFs acquired when embedded in the self-assembling peptide RAD16-I [44]; the possible mechanisms that modulate the spontaneous multipotent commitment of these cells were studied. Our main hypothesis was that early organizer genes may be involved in the initial steps of the chondrogenic process and their expression could be regulated by the mechanical properties of the scaffold matrix. Thus, our initial assays were focused on evaluating the influence of matrix properties in the spontaneous chondrogenic differentiation that MEFs suffered in the self-assembling peptide RAD16-I.

Nowadays, an increasingly number of studies demonstrate that cell morphology and function strongly depend on substrate mechanical properties [25,27–29,32,33]. Hence, the results presented in this chapter suggested that the spontaneous chondrogenic-like differentiation that MEFs suffered when cultured in RAD16-I peptide scaffold was influenced by matrix mechanical properties. Indeed, cells only created tight cell-cell networks and up-regulated the expression of the chondrogenic markers Coll II, Sox9 and PGs under certain mechanical conditions. Coincidently, our results agree with the recently published studies where MSCs differentiate toward the chondrongenic lineage in two types of compliant scaffolds with similar mechanical properties as described in this work [25,32,33]. Then, it was observed that the instructive capacity of the material was also playing a crucial role in our system. Indeed, collagen type I cultures of MEFs stained negative for PGs. These results suggested that the biomechanical and non-instructive properties of the self-assembling peptide environment might have a key role in the process [44]. Finally, the size of the construct (which affects directly biophysical parameters) was an interesting and unexpected key factor in the spontaneous chondrogenic differentiation. Certainly, this parameter could reduce the local oxygen pressure and as a consequence it would be necessary a threshold sample volume in order to engage in the differentiation process. These results are in concordance with published studies of chondrogenic differentiation using stem cells in which hypoxic conditions favored the differentiation to the chondrogenic lineage [50,51,73,76]. Nevertheless, when the chondrogenic potential of human normal dermal fibroblasts (hNDFs) in RAD16-I was evaluated in our laboratory (data not presented in this work), the chondrogenic differentiation was only obtained by chemical induction [77]. It is important to mention that hNDFs are adult cells and their differentiation potential is not necessarily the same than MEFs. However, that study provided proof of concept that hNDFs in self-assembling peptide RAD16-I gel have the potential to differentiate into the chondrogenic lineage under induction medium.

Similar results were obtained when the isolated adipogenic differentiation was analyzed in the MEFs 3D-cultures. As observed in the chondrogenic differentiation, MEFs did not commit to the adipogenic lineage when cultured in collagen type I. Moreover, an intimate cell interaction

was required to develop a tight cellular network that contracted the matrix and to start molecular events that ended with differentiation processes.

Afterwards, the molecular mechanisms regulating the multipotent commitment of MEFs in the self-assembling peptide RAD16-I were characterized. Interestingly, the balance between the chondrogenic inductor BMP4 and its antagonist Noggin played a critical role in the observed chondrogenic differentiation of MEFs cultured in RAD16-I. Thus, the chondrogenic inductor BMP4 was only expressed under mechanical conditions where the spontaneous chondrogenic differentiation was observed. At that point, its antagonist Noggin was also up-regulated. In a similar way, *in vivo* studies demonstrated that Noggin is expressed in condensing cartilage and immature chondrocytes, like many BMPs, having an important role in the regulation of chondrocyte proliferation and differentiation [11–14]. As a consequence, these results suggest that the spontaneous chondrogenic fate of the system, which is feasible only under certain mechanical conditions, could be based on its capacity to self-modulate the expression pattern of molecules such as BMP, Noggin and other possible factors implicated in chondrogenesis.

Regarding to the transcription factors characteristics of iPSCs, only the expression of c-Myc and Klf4 was detected in the 3D cultures. These results confirmed that MEFs cultured in the self-assembling peptide were not reprogramming to a pluripotent stage. Besides, this is in agreement with previous results from our laboratory where MEFs combined with RAD16-I were implanted in mice and they had an excellent performance in terms of viability and local proliferation. Remarkably, they did not migrate out of the scaffold or form teratomas, which is one of the properties of pluripotent stem cells [78].

Summarizing, MEFs in the self-assembling peptide RAD16-I did not acquire pluripotency but showed a potential mesodermal lineage commitment evidenced by the expression of early markers such as Brachyury, BMP4, Noggin or PPAR. As a consequence of this commitment, only under certain culture conditions, MEFs acquired the capacity to differentiate into chondrogenic and adipogenic lineages.

Up to now, few studies reported the commitment and differentiation of MEFs into the mesenchymal lineage: differentiation into adipocytes [57], osteoblastic cells [45] or chondrogenic lineage [79]. Interestingly, in all cases the addition of induction media was necessary to obtain the desired differentiation. Instead, chondrogenic and adipogenic differentiation of MEFs was observed in our system without the need of supplements in the culture media. These results suggested that culture conditions in the self-assembling peptide provided a unique environment in which MEFs could be acquiring a multipotent state, from which they could give rise to most of the cell types of mesodermal germ lineages [44,45]. The multipotent commitment of these cells

could be explained with the recently published study of Saeed and coworkers [41]. They reported that MEFs were not distinguishable from Bone Marrow Stem Cells (BMSCs) based on typical BMSCs CD surface marker expression. In addition, they confirmed that MEFs contain a subpopulation of stem cells that behave in *ex vivo* and *in vivo* assays similar but not identical to MSC derived from bone marrow [41]. Thus, it is not clear whether the observed cell behavior is due to transdifferentiation of committed fibroblasts or to differentiation of resident stem cells.

Finally, it was hypothesized that RAD16-I scaffold could support the chondrogenic differentiation of other cell types. In order to test this hypothesis, the use of the self-assembling peptide RAD16-I as a support scaffold for chondrogenic differentiation using dedifferentiated bovine chondrocytes was evaluated. As mentioned before, several studies reported the redifferentiation of dedifferentiated articular chondrocytes using high density 3D cultures in a variety of materials such as agarose [67], alginate beads [68–70], fibrin glue [71] or compressing cells into pellets [72,73]. In our system, bovine dedifferentiated chondrocytes appeared to have a similar cellular behavior to MEFs embedded in the self-assembling peptide RAD16-I. Briefly, the material allowed the development of a tight cell network that culminated with the contraction of the structure in a few days. We hypothesized that these intimate cell-cell interactions reactivated the expression of molecular regulators that started the chondrogenic differentiation process as observed in MEFs. Interestingly, some recovery was observed in the expression of PGs by the dedifferentiated chondrocytes, which evidenced the potentiality of this scaffold for its use in cartilage tissue engineering applications. However, this recovery was not enough to acquire full chondrogenic properties as it was observed in the Collagen type I expression.

Altogether, it was speculated that the combination of the self-assembling peptide RAD16-I with chondrogenic inductors could promote an enhanced redifferentiation of dedifferentiatied chondrocytes. Future avenues of research would include the dedifferentiation and redifferentiation of human chondrocytes. The way we envision a future clinical application of our technology would consist in obtaining small cartilage constructs which could be used as building blocks to fill the cartilage defect of the patient and bonded with another carrier scaffold. This strategy has the advantage that cartilage defect shape and size are not a drawback.

## 2.6 Concluding Remarks

- MEFs cultured under certain biomechanical conditions (G' around 0.1 kPa), were able to develop a rich interconnected cellular network which promoted increase of several basic parameters including cell density, cell-cell contact and matrix storage modulus. This process created a unique environment, which favored the system to engage in a spontaneous chondrogenesis differentiation evidenced by the expression of the chondrogenic markers Sox9, Coll II and proteoglycans.

- MEFs developed an isolated spontaneous adipogenic differentiation in RAD16-I which was favored by the formation of a tight cell network. Interestingly, it was described for the first time the adipogenic differentiation of MEFs in 2D and 3D cultures by the addition of the growth factor PDGF to the culture media.

- Matrix instruction played an important role in the multipotent commitment acquired by MEF in the self-assembling peptide RAD16-I since cultures in collagen type I did not engage neither in the spontaneous chondrogenic nor adipogenic differentiation.

- The balance Noggin/BMP4 was found to play a critical role in the observed chondrogenic differentiation of MEFs cultured in RAD16-I. Remarkably, the chondrogenic inductor BMP4 was only expressed under mechanical conditions where the spontaneous chondrogenic differentiation was observed.

- The observed spontaneous chondrogenic differentiation of MEFs in the self-assembling peptide together with the partial redifferentiation of dedifferenitiated bovine chondrocytes evidenced the potential of this scaffold for its use in cartilage tissue engineering applications.

## 2.7 References


1. Brittberg, M. & Lindahl, A. in *Tissue Eng.* (Blitterswijk, C. van et al.) 533–557 (Elsevier Inc., 2008).

2. Vinatier, C., Mrugala, D., Jorgensen, C., Guicheux, J. & Noël, D. Cartilage engineering: a crucial combination of cells, biomaterials and biofactors. *Trends Biotechnol.* **27,** 307–14 (2009).

3. Quintana, L., zur Nieden, N. I. & Semino, C. E. Morphogenetic and Regulatory Mechanisms During Developmental Chondrogenesis : *Tissue Eng Part B* **15,** 29–41 (2009).

4. Hall, B. K. & Miyake, T. Divide, accumulate, differentiate: cell condensation in skeletal development revisited. *Int. J. Dev. Biol.* **39,** 881–93 (1995).

5. DeLise, a M., Fischer, L. & Tuan, R. S. Cellular interactions and signaling in cartilage development. *Osteoarthritis Cartilage* **8,** 309–34 (2000).

6. Heinegård, D. & Saxne, T. The role of the cartilage matrix in osteoarthritis. *Nat. Rev. Rheumatol.* **7,** 50–6 (2011).

7. Long, F. & Ornitz, D. M. Development of the endochondral skeleton. *Cold Spring Harb. Perspect. Biol.* **5,** 1–20 (2013).

8. Goldring, M. B., Tsuchimochi, K. & Ijiri, K. The control of chondrogenesis. *J. Cell. Biochem.* **97,** 33–44 (2006).

9. Anderson, R. M., Lawrence, A. R., Stottmann, R. W., Bachiller, D. & Klingensmith, J. Chordin and noggin promote organizing centers of forebrain development in the mouse. *Development* **129,** 4975–87 (2002).

10. Sasai, Y., Lu, B., Piccolo, S. & De Robertis, E. M. Endoderm induction by the organizer-secreted factors chordin and noggin in Xenopus animal caps. *EMBO J* **15,** 4547–55 (1996).

11. Yoshimura, Y. *et al.* Colocalization of noggin and bone morphogenetic protein-4 during fracture healing. *J Bone Min. Res* **16,** 876–84 (2001).

12. Zehentner, B. K., Haussmann, A. & Burtscher, H. The bone morphogenetic protein antagonist Noggin is regulated by Sox9 during endochondral differentiation. *Dev Growth Differ* **44,** 1–9 (2002).

13. Brunet, L. J. Noggin, Cartilage Morphogenesis, and Joint Formation in the Mammalian Skeleton. *Science (80-. ).* **280,** 1455–1457 (1998).

14. Shum, L., Wang, X., Kane, A. a & Nuckolls, G. H. BMP4 promotes chondrocyte proliferation and hypertrophy in the endochondral cranial base. *Int. J. Dev. Biol.* **47,** 423–31 (2003).

15. Pizette, S. & Niswander, L. BMPs are required at two steps of limb chondrogenesis: formation of prechondrogenic condensations and their differentiation into chondrocytes. *Dev Biol.* **219,** 237–49 (2000).

16. Nifuji, A., Kellermann, O. & Noda, M. Noggin inhibits chondrogenic but not osteogenic differentiation in mesodermal stem cell line C1 and skeletal cells. *Endocrinology* **145,** 3434–42 (2004).

17. Gong, Y. *et al.* Heterozygous mutations in the gene encoding noggin affect human joint morphogenesis. *Nat. Genet.* **21,** 302–4 (1999).

18. Marcelino, J. *et al.* Human disease-causing NOG missense mutations: effects on noggin secretion, dimer formation, and bone morphogenetic protein binding. *Proc. Natl. Acad. Sci. U. S. A.* **98,** 11353–8 (2001).

19. Cho, K. W. Y., Blumberg, B., Steinbeisser, H. & Robertis, E. M. De. Molecular Nature of Spemann's Organizer: the Role of the Xenopus Homeobox Gene goosecoid. *Cell* **67,** 1111–1120 (1991).

20. De Robertis, E. M. *et al.* Molecular mechanisms of cell-cell signaling by the Spemann-Mangold organizer. *Int. J. Dev. Biol.* **45,** 189–97 (2001).

21. Krause, C., Guzman, A. & Knaus, P. Noggin. *Int. J. Biochem. Cell Biol.* **43,** 478–81 (2011).

22. Filosa, S. *et al.* Goosecoid and HNF-3beta genetically interact to regulate neural tube patterning during mouse embryogenesis. *Development* **124,** 2843–54 (1997).

23. Ionescu, A. *et al.* FoxA family members are crucial regulators of the hypertrophic chondrocyte differentiation program. *Dev. Cell* **22,** 927–39 (2012).

24. Technau, U. & Scholz, C. B. Origin and evolution of endoderm and mesoderm. *Int. J. Dev. Biol.* **47,** 531–9 (2003).

25. Murphy, C. M., Matsiko, A., Haugh, M. G., Gleeson, J. P. & O'Brien, F. J. Mesenchymal stem cell fate is regulated by the composition and mechanical properties of collagen-glycosaminoglycan scaffolds. *J Mech Behav Biomed Mater* **11,** 53–62 (2012).

26. Banerjee, A. *et al.* The influence of hydrogel modulus on the proliferation and differentiation of encapsulated neural stem cells. *Biomaterials* **30,** 4695–9 (2009).

27. Engler, A. J., Sen, S., Sweeney, H. L. & Discher, D. E. Matrix elasticity directs stem cell lineage specification. *Cell* **126,** 677–89 (2006).

28. Discher, D. E., Janmey, P. & Wang, Y.-L. Tissue cells feel and respond to the stiffness of their substrate. *Science* **310,** 1139–43 (2005).

29. Evans, N. D. *et al.* Substrate stiffness affects early differentiation events in embryonic stem cells. *Eur Cell Mater* **18,** 1–13; discussion 13–4 (2009).

30. Park, J. S. *et al.* The Effect of Matrix Stiffness on the Differentiation of Mesenchymal Stem Cells in Response to TGF-β. *Biomaterials* **32,** 3921–3930 (2011).

31. Candiello, J., Singh, S. S., Task, K., Kumta, P. N. & Banerjee, I. Early differentiation patterning of mouse embryonic stem cells in response to variations in alginate substrate stiffness. *J. Biol. Eng.* **7,** 9 (2013).

32. Kwon, H. J. Chondrogenesis on sulfonate-coated hydrogels is regulated by their mechanical properties. *J Mech Behav Biomed Mater* **17,** 337–46 (2013).

33. Farrell, M. J., Comeau, E. S. & Mauck, R. L. Mesenchymal stem cells produce functional cartilage matrix in three-dimensional culture in regions of optimal nutrient supply. *Eur Cell Mater* **23,** 425–40 (2012).

34. Rakar, J., Lönnqvist, S., Sommar, P., Junker, J. & Kratz, G. Interpreted gene expression of human dermal fibroblasts after adipo-, chondro- and osteogenic phenotype shifts. *Differentiation.* **84,** 305–13 (2012).

35. Singh, M., Pierpoint, M., Mikos, A. G. & Kasper, F. K. Chondrogenic differentiation of neonatal human dermal fibroblasts encapsulated in alginate beads with hydrostatic compression under hypoxic conditions in the presence of bone morphogenetic protein-2. *J. Biomed. Mater. Res. A* **98,** 412–24 (2011).

36. Junker, J., Sommar, P., Skog, M., Johnson, H. & Kratz, G. Adipogenic, chondrogenic and osteogenic differentiation of clonally derived human dermal fibroblasts. *Cells. Tissues. Organs* **191,** 105–118 (2010).

37. Sommar, P. *et al.* Engineering three-dimensional cartilage- and bone-like tissues using human dermal fibroblasts and macroporous gelatine microcarriers. *J. Plast. Reconstr. Aesthet. Surg.* **63,** 1036–46 (2010).

38. Lorenz, K. *et al.* Multilineage differentiation potential of human dermal skin-derived fibroblasts. *Exp. Dermatol.* **17,** 925–32 (2008).

39. Shui, C. & Scutt, A. M. Mouse embryo-derived NIH3T3 fibroblasts adopt an osteoblast-like phenotype when treated with 1alpha,25-dihydroxyvitamin D(3) and dexamethasone in vitro. *J. Cell. Physiol.* **193,** 164–72 (2002).

40. Chen, F. G. *et al.* Clonal analysis of nestin(-) vimentin(+) multipotent fibroblasts isolated from human dermis. *J. Cell Sci.* **120,** 2875–83 (2007).

41. Saeed, H., Taipaleenmäki, H., Aldahmash, A. M., Abdallah, B. M. & Kassem, M. Mouse embryonic fibroblasts (MEF) exhibit a similar but not identical phenotype to bone marrow stromal stem cells (BMSC). *Stem Cell Rev.* **8,** 318–28 (2012).

42. Thomson, J. a. Embryonic Stem Cell Lines Derived from Human Blastocysts. *Science (80-. ).* **282,** 1145–1147 (1998).

43. Takahashi, K. & Yamanaka, S. Induction of pluripotent stem cells from mouse embryonic and adult fibroblast cultures by defined factors. *Cell* **126,** 663–76 (2006).

44. Quintana, L. *et al.* Early tissue patterning recreated by mouse embryonic fibroblasts in a three-dimensional environment. *Tissue Eng Part A* **15,** 45–54 (2009).

45. Garreta, E., Genové, E., Borrós, S. & Semino, C. E. Osteogenic Differentiation of Mouse Embryonic Stem Cells and Mouse Embryonic Fibroblasts in a Three-Dimensional. *Tissue Eng Part A* **12,** 2215–2227 (2006).

46. Bi, W., Deng, J. M., Zhang, Z., Behringer, R. R. & de Crombrugghe, B. Sox9 is required for cartilage formation. *Nat. Genet.* **22,** 85–9 (1999).

47. Terry, D. E., Chopra, R. K., Ovenden, J. & Anastassiades, T. P. Differential Use of Alcian Blue and Toluidine Blue Dyes for the Quantification and Isolation of Anionic Glycoconjugates from Cell Cultures : Application to Proteoglycans and a High-Molecular-Weight Glycoprotein Synthesized by Articular Chondrocytes. *Anal Biochem* **285,** 211–219 (2000).

48. Knudson, C. B. & Knudson, W. Cartilage proteoglycans. *Semin Cell Dev Biol.* **12,** 69–78 (2001).

49. Kopesky, P., Vanderploeg, E., Kurz, B. & Grodzinsky, A. J. Self-assembling peptide hydrogels modulate in vitro chondrogenesis of bovine bone marrow stromal cells. *Tissue Eng Part A* **16,** (2009).

50. Koay, E. J. & Athanasiou, K. a. Hypoxic chondrogenic differentiation of human embryonic stem cells enhances cartilage protein synthesis and biomechanical functionality. *Osteoarthritis Cartilage* **16,** 1450–6 (2008).

51. Merceron, C. *et al.* Differential effects of hypoxia on osteochondrogenic potential of human adipose-derived stem cells. *Am J Physiol Cell Physiol* **298,** C355–64 (2010).

52. Schipani, E. Hypoxia and HIF-1 alpha in chondrogenesis. *Semin. Cell Dev. Biol.* **16,** 539–46 (2005).

53. Zur Nieden, N. I., Kempka, G., Rancourt, D. E. & Ahr, H.-J. Induction of chondro-, osteo- and adipogenesis in embryonic stem cells by bone morphogenetic protein-2: effect of cofactors on differentiating lineages. *BMC Dev. Biol.* **5,** 1 (2005).

54. Kawai, M. & Rosen, C. J. PPARγ: a circadian transcription factor in adipogenesis and osteogenesis. *Nat Rev Enocrinol.* **6,** 629–636 (2010).

55. Caplan, A. I. & Correa, D. PDGF in bone formation and regeneration: new insights into a novel mechanism involving MSCs. *J. Orthop. Res.* **29,** 1795–803 (2011).

56. Graham, S. *et al.* Investigating the role of PDGF as a potential drug therapy in bone formation and fracture healing. *Expert Opin. Investig. Drugs* **18,** 1633–54 (2009).

57. Alexander, D. L., Ganem, L. G., Fernandez-Salguero, P., Gonzalez, F. & Jefcoate, C. R. Aryl-hydrocarbon receptor is an inhibitory regulator of lipid synthesis and of commitment to adipogenesis. *J. Cell Sci.* **111 ( Pt 2,** 3311–22 (1998).

58. Doetschman, T. C., Eistetter, H., Katz, M., Schmidt, W. & Kemler, R. The in vitro development of blastocyst-derived embryonic stem cell lines: formation of visceral yolk sac, blood islands and myocardium. *J. Embryol. Exp. Morphol.* **87,** 27–45 (1985).

59. Leahy, A., Xiong, J. W., Kuhnert, F. & Stuhlmann, H. Use of developmental marker genes to define temporal and spatial patterns of differentiation during embryoid body formation. *J. Exp. Zool.* **284,** 67–81 (1999).

60. Hoffmann, A. *et al.* The T-box transcription factor Brachyury mediates cartilage development in mesenchymal stem cell line C3H10T1/2. *J. Cell Sci.* **115,** 769–81 (2002).

61. Chung, C. & Burdick, J. A. Engineering cartilage tissue. *Adv. Drug Deliv. Rev.* **60,** 243–62 (2008).

62. Brodkin, K. R., García, a J. & Levenston, M. E. Chondrocyte phenotypes on different extracellular matrix monolayers. *Biomaterials* **25,** 5929–38 (2004).

63. Martin, I., Vunjak-Novakovic, G., Yang, J., Langer, R. & Freed, L. E. Mammalian chondrocytes expanded in the presence of fibroblast growth factor 2 maintain the ability to differentiate and regenerate three-dimensional cartilaginous tissue. *Exp. Cell Res.* **253,** 681–8 (1999).

64. Mandl, E. W. *et al.* Fibroblast growth factor-2 in serum-free medium is a potent mitogen and reduces dedifferentiation of human ear chondrocytes in monolayer culture. *Matrix Biol.* **23,** 231–41 (2004).

65. Murphy, C. L., Thoms, B. L., Vaghjiani, R. J. & Lafont, J. E. Hypoxia. HIF-mediated articular chondrocyte function: prospects for cartilage repair. *Arthritis Res. Ther.* **11,** 213 (2009).

66. Watt, F. M. Effect of seeding density on stability of the differentiated phenotype of pig articular chondrocytes in culture. *J. Cell Sci.* **89 ( Pt 3),** 373–8 (1988).

67. Buschmann, M. D., Gluzband, Y. a, Grodzinsky, a J., Kimura, J. H. & Hunziker, E. B. Chondrocytes in agarose culture synthesize a mechanically functional extracellular matrix. *J. Orthop. Res.* **10,** 745–58 (1992).

68. Homicz, M. R. *et al.* Human septal chondrocyte redifferentiation in alginate, polyglycolic acid scaffold, and monolayer culture. *Laryngoscope* **113,** 25–32 (2003).

69. Häuselmann, H. J. *et al.* Phenotypic stability of bovine articular chondrocytes after long-term culture in alginate beads. *J. Cell Sci.* **107,** 17–27 (1994).

70. Bonaventure, J. *et al.* Reexpression of Cartilage-Specific Genes by Dedifferentiated Human Articular Chondrocytes Cultured in Alginate bEDS. *Exp. Cell Res.* **212,** 97–104 (1994).

71. Perka, C., Spitzer, R. S., Lindenhayn, K., Sittinger, M. & Schultz, O. Matrix-mixed culture: new methodology for chondrocyte culture and preparation of cartilage transplants. *J. Biomed. Mater. Res.* **49,** 305–11 (2000).

72. Schulze-Tanzil, G. *et al.* Redifferentiation of dedifferentiated human chondrocytes in high-density cultures. *Cell Tissue Res.* **308,** 371–9 (2002).

73. Babur, B. K. *et al.* The interplay between chondrocyte redifferentiation pellet size and oxygen concentration. *PLoS One* **8,** e58865 (2013).

74. Sah, R. L. *et al.* Biosynthetic response of cartilage explants to dynamic compression. *J. Orthop. Res.* **7,** 619–36 (1989).

75. Gan, L. & Kandel, R. a. In Vitro Cartilage Tissue Formation by Co-culture of Primary and Passaged Chondrocytes. *Tissue Eng.* **13,** 831–842 (2007).

76. Malladi, P., Xu, Y., Chiou, M., Giaccia, A. J. & Longaker, M. T. Effect of reduced oxygen tension on chondrogenesis and osteogenesis in adipose-derived mesenchymal cells. *Am. J. Physiol. Cell Physiol.* **290,** C1139–46 (2006).

77. Bussmann, B. M. *et al.* Chondrogenic potential of human dermal fibroblasts in a contractile soft self-assembling peptide hydrogel. *J Tissue Eng Regen Med* (2013).

78. Dégano, I. R. *et al.* The effect of self-assembling peptide nanofiber scaffolds on mouse embryonic fibroblast implantation and proliferation. *Biomaterials* **30,** 1156–65 (2009).

79. Lengner, C. J. *et al.* Primary mouse embryonic fibroblasts: a model of mesenchymal cartilage formation. *J. Cell. Physiol.* **200,** 327–33 (2004).

# Chapter 3: Evaluation of the biologically induced osteogenic differentiation of MEFs in the self-assembling peptide RAD16-I

# 3.1 Introduction

## 3.1.1 Overview

Bone tissue is mainly composed by a natural composite of collagen type I and hydroxyapatite containing a highly vascularized network which plays a crucial role in supplying cells with oxygen and nutrients and removing waste products [1]. Unlike other tissues, bones possess the capacity to regenerate, remodel and repair in response to injury. However, the supply of additional bone grafts is needed when the required bone regeneration exceeds the natural potential for self-healing, as in large bone defects occurring after trauma, infection, tumor resection or skeletal abnormalities [2]. In the clinical setting, the gold standard to treat bone defects consists of the transplantation of autologous bone grafts, usually harvested from the iliac crest and fibular grafts. Nonetheless, some of the disadvantages are the limited availability of autologous material and donor-site morbidity [2]. Allografts and xenografts are also available but their use is often associated with infection, disease transmission, and immunological rejection [3].

Traditionally, bone tissue engineering strategies have been mainly focused on the development and application of three-dimensional porous scaffolds with similar composition to the bone. Delivery of cells and growth factors has been coupled in order favor the formation of new bone [1,4–6]. However, challenges still remain in the inability to reproduce an engineered well vascularized bone that truly mimics natural bone blood vessels. Although tissue engineering of bone has been traditionally focused on direct (intramembranous) bone formation, nowadays the interest in endochondral bone formation is increasing since it is a more physiological approach which recreates most aspects of *in vivo* bone formation. These studies consist mainly on creating a cartilage template *in vitro* followed by its implantation *in vivo* where the template is vascularized and remodeled [7].

## 3.1.2 Endochondral Ossification

The osseous tissues in mammals develop through two distinct processes, intramembranous ossification and endochondral ossification. Intramembranous bone formation, which occurs in many of the craniofacial bones, involves direct differentiation of mesenchymal cells into the bone-forming osteoblasts, which deposit and mineralize the bone matrix. In contrast, endochondral ossification, which occurs in the remainder of the mammalian skeleton, generates bone via a cartilage intermediate [8,9].

Endochondral bone development begins with the formation of a cartilage template (Figure 3.1.1). Briefly, as it is detailed in Chapter 2 for chondrogenic differentiation, the first step is mesenchymal condensation after which cells in the core of the condensation differentiate into chondrocytes that secrete a cartilage matrix rich in collagen types II, IX, and XI, and specific proteoglycans such as aggrecan. Then, cells at the periphery of the condensation form the

perichondrium, which continues to express collagen type I and demarcates the developing skeletal element from the surrounding mesenchyme. All chondrocytes undergo rapid proliferation that drives the linear growth of the skeletal elements and form the model for the future bone. Then, the chondrocytes stop dividing and increase their volume dramatically, becoming hypertrophic chondrocytes. The orderly maturation of chondrocytes produces zones of proliferation, hypertrophy, and bone formation, linearly progressing from the articular ends (epiphysis) to the midshaft (diaphysis) of the skeletal element. The hypertrophic chondrocytes are characterized by the expression of type X collagen that enables the mineralization by calcium carbonate. Later, the terminal hypertrophic chondrocytes express additional molecular markers such as matrix metalloproteinase 13 (MMP13), which plays a critical role in cleaving the extracellular matrix proteins within the hypertrophic cartilage and thus facilitating vascular invasion. This invasion brings osteoprogenitors that differentiate into osteoblasts, which establish the primary ossification center to generate the trabecular bone [10]. These osteoblast cells replace apoptotic chondrocytes and generate bone matrix and thus are the crucial cellular mediators of endochondral ossification [11]. Moreover, vascularization leads to further degradation of the matrix by MMP9[12]. Only a small region at either end of the growing bone will remain cartilaginous. This structure, called the growth plate cartilage, will control longitudinal growth of the bone [13].

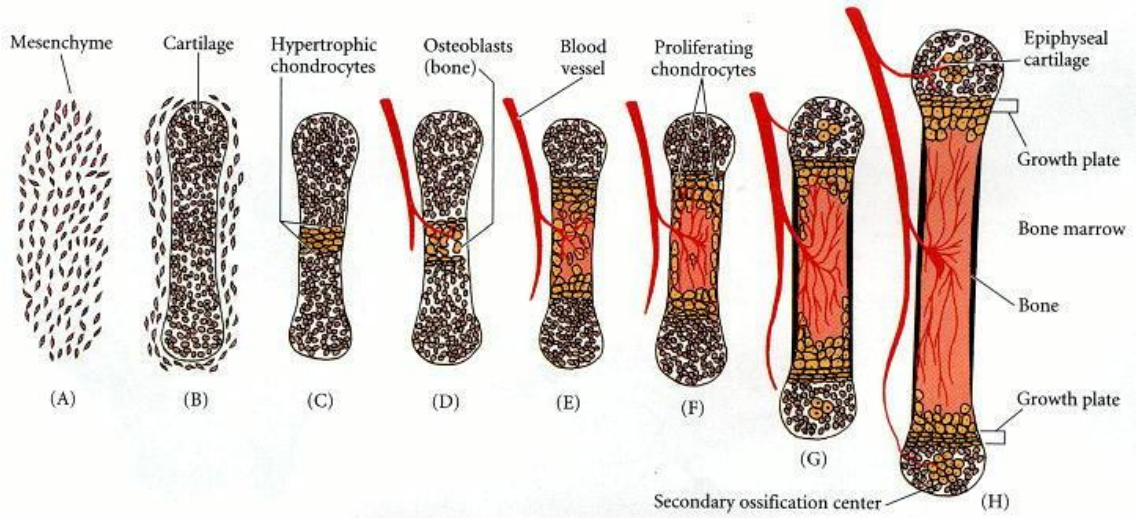


**Figure 3.1.1 Schematic diagram of** endochondral ossification. (A, B) Mesenchymal cells condense and differentiate into chondrocytes to form the cartilaginous model of the bone. (C) Chondrocytes in the center of the shaft undergo hypertrophy and apoptosis while they change and mineralize their extracellular matrix. Their deaths allow blood vessels to enter. (D, E) Blood vessels bring in osteoblasts, which bind to the degenerating cartilaginous matrix and deposit bone matrix. (F-H) Bone formation and growth consist of ordered arrays of proliferating, hypertrophic, and mineralizing chondrocytes. Secondary ossification centers also form as blood vessels enter near the tips of the bone. (Image from Developmental Biology 6th Edition. Gilbert SF)

The orderly progression from proliferating chondrocytes to bone formation is subjected to regulation by key extracellular signals and nuclear factors. Among them, hormones such as growth hormone (GH), insulin-like growth factors (IGFs), thyroid hormone, androgen, estrogen and glucocorticoids tightly regulate longitudinal bone growth. Moreover, locally produced factors such as bone morphogenetic proteins (BMPs), fibroblast growth Factors (FGFs), TGFβ, Wnts, Ihh, parathyroid hormone-related peptide and retinoids are known to influence the process (Figure 3.1.2). Lastly, a number of nuclear factors have also been shown to regulate chondrocyte hypertrophy such as Sox9 and Runx2 [9,13–16]..

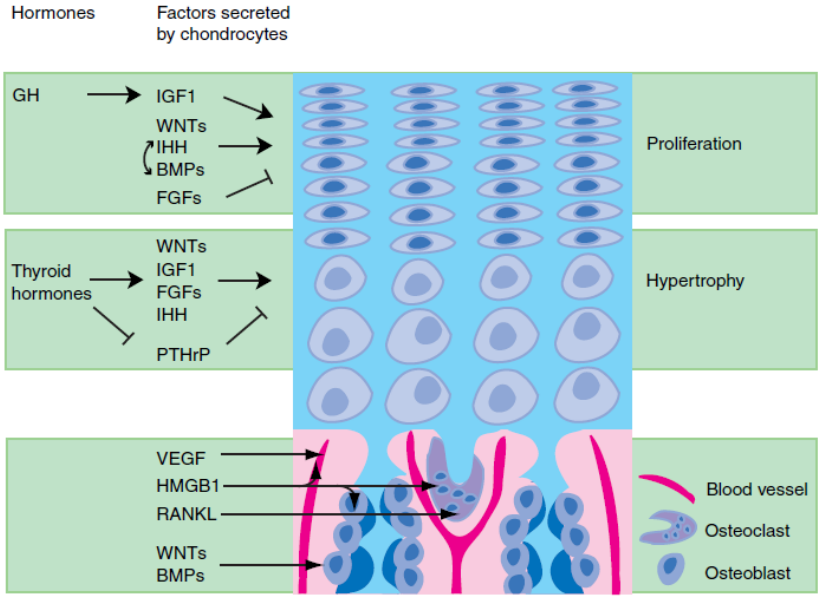


**Figure 3.1.2. Overview of the effects of factors secreted by chondrocytes on growth plate cell function and invasion.** Under the control of circulating hormones, chondrocytes secrete growth factors that act on chondrocytes to regulate their proliferation and hypertrophy (upper two panels), and on cells of the ossification front (lower panel), to regulate their invasion of the growth plate cartilage. Arrows indicate stimulatory pathways, and crossed lines indicate inhibitory pathways. (Image from Mackie et al 2008 [14])

### 3.1.3 Role of endothelial cells in the endochondral ossification process

As detailed in the previous section, endochondral bone formation is characterized by the blood vascular invasion into previously avascular cartilage. At early stages of differentiation, since cartilage is an avascular tissue, it strongly produces anti-angiogenic factors such as transforming growth factor beta (TGF-β1), chondrocyte inhibitor of angiogenesis (hCHIAMP), TIMP-1, TIMP-2, and Chondromodulin-I (ChM-I) [11]. However, hypertrophic chondrocytes in mature cartilage rapidly suffer an angiogenic switch characterized by the secretion of angiogenic molecules that stimulate endothelial cell migration from the subchondral bone into growth plates, including vascular endothelial growth factor (VEGF), transferrin, acid and basic fibroblast growth factor (FGF) or connective tissue growth factor (CTGF) [11]. Nowadays, a

wealth of data has demonstrated that an intimate functional relationship exists between endothelial cells (ECs) and osteoblasts (OBs) during bone formation and repair. Several studies have identified and characterized factors involved in the "dialog" between both types of cells suggesting that this cell-to-cell communication could be crucial to the coordinated cell behavior necessary for the development and remodeling of bone [17]. In addition to the angiogenic factors secreted by the hypertrophic chondrocytes, ECs produce growth factors including bone morphogenetic protein-2 (BMP2), vasoconstrictor endothelin-1 (ET1) and insulin-like growth factor (IGF) which affect the migration and proliferation of OBs and the differentiation of osteoprogenitor cells. The vasculature is crucial for the progressive conversion of the cartilage scaffolds into bones during endochondral ossification. As a consequence, it plays a crucial role for bone health throughout life. For this reason, failure in the blood supply may contribute to osteoporosis, and critically hamper fracture healing [18]. In the last years, different groups have been focused on characterizing the crosstalk between ECs and OBs in order to obtain new strategies for bone tissue engineering [19]. Coculture models on conventional 2D surfaces or within 3D structures have been used for the analysis of the cell-to-cell communication. The 3D models could be obtained without scaffold by the formation of spheroids, or with scaffold by the association of these two cell types into a biomaterial composite [19,20]. Biocompatible scaffolds offer an adequate 3D architecture and design to promote the rate of bone formation and vascularization by enhancing cell contact between the two cell types. Several types of biomaterials have been used for this application such as polylactide-glycolic acid (PLGA) [21], polyurethane [22], alginate [23] or silk fibroin fibers [24]. Regarding to the cell types used, different types of endothelial cells have been used such as human umbilical vein endothelial cells (HUVECs), human dermal microvascular endothelial cells (HDMECs) or endothelial progenitor cells [19]. Moreover, mesenchymal stem cells and osteoblasts have been mainly used as osteoprogenitor cells [25–27]. Interestingly, independently of the method used, the osteogenic and angiogenic potentials in the cocultures increased as compared with the monocultures, which evidenced the importance of the crosstalk between both types of cells in the osteogenic differentiation and the potential role of ECs as osteogenic mediators.

## 3.2 Hypothesis and specific aims

As it was detailed in Chapter 2, when mouse embryonic fibroblasts (MEFs) were cultured *in vitro* in the self-assembling peptide scaffold RAD16-I under certain biomechanical conditions, they acquired multipotential capacity engaging into a spontaneous process of chondrogenic differentiation. However, MEFs only underwent osteogenic differentiation under specific chemical induction as it was published in Quintana et al 2009.

In view of these results together with the ability of ECs to act as osteogenic mediators, we hypothesized that the presence of ECs could promote a switch in MEFs to an osteogenic-like commitment due to a crosstalk between the chondrogenic-like cells and the ECs recreating an endochondral ossification process. Therefore, the specific aims for this chapter are the following:

(1) To develop a coculture system using ECs and MEFs in order to induce the switch of MEFs to an osteogenic commitment.
(2) To evaluate the osteogenic-like commitment of the coculture system by analyzing the expression of hypertrophic markers and matrix mineralization.

## 3.3 Materials and Methods

### 3.3.1 Culture of mouse embryonic fibroblasts (MEFs)

MEFs isolated from C57BL=6 embryos at day 14 were purchased from the American Type Culture Collection (scrc-1008; ATCC). The use of these cells has been approved by the Ramon Llull University Ethics Committee (CER URL 2013-001). MEFs (<10th passage) were cultured in 75-cm2 flasks in fibroblast medium (FM), which contains high-glucose Dulbecco's modified Eagle medium (DMEM; D5671, Sigma) supplemented with 15% (v/v) Fetal Bovine Serum (FBS) (DE14-801F, Lot: 1SB003, Lonza), 100 U/mL Penicillin / 0.1 mg/mL Streptomycin (P11-010, PAA), 2mM L-Glutamine (M11-004, PAA), 1mM Sodium Piruvate (11360-039, Gibco) and 100µM Minimum Essential Medium Non-essential Amino Acid solution (M7145, Sigma). Cultures were maintained in the incubator in humidified atmosphere at 37ºC and 5% $CO_2$.

### 3.3.2 Culture of human umbilical vein endotelial cells (HUVECs)

Human Umbilical Vein Endothelial Cells (HUVECs) (CC-2519, Lot: 3F0060, Lonza) were cultured in 25-cm2 flasks, previously coated with 0.1% (w/v) gelatin (G9391, Sigma), in Endothelial Basal Medium-2 (EBM-2) (CC-3156, Lonza) supplemented with Endothelial Cell Growth Media SingleQuots kit (EGM-2) (4176, Lonza). Cultures were maintained in the incubator at 37ºC and 5% CO2.

### 3.3.3 3D culture technique

To obtain a 3D culture, a solution of commercial 1% (w/v) RAD16-I (PuraMatrix™,354250, Beckton Dickinson) was diluted in sucrose 10% (w/v) (S1888, Sigma), to obtain a concentration of 0.14% (w/v). This solution was mixed with an equal volume of a cell suspension (4 x $10^6$ cells/mL) in sucrose 10% (w/v), to obtain a final concentration of 2 x $10^6$ cells/mL in 0.07% (w/v) of RAD16-I in sucrose 10% (w/v). 80µL of this mix were loaded into 9mm diameter cell culture inserts (PICM01250, Millipore), previously placed into a 6-well culture plate and equilibrated with culture media. Immediately, cell-peptide cultures were placed for 30 minutes in the incubator at 37°C and 5% $CO_2$, to allow the formation of the hydrogel by the action of the high ionic strength and the neutral pH of the medium. Elapsed this time, to dilute the content of sucrose, subsequent washing steps were performed by aspiration of the culture media in the well (outside of the insert), and the addition of the same amount (500µL) of fresh medium. The plate was placed again in the incubator for 10 minutes and this step was repeated 3 times, after which 2.5mL of fresh medium were added outside the insert and the plate placed in the incubator for 30 more minutes, to finally allow the construct to form, preventing its rupture. At this point, the addition of medium over the cell culture began, by adding 10µL in the inner wall of the insert letting it slowly slide to the gel, until a volume of 40µL is reached. The plate was placed once again in the incubator for 15 minutes and then the addition of fresh medium over the cell

construct continued, by addition of 20µL inside the insert, until a final volume of 200µL. The 3D cell cultures were maintained in the incubator at 37°C and 5% $CO_2$, for 5, 14 or 28 days. The medium was changed every second day by removing 500µL of medium from the well and the addition of 500µL of fresh medium inside the insert. (Figure 2.3.1, Chapter 2).

### 3.3.4 Coculture of MEFs with HUVECs

In order to coculture MEFs with HUVECs, two protocols were performed:

1) In the first method, MEFs 3D-cultures at final concentration of 2 x $10^6$ cells/mL in 0.07% (w/v) RAD16-I were prepared as usual. After 1, 5 or 10 days of culture, a suspension of 120.000 HUVECs in sucrose 10% (w/v) was loaded on top of the 3D cultures and maintained for 10 days in FM.

2) The second method consisted on the encapsulation of both cell types together. 3D-cultures were prepared following the 3D culture protocol but combining a solution of HUVECs and MEFs with the self-assembling peptide RAD16-I to obtain at a final concentration of 1 x $10^6$ cells/mL of each cell type and 0.07% (w/v) RAD16-I. Cultures were maintained for 5 or 21 days in FM (Figure 3.3.1).

In both methods, medium was changed every second day and the cultures were maintained in an incubator at 37°C and 5% $CO_2$.

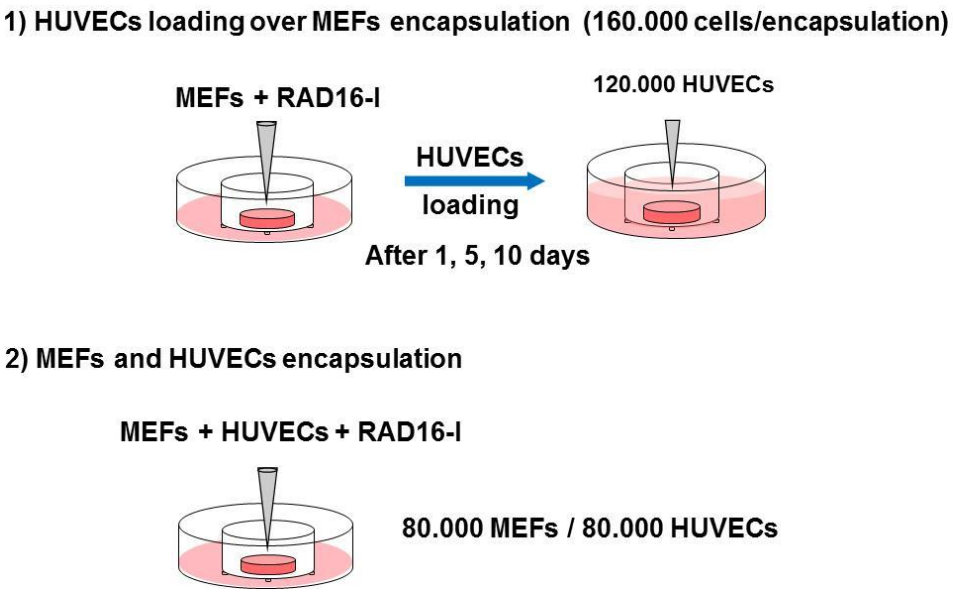


**Figure 3.3.1. MEFs and HUVECs coculture schematic protocols.** 1) Loading HUVECs suspension over a MEFs 3D encapsulation in 0.07% (w/v) RAD16-I after 1, 5 or 10 days of regular culture in FM.The cocultures were maintained for 10 days independently of the day of loading. 2) Encapsulation of HUVECs and MEFs together by mixing 80.000 cells of each type and maintaining the cocultures for 5 and 21 days.

### 3.3.5 Reverse Transcription Polymerase Chain Reaction

The RNA was extracted from the samples using peqGold total RNA kit (12-6834-02, Lot: 072412, PeqLab). After the removal of the genomic DNA, cDNA was synthesized using QuantiTect Reverse Transcription kit (205311, Qiagen). The cDNA obtained was then analyzed by RT-PCR, using either Deep Vent DNA Polymerase (M0258S, New England Biolabs) or Taq DNA Polymerase master mix (D1806, Sigma). In both cases, 50ng of cDNA sample were added, dNTPs at a final concentration of 200µM and primers at a final concentration of 0.3µM (Table 3.3.1). In the case of Deep Vent, 0.2 units of polymerase were added, instead of 1 unit of polymerase added when Taq Polymerase was used. The amplification reaction was performed according the following parameters: Stage 1: 5 min at 95°C, Stage 2: 40 cycles of 30s at 95°C, 15s at T°m (depending on the primers used) and 20s at 72°, Stage 3: 1 min at 72°C. The gene used as a housekeeping was the ribosomal subunit 18S. DNA fragments were visualized under UV light in a 2% (w/v) agarose gel to estimate their size.

**Table 3.3.1. Designed primers used for RT-PCR**

| Gene | F/R | Sequence (5' - 3') | Length |
|---|---|---|---|
| **18s** | F | GCTACCACATCCAAGGAAGGCAG | 234bp |
| | R | CGCTCCCAAGATCCAACTACGAG | |
| **Coll I** | F | TGACTGGAAGAGCGGAGAGT | 151bp |
| | R | GTTCGGGCTGATGTACCAGT | |
| **Coll X** | F | CAAGCCAGGCTATGGAAGTC | 154bp |
| | R | AGCTGGGCCAATATCTCCTT | |
| **Runx2** | F | GCCGGGAATGATGAGAACTA | 180bp |
| | R | GGACCGTCCACTGTCACTTT | |
| **VEGF-A** | F | TCACCGCCTTGGCTTGTCACA | 93bp |
| | R | GGAGAGATGAGCTTCCTACAG | 225bp |

### 3.3.6 Western Blot

After the lysis of the samples with buffer for protein extraction, a quantification step was performed to determine total protein content using BCA Protein Assay kit (23225, Pierce). Acrylamide gels were prepared according to the size of the proteins, generally in concentrations of 7 or 12% (w/v). Cell lysates (5µg of each sample) were mixed with protein loading buffer containing 5% (v/v) β-mercaptoethanol, and this mix was heated at 95°C for 10 minutes. Samples and protein ladder (161-0374, Bio Rad) were run applying 150V during 1h in electrophoresis buffer (30g Tris-base (154563, Sigma), 144g Glycine (0167, Amresco) and 10g SDS (L5750, Sigma) in 1L $H_2O$). After the run, proteins were transferred to a PVDF membrane (LC 2005, Invitrogen) applying 40V during 2h at RT using transfer buffer (3.03g Tris-base, 36g Glycine, 200mL Methanol and $H_2O$ up to 1L). Then, the membrane was incubated at RT for 2h in blocking buffer (4% (w/v) non-fat powered milk in PBST). Membranes were incubated for

1h at RT with primary antibodies at a final concentration of 1µg/mL in PBST (Table 3.3.2). Then a secondary antibody IgG-HRP was added at a concentration of 1µg/mL, and incubated at RT for 1h (Table 3.3.3). Finally, the membrane was revealed for HRP detection (34080, Pierce). Chemiluminescent images were taken in the ImageQuant™ LAS 4000 mini (GE HealthCare). Images were analyzed with *ImageQuant™ Image Analysis Software 7.0*. Actin was used as an internal protein standard.

**Table 3.3.2. Primary antibodies used for Western Blot**

| Primary Antibodies | Molecular Weight | Catalog # | Lot | Brand |
|---|---|---|---|---|
| **Actin** | 43kDa | sc-1615 | K0612 | Santa Cruz |
| **Collagen 1A1** | 140-210kDa (prec)<br>70-90kDa (mature) | sc-8784 | B1211 | Santa Cruz |
| **Collagen 2A1** | 190kDa | sc-7764 | F2912 | Santa Cruz |
| **Collagen 10A1** | 66kDa | sc-323750 | K1011 | Santa Cruz |
| **Runx2** | 55kDa | sc-10758 | D1411 | Santa Cruz |

**Table 3.3.3.HRP-Labeled secondary antibodies used for Western Blot**

| Secondary Antibodies | Catalog # | Lot | Brand |
|---|---|---|---|
| **Donkey anti-Goat** | sc-2020 | F1212 | Santa Cruz |
| **Donkey anti-Rabbit** | sc-2317 | F2212 | Santa Cruz |

### 3.3.7 Collagenase treatment

Protein lysates were treated with collagenase from *Clostridium histolyticum* (C0130, Sigma) in order to degrade the collagen present in the samples. For each protein lysate, the volume necessary to obtain 10 µg of protein were mixed with equal volume of collagenase solution at 2mg/ml to obtain a final concentration of 1 mg/ml. Samples were incubated with the collagenase at 37 ºC for different times: 30 min, 1 hour and overnight. After that samples were analyzed by WB.

### 3.3.8 Cell viability

The live/dead staining was performed to qualitatively determine proportion of live and dead cells. Cell cultures were washed 3 times with PBS and then covered with a solution 2µM of EthD-1 and Calcein AM in PBS (L3224, Invitrogen). After 15 minutes of incubation at RT in dark chamber, the solution was removed and the sample washed 3 times with PBS, after which the sample was analyzed under fluorescence microscope (Zeiss Axiovert 200M inverted microscope with coupled ApoTome system).

### 3.3.9 Von Kossa staining

Von Kossa staining was performed to detect matrix mineralization. Cell cultures were washed with PBS and fixed with PFA 2% (w/v) in PBS for 1h at RT. Then, cultures were washed several times with distilled water, to completely remove the PBS in order to prevent their precipitation with the silver nitrate solution. Then, cultures were incubated for 1h with a

solution of 5% (w/v) silver nitrate (209139, Sigma) in dark chamber, time after which the culture was washed several times with distilled water and placed under a bright light source for 10 minutes. Finally, samples were observed under phase contrast microscopy using an inverted Nikon microscope (Nikon eclipse TS100).

### 3.3.10 Labeling of HUVECs

HUVECs were labeled using Qtracker 565 Cell Labeling kit (Q25031MP, Invitrogen), following the manufacturer's protocol. Briefly, the labeling solution was prepared mixing equal volumes of components A and B in EBM-2. Then, a 2D culture of HUVECs (in a 25-cm2 cell culture flask) was incubated with this solution for 1 hour at 37°C. Labeling solution was completely aspirated and 5mL of fresh medium were added. The culture was then cultured as usual. This labeling permits the identification and localization of the cells due to fluorescent emission at 565 nm of the nanocrystals which allows their observation under fluorescence microscope. (Zeiss Axiovert 200M inverted microscope with coupled ApoTome system).

### 3.3.11 Statistics

All values were expressed as mean ± SD. Statistical differences were analyzed with GraphPad Prism 6 when samples were prepared in triplicate for the condition analyzed. When comparing two groups, unpaired student's t test was used to test for the significance level. When comparing three or more groups statistical analysis was carried out by 1-way or 2-way ANOVA, as appropriate, followed by Tukey post analysis.

## 3.4 Results

First of all, in order to evaluate if the MEFs 3D-cultures undergoing spontaneous chondrogenic differentiation were committed to a terminal differentiation of hypertrophic chondrocytes, the transcription factor Runx2 and the hypertrophic marker Collagen type X (Coll X) were studied. For this purpose, cultures of MEFs were prepared at the peptide concentration where the spontaneous chondrogenesis was previously observed (0.07% (w/v) RAD16-I) and they were maintained for 5, 14 and 28 days.

When analyzing Coll X expression by western blot (WB), it was observed that the anti-Coll X antibody bounded to two different proteins, and depending on the band considered as correct, the results totally changed (Figure 3.4.1, A). Thus, samples were treated with collagenase to degrade the collagen band and to elucidate which was the correct band. Collagenase treatment was performed with the protein lysates following the manufacturer's protocol and using different times of incubation. Interestingly, it was found that the band degraded by the collagenase was the one weighing 54 kDa, which was then only present in 2D cultures (Figure 3.4.1, B). The weight of the band corresponded with the theoretical value provided by the manufacturer (55 kDa). Thus, Coll X was only expressed in 2D cultures and its expression was down-regulated in 3D.

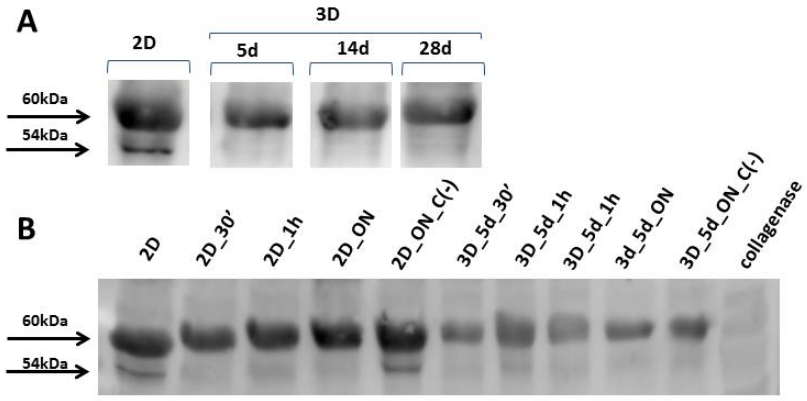


**Figure 3.4.1. Collagen type X analysis by western blot. (**A) Coll X was analyzed by WB in the MEFs 2D cultures and 3D cultures maintained for 5, 14 and 28 days. (B) WB of MEFs 2D cultures and 3D cultures maintained for 5 days treated with the collagenase. Results show from left to right for each sample: lysate without treatment, lysate treated for 30 minutes, 1 hour and overnight (ON) at 37ºC, and sample maintained ON at 37ºC without collagenase as negative control.

Remarkably, the results obtained after collagenase treatment and with RT-PCR, showed a clear expression of Coll X in the 2D controls but absent in 3D-cultures (Figure 3.4.2), suggesting that the system did not undergo hypertrophy in the scaffold system and maintained its chondrogenic commitment. Instead, results obtained using both techniques (WB and RT-PCR) showed that Runx2 was expressed in 2D cultures and down-regulated but still expressed in 3D once (Figure 3.4.2). Although Runx2 is a transcription factor that plays an important role in the maturation of

chondrocytes to a hypertrophic stage, the presence of Sox9 (as observed with qPCR and WB in Chapter 2) might have a dominant effect against hypertrophy as previously reported [28].

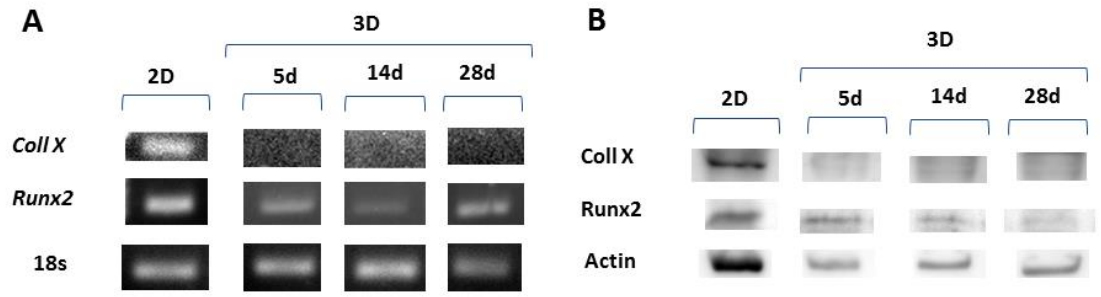


**Figure 3.4.2. Hypertrophic characterization of MEFs cultured in 0.07% (w/v) RAD16-I scaffold.** **(**A) RT-PCR results of Coll X and Runx2 after 5, 14 and 28 days of culture. 18s was used as housekeeping gene. (B) WB results of Coll X and Runx2 when MEFs were cultured for 5, 14 and 28 days.

### 3.4.1 Switch to osteogenic-like differentiation due to biological induction

It was observed that 3D-constructs undergoing spontaneous chondrogenesis did not undergo hypertrophy (by the absence of Coll X expression). Thus, it was hypothesized that the presence of endothelial cells could promote osteogenic-like commitment since several studies suggest the potential role of endothelial cells as osteogenic mediators [19,25].

In order to test the hypothesis, two types of cocultures were prepared with MEFs and endothelial cells to promote cross-talk between both cell types (See Materials and Methods 3.3.4). One type consisted of preparing cultures of MEFs at low peptide concentration (0.07% (w/v)) to promote spontaneous chondrogenic differentiation. Then, after 1, 5 and 10 days of culture, a suspension of HUVECs was added on top of the cell construct and the cocultures were maintained for 10 days independently of the loading day. From this point onwards, this type of coculture will be referred as "loading coculture". On the other hand, the second type consisted of the encapsulation of both cell types together obtaining a final concentration of $1x10^6$ cells/mL of each type and 0.07% (w/v) RAD16-I. These cocultures were maintained for 5 and 21 days. In this case, this type of coculture will be referred as "encapsulation coculture" in this thesis. Before starting with the 3D coculture systems, HUVECs 2D cultures were prepared in order to study their maintenance in fibroblast media, since it would be the culture media of the 3D cocultures. Cells were seeded at 20.000 cells/$cm^2$ and maintained in different types of media: complete FM; conditioned FM from MEFs 2D cultures; conditioned FM from MEFs 3D cultures in 0.07% (w/v) RAD16-I undergoing chondrogenesis; and conditioned FM from 3D cultures of MEFs in 0.25% (w/v) RAD16-I (Figure 3.4.3). Cultures in complete endothelial medium (EBM) were used as benchmark. As expected, lower viability was observed in endothelial cells cultured in FM than in control EBM. However, viability appeared to increase when HUVECs were cultured in conditioned FM from cultures undergoing chondrogenesis after

14 days of culture (Figure 3.4.3). These results suggested that MEFs could be secreting factors that promoted the maintenance of endothelial cells.

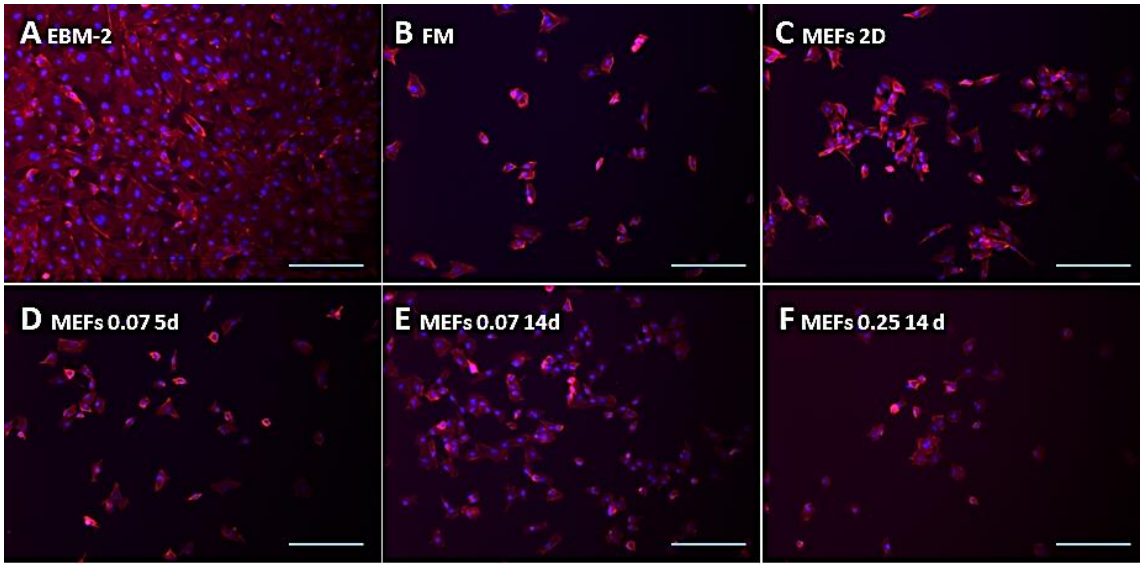


**Figure 3.4.3. HUVECs maintenance in fibroblast media.** 2D cultures were prepared and maintained for 3 days in (A) complete endothelial media used as control, (B) complete FM, (C) conditioned FM from MEFs 2D cultures, (D) conditioned FM from 3D cultures of MEFs in 0.07% (w/v) RAD16-I after 5 days and (E) 14 days and (F) conditioned FM from 3D cultures of MEFs in 0.25% (w/v) RAD16-I. (Scale bar=200 µm)

### *Loading cocultures for the biological osteogenic induction of MEFs*

The *loading coculture* was the first type of coculture prepared, which consisted of adding the HUVECs on top of the MEFs 3D cultures after 1, 5 and 10 days of culture. For better localization and identification in the cocultures, HUVECs were labeled. Briefly, a custom targeting peptide was used to deliver nanocrystals into the cytoplasm of live cells, these nanocrystals were distributed in vesicles and their fluorescent emission at 565 nm allowed their observation under fluorescence microscope (Figure 3.4.4).

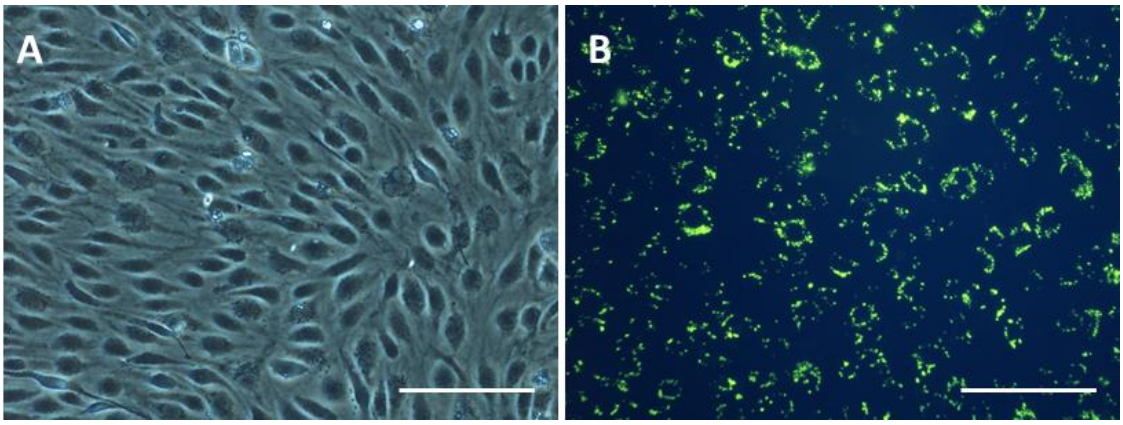


**Figure 3.4.4. HUVECs labeling with fluorescent nanocrystals. (**A) Phase contrast image and (B) Fluorescence image of passage 4 HUVECs labeled with Qtracker® 565. (Scale bar=200µ)

Remarkably, HUVECs loaded on top of MEFs 3D cultures were mainly localized in the edges of the constructs as it was observed by fluorescence microscopy after 1 and 7 days of the loading (Figure 3.4.5).

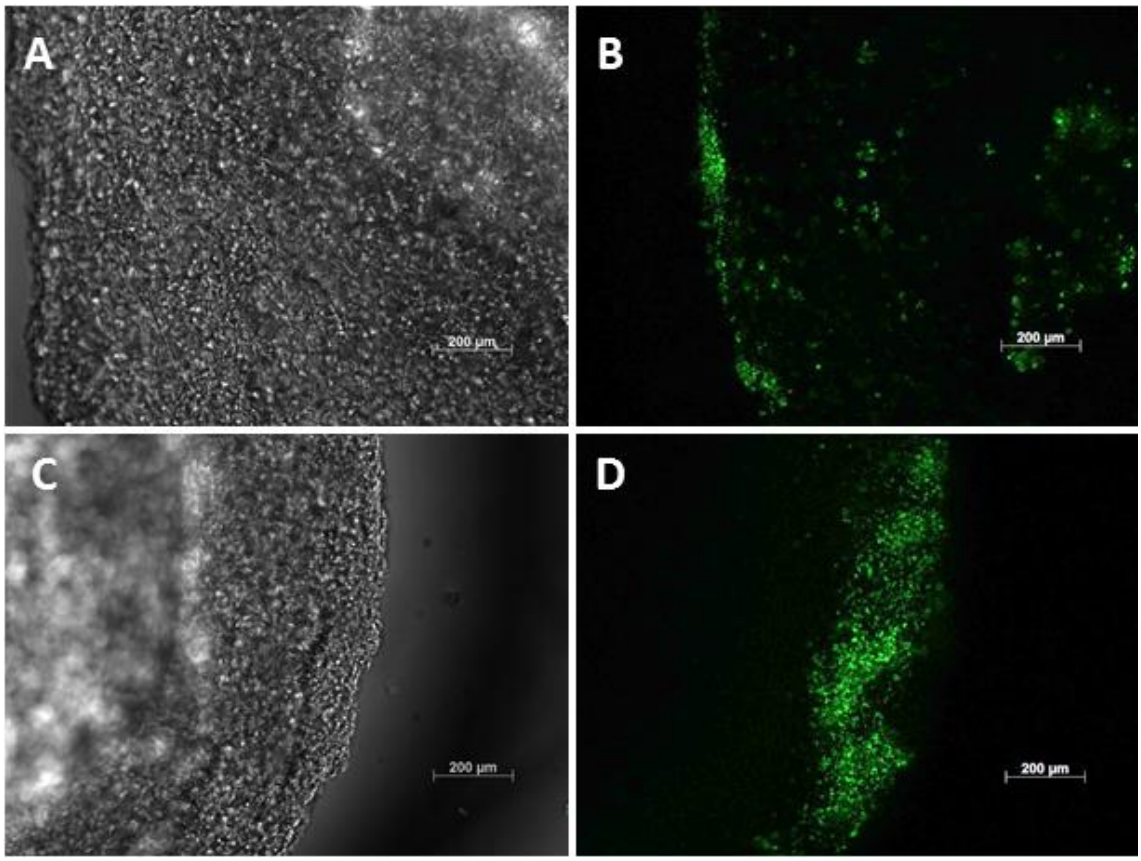


**Figure 3.4.5. HUVECs on top of MEFs 3D cultures. (**A) Phase contrast image and (B) Fluorescence image of HUVECs after 1 day of loading. (C) Phase contrast image and (D) Fluorescence image of HUVECs after 7 day of loading.

In addition, independently of the day of HUVECs addition, it was observed that a part of cells fell into the bottom of the cell culture insert, being capable of grow in the membrane. Surprisingly, the cells just below the 3D cell culture grew and proliferate in higher proportion (Figure 3.4.6, A,B), compared with those cells in the periphery of the cell culture insert which showed a rounded morphology (Figure 3.4.6, C,D). These results suggested that MEFs were secreting factors that favored the maintenance of endothelial cells as previously observed in the 2D cultures with conditioned media. Fluorescence images clearly elucidate that the cells growing below the MEFs 3D cultures were the endothelial cells and not fibroblasts.

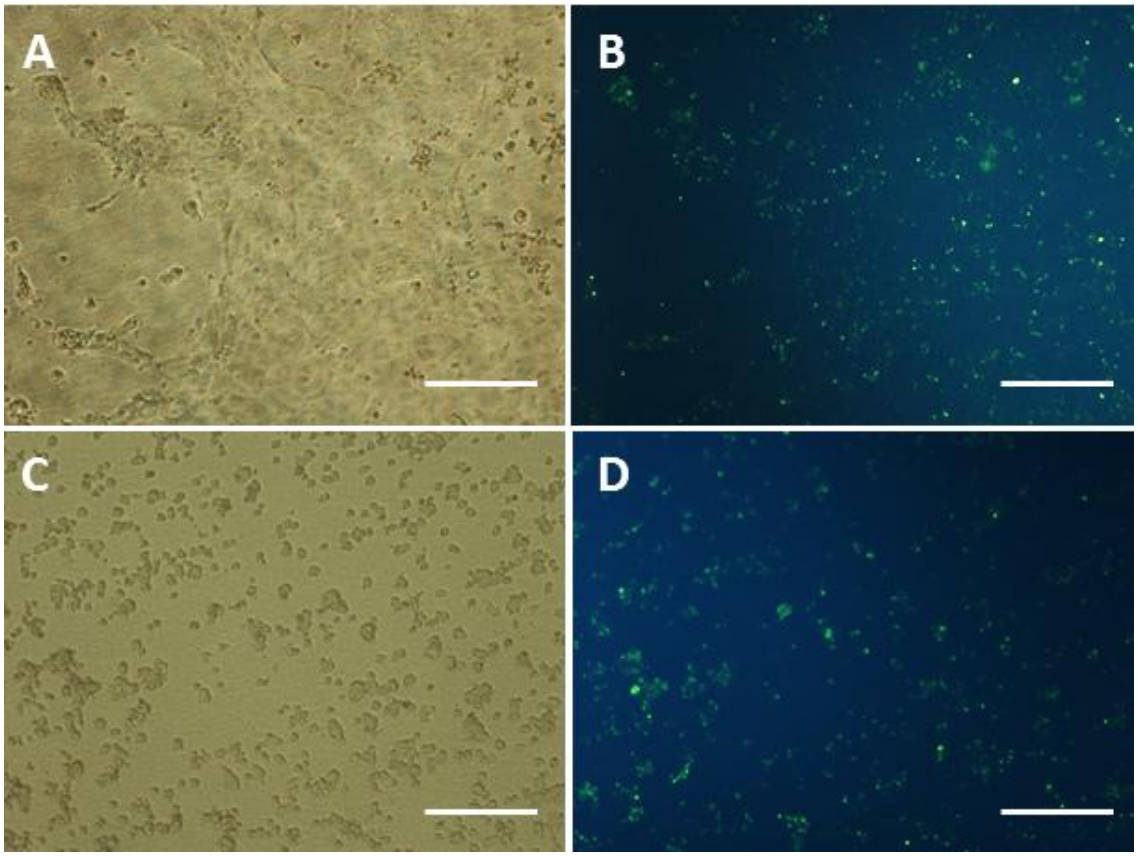


**Figure 3.4.6. HUVECs growing in the cell culture insert membrane**. (A) Phase contrast image and (B) Fluorescence image of HUVECs below the MEFs 3D cultures. (C) Phase contrast image and (D) Fluorescence image of HUVECs in the periphery of the MEFs 3D cultures. (Scale bar=200 μm)

Then, the possible switch to osteogenic commitment after 10 days of coculture independently of the day of loading (5 or 10 days), was evaluated by assessing the expression of hypertrophic markers (Coll X, Runx2) and the angiogenic factor VEGF [13,29]. In addition, the expression of Coll I and II was also studied over time to assess the change to hypertrophy, which is the first step in the endochondral ossification process. Finally, in order to confirm ossification, von Kossa staining was performed to detect calcium mineralization of the extracellular matrix which is the final step of osteogenic differentiation [30].

In terms of hypertrophic markers, RT-PCR results showed an expression of Runx2 which seemed higher in cocultures than in MEFs 3D-constructs (Figure 3.4.7). Instead, the expression of Runx2 was observed with WB only in cocultures when endothelial cells were loaded after 10 days of culture (Figure 3.4.8, A). The results obtained were contradictory since a clear expression of Runx2 was observed by RT-PCR. Therefore, we speculated that this effect could be influenced by the fact that Runx2 is a transcription factor expressed in low amounts and hence it may be difficult to observe by WB.

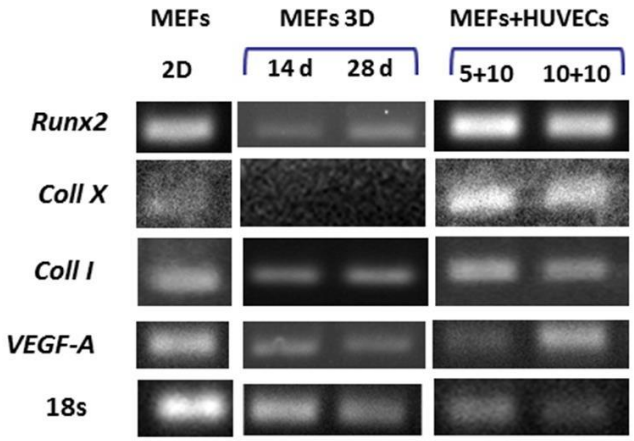


**Figure 3.4.7. RT-PCR of MEFs and loading cocultures.** Runx2, Coll X, Coll I and VEGF expression of 2D cultures of MEFs, 3D cultures of MEFs after 14 and 28 days of culture in 0.07%(w/v) RAD16-I and 3D cocultures where HUVECs were loaded after 5 days (5+10) or loaded after 10 days (10+10) and cocultured for 10 more extra days.

Remarkably, RT-PCR results showed a clear up-regulation of Coll X only in cocultures containing endothelial cells (Figure 3.4.7). However, WB showed that its expression was weak at both times of culture (Figure 3.4.8, A). This was the first time that Coll X was expressed in our 3D-culture system and as a consequence it could be an evidence of the hypertrophic switch of MEFs due to their cross-talk with endothelial cells. Besides, VEGF expression, which it is necessary for the angiogenic switch during bone development, was observed by RT-PCR in all the cultures tested which suggested a constitutive expression of this marker in MEFs (Figure 3.4.7).

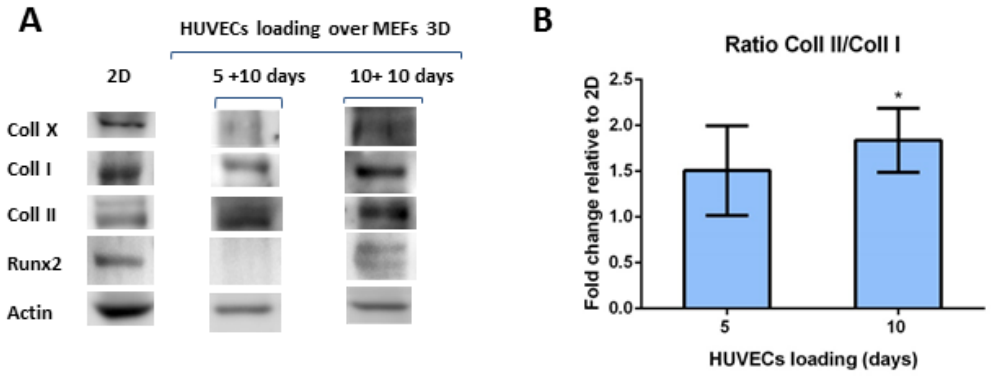


**Figure 3.4.8. Western blot of MEFs and loading cocultures.** (A) Runx2, Coll I, II and X expression of 2D cultures of MEFs and 3D cocultures where HUVECs were loaded after 5 days (5+10) or loaded after 10 days (10+10) and cocultured for 10 more extra days. Actin expression was used as internal control. (B) Ratio Coll II/ Coll I calculated from the western blot band areas normalized by Actin from (A). (Statistical differences are indicated as* for $p<0.05$, Unpaired t-student, n=3).

Then, the expression of collagens type I and II was also studied, according to the results obtained by WB, Coll I was expressed all the days of culture, while Coll that the expression of Coll II was up-regulated over the time of the culture (Figure 3.4.8, A). These observations were reflected in the ratio Coll II / Coll I, which increased over the time of culture (Figure 3.4.8, B).

These results suggested that MEFs were committing to chondrogenic lineage, which is necessary for further endochondral ossification. However, the ratio Coll II/ Coll I was lower than the observed in the MEFs 3D-constructs described in Chapter 2 (Figure 2.4.5).

Finally, Von Kossa staining was performed to determine the mineralization of the ECM. In this staining, the calcium ions, mainly in phosphate and carbonate salts, are substituted by silver cations from a silver nitrate solution supplied to the cell culture, which subsequently reduces, forming black precipitates observable under the microscope. Remarkably, mineralization of the extracellular matrix was only observed in the coculture system by evident formation of black silver precipitates easily observed under the microscope. Besides, it was observed that when HUVECs were loaded after 1 or 5 days of MEFs culture, mineralization was confined mostly at the edges of the constructs but when the HUVECs were loaded after 10 days, mineralization was more generalized in the surface of the cocultures (Figure 3.4.9).

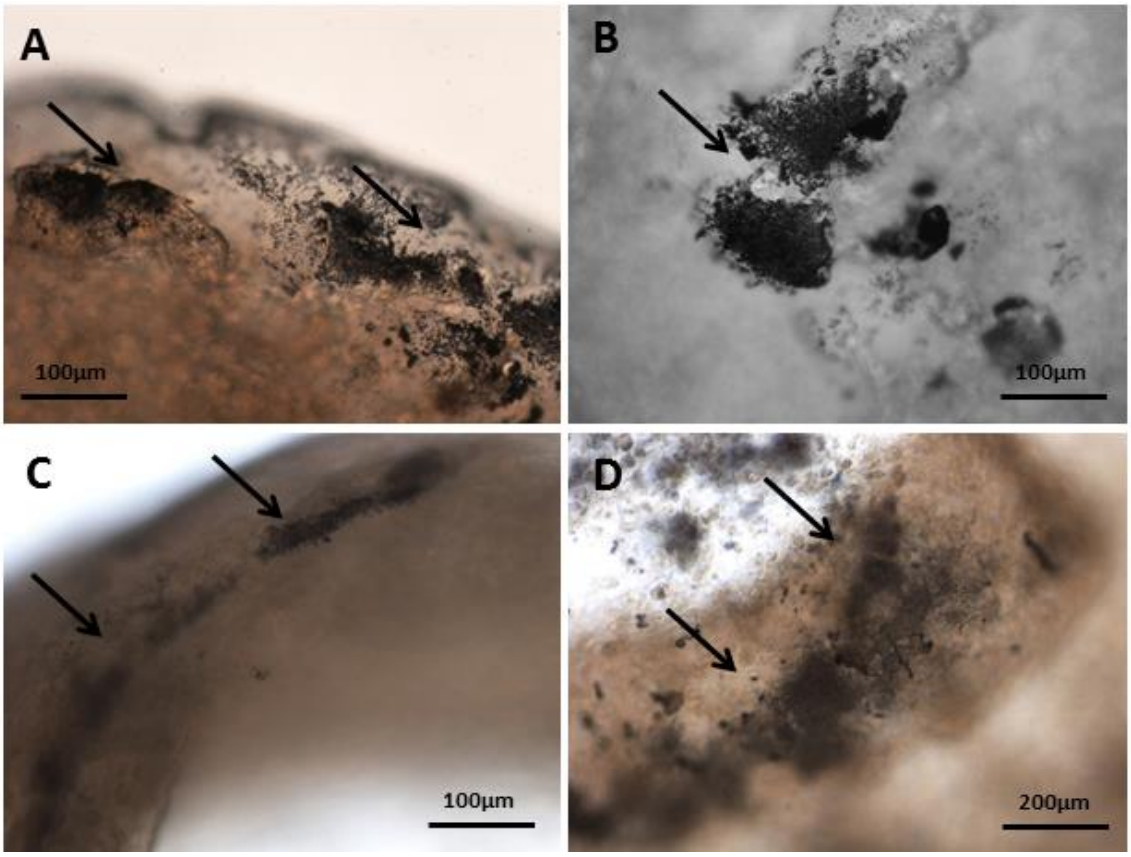


**Figure 3.4.9. Von Kossa staining of loading cocultures.** HUVECs were loaded over MEFs cultures after (A, B) 1, (C) 5, (D) and 10 days of culture and fixed 10 days later.

When looking at the fluorescence images of cocultures where the endothelial cells were loaded after 5 days of culture and fixed after 10 days of coculture, HUVECs were located over the MEFs cultures and were associated to zones on which the Von Kossa staining was positive (Figure 3.4.10). These results suggested that matrix mineralization was developed at the interaction site between MEFs and endothelial cells.

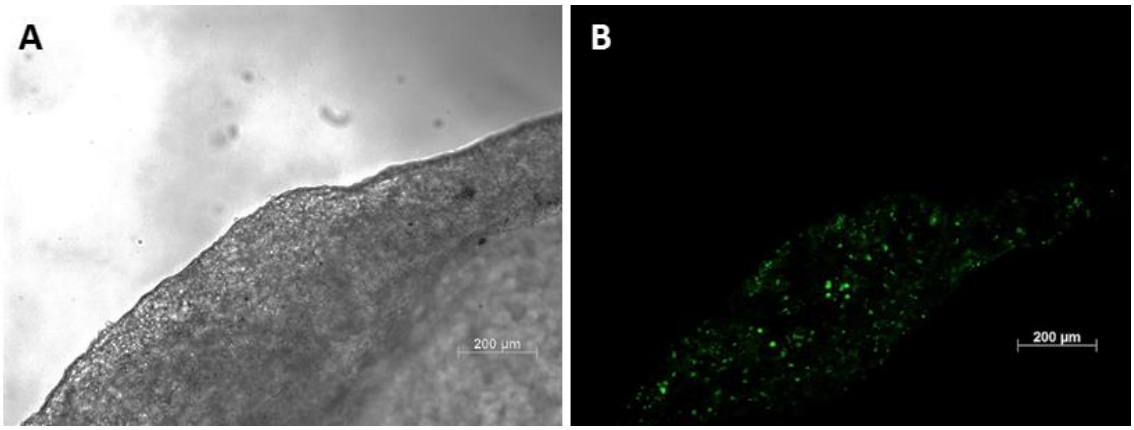


**Figure 3.4.10. Localization of labeled HUVECs.** Endothelial cells were loaded after 5 days of culture and fixed 10 days later. (A) Phase contrast image and (B) Fluorescence image.

### *Encapsulation cocultures for the biological osteogenic induction of MEFs*

The second type of cocultures prepared consisted of the encapsulation of MEFs and HUVECs in 0.07% (w/v) RAD16-I and at a final concentration of $1x10^6$ cells/mL for each cell type in order to maintain the cell density of $2x10^6$ cells/mL used in the MEFs 3D cultures. Then, these cocultures were maintained for 5 and 21 days with FM.

First of all, it was observed that MEFs migrated in the cocultures, proliferated and developed cell-cell networks as described in Chapter 2 for MEFs cultures (Figure 3.4.11, A, B). However, although final cell density was the same in the cocultures and in the cultures of MEFs, the amount of fibroblasts was half as much and as a consequence the cell network was weaker and the structure did not contract as observed before (Figure 3.4.11, C). Then, viability was evaluated qualitatively using a live and dead staining which showed that almost all cells were alive after 21 days of coculture (Figure 3.4.11, D).

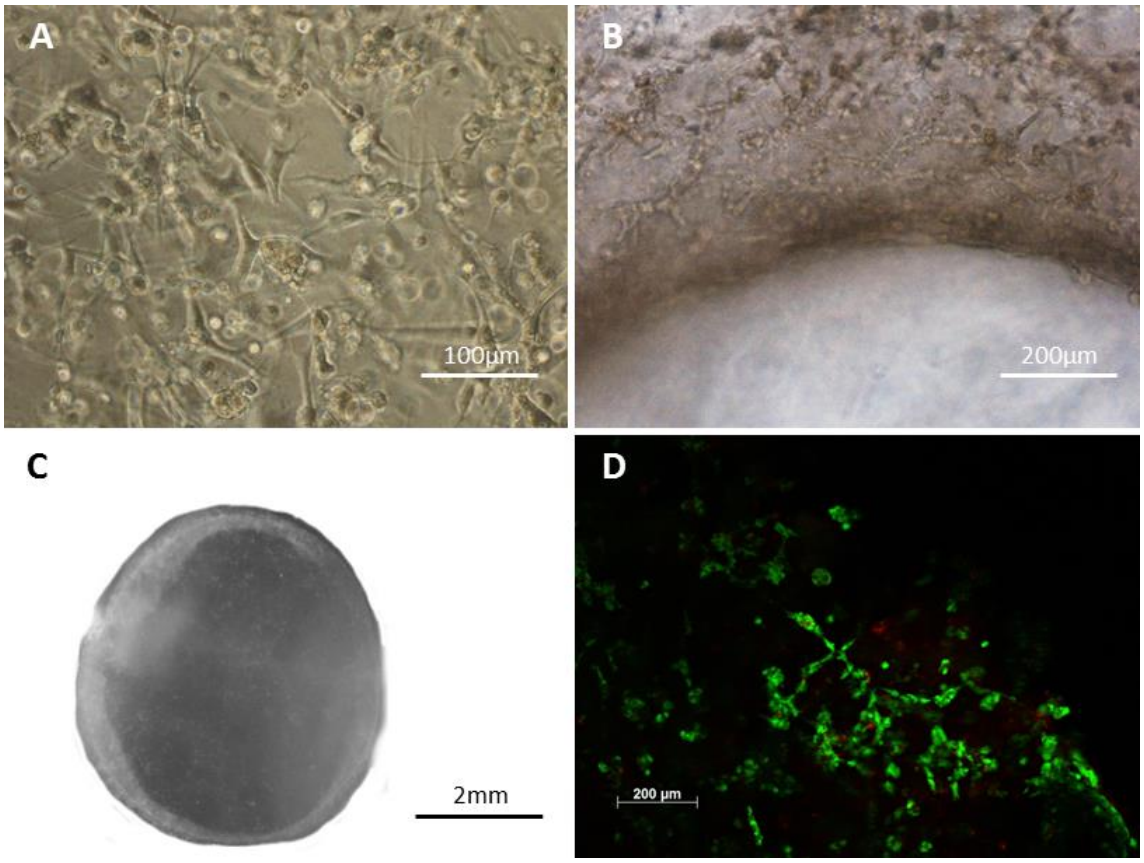


**Figure 3.4.11. Encapsulation cocultures behavior.(**A) Phase contrast image of cocultures after 1 day and (B) 5 days of culture. (C) Coculture morphology after 5 days of culture, same contraction was observed after 21 days of culture. (D) Live and dead staining after 21 days of culture.

In addition, HUVECs labeled with the nanocrystals as previously described were used for the encapsulation cocultures. The visualization of the cocultures under fluorescent microscopy allowed the localization of the labeled cells (Figure 3.4.12).

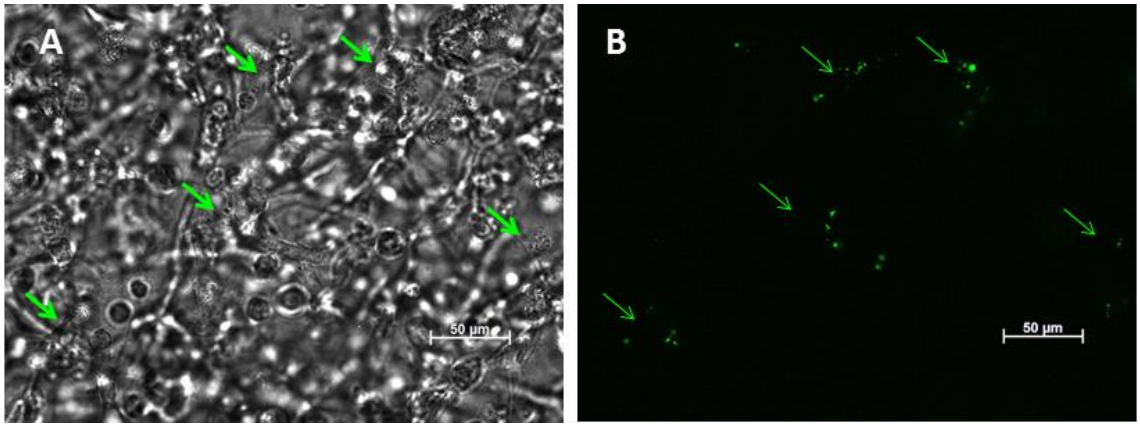


**Figure 3.4.12. Labeled HUVECs localization. (**A) Phase contrast image and (B) Fluorescence image of encapsulation cocultures after 1 day of culture.

Then, RNA extraction of the samples was performed in order to obtain cDNA for the analysis of gene expression. However, due to the low cell density after 21 days of culture, the obtained concentrations of RNA were very low. In addition, the ratios 260/230 and 260/280 obtained indicated presence of proteins, solvent or other contaminants. As a consequence, the RT-PCR with those samples was not performed, and samples were only analyzed for protein expression with WB.

Regarding hypertrophic markers, the expression of Runx2 was only observed in 2D control samples of MEFs but not in any coculture (Figure 3.4.13, A). These results could be influenced by the fact that Runx2 is a transcription factor expressed by MEFs, and in this type of coculture the quantity of this cell type is half as much as in the regular encapsulations. Hence, it may be difficult to observe the expression of Runx2 with WB like in the loading cocultures where Runx2 was perfectly observed by RT-PCR but its expression was not detected with WB. Remarkably, a weak band was observed again related to the expression of Coll X after 5 and 21 days of coculture which could indicate a change in cell behavior to osteogenic commitment (Figure 3.4.13, A).

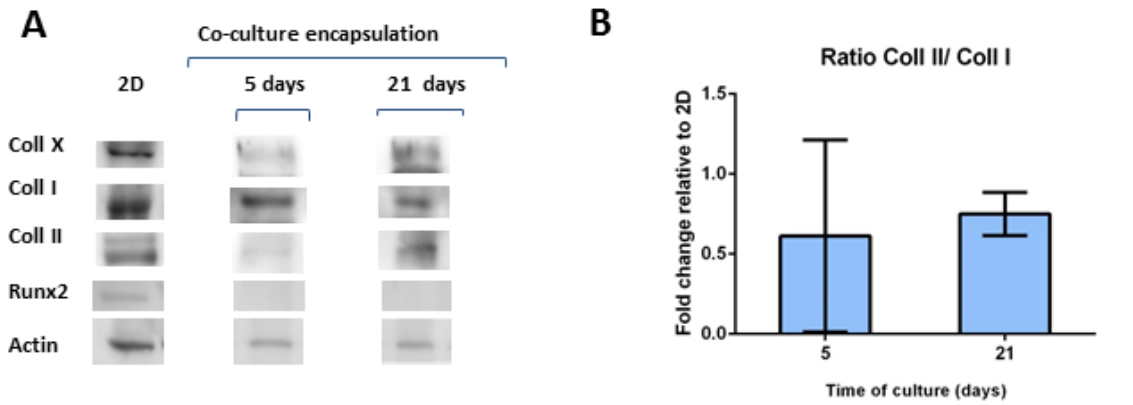


**Figure 3.4.13. Western blot of MEFs and cocultures.** (A) Runx2, Coll I, II and X expression of 2D cultures of MEFs, encapsulation cocultures after 5 and 21 days of culture. Actin expression was used as internal control. (B) Ratio Coll II/ Coll I calculated from the western blot band areas normalized by Actin from (A).

Then, the expression of collagens type I and II was also studied, according to the results obtained by WB, Coll I was expressed all the days of culture, while Coll II seemed to be expressed at day 21 of culture (Figure 3.4.13, A). These observations were reflected in the ratio Coll II / Coll I, which increased over the time of culture (Figure 3.4.13, B). However, these values were not significantly different from values obtained for 2D cultures of MEFs used as control. These results suggested that MEFs were not committing to chondrogenic lineage, which is the first step of endochondral ossification, contrary to loading cocultures described before.

Finally, Von Kossa staining after 21 days of culture revealed an isolated and localized mineralization in some areas with tubular structures, which suggested the presence of endothelial cells (Figure 3.4.14). We hypothesized that this mineralization was located in areas of direct interaction between fibroblasts and endothelial cells where cells engaged in a local remodeling of the ECM.

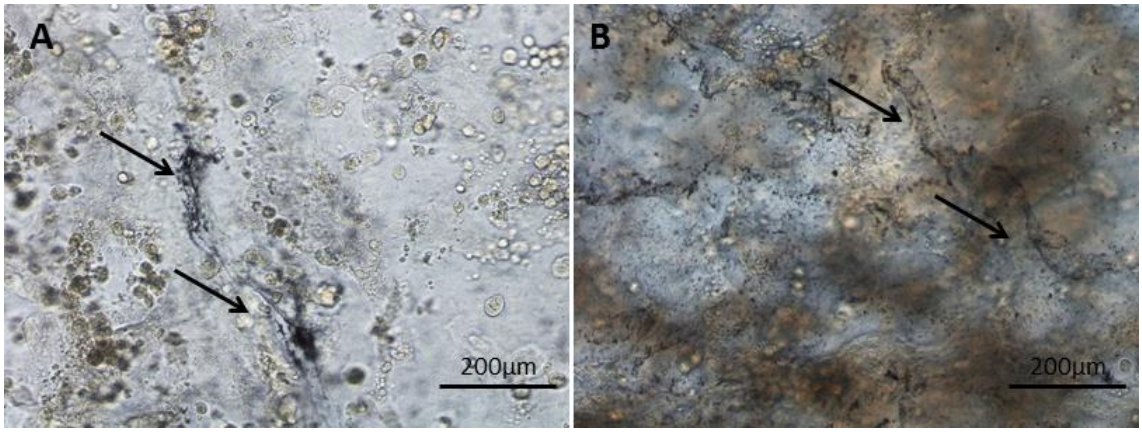


**Figure 3.4.14. Von Kossa staining of encapsulation cocultures after 21 days of culture**. Arrows indicate mineralized areas.

### *Cocultures of MEFs and HUVECs in 2D*

Finally, 2D cocultures were prepared to better understand the dialog between fibroblasts and endothelial cells observed in the previous sections. For this purpose, HUVECs and MEFs were cultured separately in 2D at a seeding density of 30.000 cell/cm$^2$ and maintained during 3 days in complete endothelial and fibroblast media respectively. Then, a suspension of HUVECs to a final concentration of 15.000 cells/cm$^2$ was loaded on MEFs cultures, and maintained for 7 days in different culture mediums: FM, FM+EBM (1:1) or EBM.

Over the time, some areas with higher densities of cells were generated over the MEFs 2D cultures. These areas were better localized when the cell nuclei were stained with DAPI. Interestingly, this effect was exaggerated when cocultures were maintained in complete endothelial culture medium (Figure 3.4.15). These results suggested that the growth factors added in the culture media together with the intimate cell interactions between fibroblasts and endothelial cells induced the formation of these structures. Remarkably, it was also observed that some cells underwent adipogenic differentiation evidenced by formation of lipid droplets stained with Nile Red (Figure 3.4.15, D,F). This lipid formation was only observed in the presence of EBM, which is composed of a cocktail of growth factors that could induce the adipogenic differentiation.

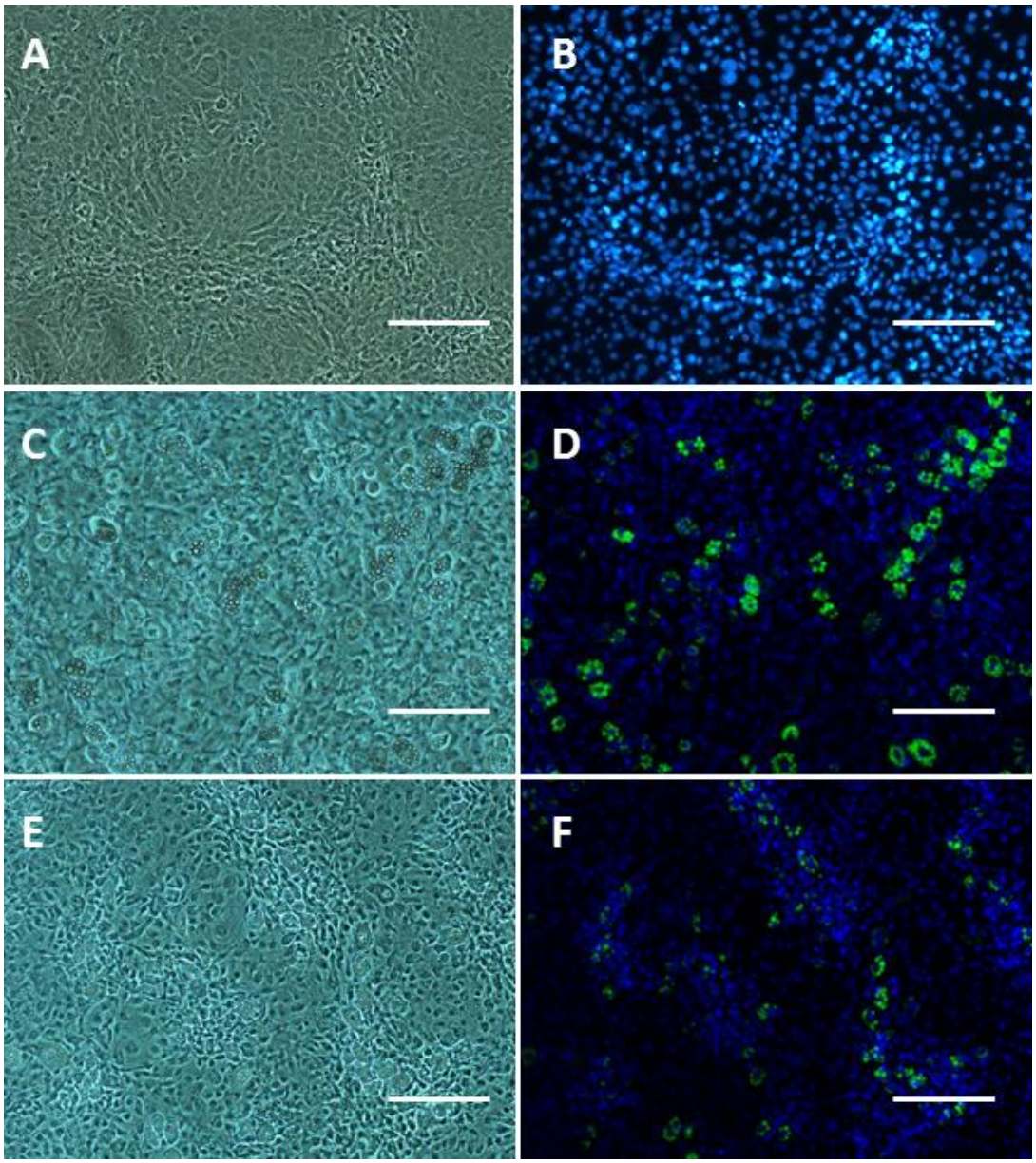


**Figure 3.4.15. 2D cocultures of MEFs and HUVECs.** Cultures were prepared as described and maintained for 7 days in (A, B) Fibroblast media (FM); (C, D) Endothelial media and Fibroblast media (FM+EBM) (1:1) and (E, F) Endothelial media (EBM). (B, D, F) Fluorescence images show the nuclei stained with DAPI (blue) and lipid droplets stained with Nile Red (green). **(**Scale bar=200µm)

In view of the results obtained in the previous chapter where MEFs underwent adipogenesis in presence of PDGF together with the mesodermal origin of fibroblasts, we hypothesized that MEFs were the cell type that committed to the observed adipogenesis. In addition, it was reported that endothelial cells enhanced the adipogenic potential of preadipocytes which could indicate a combined effect with the growth factors present in the culture media [31]. On the other hand, some studies suggested an endothelial origin of murine and human adipocytes [32,33], which could indicate that HUVECs were responsible for the adipogenic differentiation observed in the cocultures. Thus, the cell type involved in the formation of lipid droplets observed in the 2D cocultures described in this section remained unclear.

Finally, with the purpose to elucidate the cell type that formed the areas of high cell density, Platelet Endothelial cell adhesion molecule (PECAM) was analyzed. PECAM is a major constituent of endothelial cell intercellular junction, and it is not present in fibroblasts [34]. The expression of PECAM was analyzed by immunofluorescence in order to locate its expression. As expected, the areas of high cell density that recreated tubular structures were clearly positive for the expression of the endothelial cell marker, which evidenced that these areas were mainly composed by HUVECs (Figure 3.4.16).

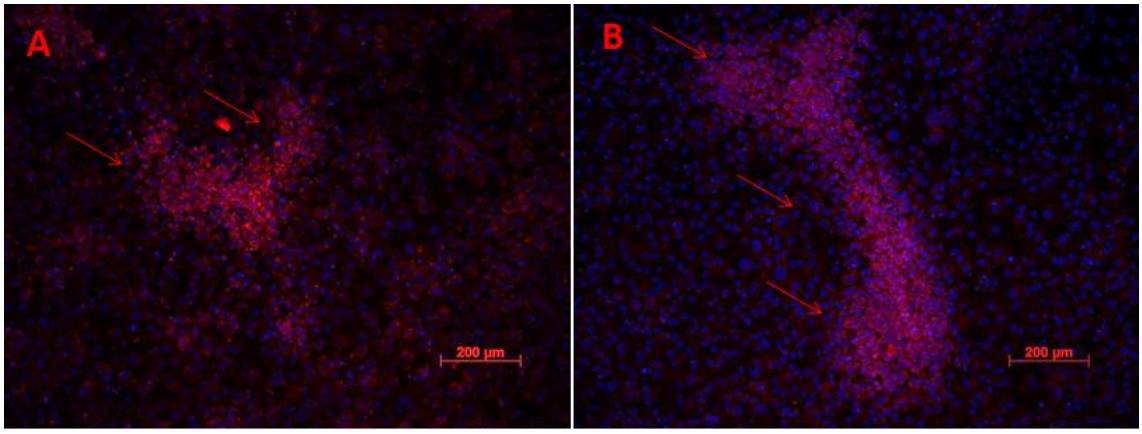


**Figure 3.4.16. PECAM immunofluorescence.** Cultures were prepared as described and maintained for 7 days A) Endothelial media and Fibroblast media (1:1) and B) Endothelial media. PECAM protein was immunostained with an antibody anti-PECAM developed with a secondary antibody Alexafluor680-congugated (red). Nuclei were stained with DAPI (blue).

## 3.5 Discussion

Bone grafts are needed when the required bone regeneration exceeds the natural potential for self-healing, as in large bone defects occurring after trauma, infection, tumor resection or skeletal abnormalities [2]. Although in the clinical setting, the gold standard to treat bone defects consists of the transplantation of autologous bone grafts, the availability of patients' own bone tissue that can be used for these procedures is limited [2]. Even though several strategies of bone tissue engineering have been developed, challenges still remain in the inability to reproduce an engineered well vascularized bone that truly mimics natural bone blood vessels. This parameter is crucial to ensure optimal cell survival and implant integration after *in vivo* engraftment [35]. For years it has been recognized that engineering of large bone constructs will be feasible only if the hurdle of vascularization is overcome [36].

Although tissue engineering of bone has been traditionally focused on direct (intramembranous) bone formation, nowadays several groups are interested in endochondral bone formation since it is a more physiological approach which recreates most aspects of *in vivo* bone formation. These studies consists mainly of creating a cartilage template *in vitro* followed by its implantation *in vivo* where the template is vascularized and remodeled [7,36–39]. Since cartilage is an avascular

tissue, its cells are equipped to survive the poor oxygenation and nutritional conditions inherent to implanted tissues [36]. For this reason, forming bone through the production of a cartilaginous template may circumvent issues with supply of oxygen and nutrients of larger engineered constructs. Moreover, our long bones grow and most fractures heal through this mechanism which evidences the attractive characteristics of endochondral bone tissue engineering [36].

Following this hypothesis, the switch from chondrogenic to ostegenic-like commitment of MEFs in the self-assembling peptide RAD16-I has been described in this thesis. Up to now, osteogenic differentiation with MEFs in our laboratory had only been obtained thanks to the addition of specific chemical induction [40,41]. In that case, MEFs cultured in the self-assembling peptide were maintained with fibroblast media supplemented with dexamethasone, β-glycerophosphate, ascorbic acid and 1α,25-(OH)2 vitamin D3 as previously described [42]. Osteogenic differentiation was assessed based on matrix mineralization, collagen I synthesis, ALP activity, and expression of the osteoblast transcription factor Runx2 [40,41]. Similar results were also reported using mouse and human fibroblast, in both cases the osteogenic differentiation was obtained only when cells were maintained in osteogenic induction media [43,44].

However, a more physiological approach was described in this chapter which consisted on challenging the 3D-cultures of MEFs undergoing chondrogenesis to coculturing them with endothelial cells. It was hypothesized that the presence of endothelial cells could promote a switch in MEFs to an osteogenic-like commitment due to a crosstalk between the chondrogenic-like cells and the endothelial cells recreating an endochondral ossification process. Under these new conditions, the hypertrophic markers Coll X and Runx2 were up-regulated and von Kossa staining clearly showed matrix mineralization at the interaction site between MEFs and endothelial cells. These results evidenced that MEFs switched to osteogenic commitment due to the biological induction of the endothelial cells. Remarkably, this is the first description of osteogenic differentiation of fibroblast due to the crosstalk with endothelial cells. In spite of a deeper understanding of the osteogenic switch is needed, preliminary results suggest that the future *in vivo* implantation of the MEFs 3D-constructs in a mouse model of ectopic bone formation or in a fracture site would promote the formation of a vascularized bone graft. Coculture systems of MSCs and endothelial cells have also been reported as strategies for bone tissue engineering. In that cases, the main objective was to obtain pre-vascularized bone grafts *in vitro* and to avoid the aforementioned vascularization problems once the graft is implanted *in vivo* [19,45].

Interestingly, when cocultures of fibroblasts and endothelial cells were prepared in 2D, cell behavior radically changed. Osteogenic differentiation was not observed; however, some cells

underwent adipogenic differentiation evidenced by formation of lipid droplets. Since MEFs in the 2D cultures did not engage in the spontaneous chondrogenic differentiation observed in 3D, obtained results agree with the hypothesis that it is necessary a first step of chondrogenic commitment to later continue with the osteogenic differentiation process. Instead, 2D cocultures could be used to better understand the adipogenic differentiation of MEFs or to support the model for how adipogenesis and angiogenesis are coordinated during adipose tissue expansion [31–33].

## 3.6 Concluding Remarks

- MEFs undergoing chondrogenesis in the self-assembling peptide RAD16-I switched to osteogenic-like commitment due the biological induction of ECs in a coculture system. This is the first description of the osteogenic differentiation of fibroblast due to the crosstalk with endothelial cells.

- The osteogenic commitment of MEFs was evidenced by the expression of collagen type X and matrix mineralization. Additionally, other factors expressed by the mentioned cocultures were Runx2 and VEGF-A, which could promote the possible formation of new blood vessels, necessary for the endochondral ossification.

- Von Kossa staining showed matrix mineralization in areas of direct interaction between MEFs and ECs, which suggested an effective cross talk between MEFs and HUVECs that could be studied more in detail in future research projects.

- Preliminary results of osteogenic differentiation suggest that future *in vivo* implantation of the MEFs 3D-constructs in a mouse model of ectopic bone formation or in a fracture site would promote the formation of a vascularized bone graft.

## 3.7 References


1. Reis, R. L. From nano- to macro-scale : nanotechnology approaches for spatially controlled delivery of bioactive factors for bone and cartilage engineering R eview. **7,** 1045–1066 (2012).

2. Saxer, M. J. F., Schreiner, C. S. S., Scherberich, P. S. A. & Martin, M. H. I. Perspective on the Evolution of Cell-Based Bone Tissue Engineering Strategies. 1–7 (2012). doi:10.1159/000338362

3. Grayson, W. L. *et al.* Engineering anatomically shaped human bone grafts. **107,** 1–6 (2010).

4. Zakaria, S. Nanophase hydroxyapatite as a biomaterial in advanced hard tissue engineering: A review. *Tissue Eng Part B* 1–38 (2012).

5. Teixeira S, Fernandes H, Leusink A, van Blitterswijk C, Ferraz MP, Monteiro FJ, de B. J. In vivo evaluation of highly macroporous ceramic scaffolds for bone tissue engineering. *J Biomed Mater Res A* **93,** 567–75 (2010).

6. Nguyen, L. H. *et al.* Vascularized Bone Tissue Engineering :Approaches for Potential Improvement. *Tissue Eng Part B* **18,** (2012).

7. Lenas, P., Jr, M. M. & Luyten, F. Developmental engineering: a new paradigm for the design and manufacturing of cell-based products. Part II. From genes to networks: tissue engineering from the. *Tissue Eng Part B* **15,** 395–422 (2009).

8. Dreier, R. Hypertrophic differentiation of chondrocytes in osteoarthritis: the developmental aspect of degenerative joint disorders. *Arthritis Res Ther* **12,** 1–11 (2010).

9. Long, F. & Ornitz, D. M. Development of the endochondral skeleton. *Cold Spring Harb. Perspect. Biol.* **5,** 1–20 (2013).

10. Maes, C. *et al.* Osteoblast precursors, but not mature osteoblasts, move into developing and fractured bones along with invading blood vessels. *Dev. Cell* **19,** 329–44 (2010).

11. Gerber, H. P. & Ferrara, N. Angiogenesis and bone growth. *Trends Cardiovasc. Med.* **10,** 223–8 (2000).

12. Vu, T. H. *et al.* MMP-9/gelatinase B is a key regulator of growth plate angiogenesis and apoptosis of hypertrophic chondrocytes. *Cell* **93,** 411–22 (1998).

13. Ortega, N., Behonick, D. J. & Werb, Z. Matrix remodeling during endochondral ossification. *Trends Cell Biol* **14,** 86–93 (2004).

14. Mackie, E. J., Ahmed, Y. a, Tatarczuch, L., Chen, K.-S. & Mirams, M. Endochondral ossification: how cartilage is converted into bone in the developing skeleton. *Int. J. Biochem. Cell Biol.* **40,** 46–62 (2008).

15. Dy, P. *et al.* Sox9 directs hypertrophic maturation and blocks osteoblast differentiation of growth plate chondrocytes. *Dev. Cell* **22,** 597–609 (2012).

16. Akiyama, H. *et al.* Osteo-chondroprogenitor cells are derived from Sox9 expressing precursors. *Proc. Natl. Acad. Sci. U. S. A.* **102,** 14665–70 (2005).

17. Carano, R. A. D. & Filvaroff, E. H. Angiogenesis and bone repair Bone healing. **8,** 980–989 (2003).

18. Maes, C. Role and regulation of vascularization processes in endochondral bones. *Calcif. Tissue Int.* **92,** 307–23 (2013).

19. Grellier, M., Bordenave, L. & Amédée, J. Cell-to-cell communication between osteogenic and endothelial lineages: implications for tissue engineering. *Trends Biotechnol.* **27,** 562–71 (2009).

20. Rouwkema, J., de Boer, J. & Van Blitterswijk, C. Endothelial cells assemble into a 3-dimensional prevascular network in a bone tissue engineering construct. *Tissue Eng.* **12,** 2685–2693 (2006).

21. Sun, H., Qu, Z., Guo, Y., Zang, G. & Yang, B. In vitro and in vivo effects of rat kidney vascular endothelial cells on osteogenesis of rat bone marrow mesenchymal stem cells growing on polylactide-glycoli acid (PLGA) scaffolds. *Biomed. Eng. Online* **6,** 41 (2007).

22. Hofmann, A. *et al.* The effect of human osteoblasts on proliferation and neo-vessel formation of human umbilical vein endothelial cells in a long-term 3D co-culture on polyurethane scaffolds. *Biomaterials* **29,** 4217–26 (2008).

23. Grellier, M. *et al.* The effect of the co-immobilization of human osteoprogenitors and endothelial cells within alginate microspheres on mineralization in a bone defect. *Biomaterials* **30,** 3271–8 (2009).

24. Fuchs, S. *et al.* Dynamic processes involved in the pre-vascularization of silk fibroin constructs for bone regeneration using outgrowth endothelial cells. *Biomaterials* **30,** 1329–38 (2009).

25. Ma, J. & Beucken, J. van den. Coculture of osteoblasts and endothelial cells: optimization of culture medium and cell ratio. *Tissue Eng. Part C* **17,** 349–357 (2010).

26. Xue, Y., Xing, Z., Hellem, S., Arvidson, K. & Mustafa, K. Endothelial cells influence the osteogenic potential of bone marrow stromal cells. *Biomed. Eng. Online* **8,** 34 (2009).

27. Kim, J. *et al.* Synergistic effects of nanotopography and co-culture with endothelial cells on osteogenesis of mesenchymal stem cells. *Biomaterials* **34,** 7257–68 (2013).

28. Zhou, G. *et al.* Dominance of SOX9 function over RUNX2 during skeletogenesis. *Proc. Natl. Acad. Sci. U.S.A* **103,** 19004–9 (2006).

29. Zelzer, E. *et al.* VEGFA is necessary for chondrocyte survival during bone development. *Development* **131,** 2161–71 (2004).

30. Garreta, E., Genové, E., Borrós, S. & Semino, C. E. Osteogenic Differentiation of Mouse Embryonic Stem Cells and Mouse Embryonic Fibroblasts in a Three-Dimensional. *Tissue Eng Part A* **12,** 2215–2227 (2006).

31. Lai, N., Jayaraman, A. & Lee, K. Enhanced proliferation of human umbilical vein endothelial cells and differentiation of 3T3-L1 adipocytes in coculture. *Tissue Eng Part A* **15,** 1053–61 (2009).

32. Frontini, A., Giordano, A. & Cinti, S. Endothelial cells of adipose tissues A niche of adipogenesis. *Cell Cycle* **11,** 2765–2766 (2012).

33. Tran, K. *et al.* The vascular endothelium of the adipose tissue give rise to both white and brown fat cells. *Cell Metab* **15,** 222–229 (2013).

34. Newman, P. J. Perspectives Series : Cell Adhesion in Vascular Biology The Biology of PECAM-1. **99,** 3–8 (1997).

35. Auger, F. a, Gibot, L. & Lacroix, D. The Pivotal Role of Vascularization in Tissue Engineering. *Annu. Rev. Biomed. Eng.* 177–200 (2013). doi:10.1146/annurev-bioeng-071812-152428

36. Gawlitta, D., Ph, D., Farrell, E., Malda, J. & Creemers, L. B. Modulating Endochondral Ossification. *Tissue Eng Part B* **16,** 385–395 (2010).

37. Jukes, J. & Both, S. Endochondral bone tissue engineering using embryonic stem cells. *Proc. Natl. Acad. Sci. U.S.A* **105,** 6840–6845 (2008).

38. Scotti, C. Recapitulation of endochondral bone formation using human adult mesenchymal stem cells as a paradigm for developmental engineering. *Proc. Natl. Acad. Sci. U.S.A* **107,** 7251–7256 (2010).

39. Farrell, E. *et al.* In-vivo generation of bone via endochondral ossification by in-vitro chondrogenic priming of adult human and rat mesenchymal stem cells. *BMC Musculoskelet Disord* **12,** 31 (2011).

40. Quintana, L. *et al.* Early Tissue Patterning Recreated by Mouse Embryonic Fibroblasts in a Three-Dimensional Environment. *Tissue Eng.* **15,** (2009).

41. Garreta, E., Genove, E., Borros, S. & Semino, C. E. Osteogenic differentiation of mouse embryonic stem cells and mouse embryonic fibroblasts in a three-dimensional self-assembling peptide scaffold. *Tissue Eng.* **12,** 1–14 (2006).

42. Jaiswal, N., Haynesworth, S. E., Caplan, a I. & Bruder, S. P. Osteogenic differentiation of purified, culture-expanded human mesenchymal stem cells in vitro. *J. Cell. Biochem.* **64,** 295–312 (1997).

43. Shui, C. & Scutt, A. M. Mouse embryo-derived NIH3T3 fibroblasts adopt an osteoblast-like phenotype when treated with 1alpha,25-dihydroxyvitamin D(3) and dexamethasone in vitro. *J. Cell. Physiol.* **193,** 164–72 (2002).

44. Hee, C. K., Jonikas, M. a & Nicoll, S. B. Influence of three-dimensional scaffold on the expression of osteogenic differentiation markers by human dermal fibroblasts. *Biomaterials* **27,** 875–84 (2006).

45. Brennan, M. A., Davaine, J.-M. & Layrolle, P. Pre-vascularization of bone tissue-engineered constructs. *Stem Cell Res. Ther.* **4,** 96 (2013).

# Chapter 4: Development of a new biomaterial for tissue engineering applications based on the self-assembling peptide RAD16-I

## 4.1 Introduction

### 4.1.1 Overview

Nowadays, one of the major challenges in tissue engineering is vascularization of engineered tissues. Regardless of the specific approach, this is an important issue because any engineered tissue construct that involves living cells needs an adequate blood supply for cell survival in tissues of macroscopic dimensions [1–3]. *In vivo* almost all tissues are vascularized with a maximum distance between capillaries of 200 µm which correlates with the diffusion limit of oxygen [4]. For this reason, any engineered tissue that exceeds 400 µm must be vascularized to have easy access to oxygen and nutrients, as well as elimination of carbon dioxide and other cellular waste products (Figure 4.1.1) [2]. Only cells from skin, cartilage and cornea can be supplied with nutrients from blood vessel systems that are further away [4].

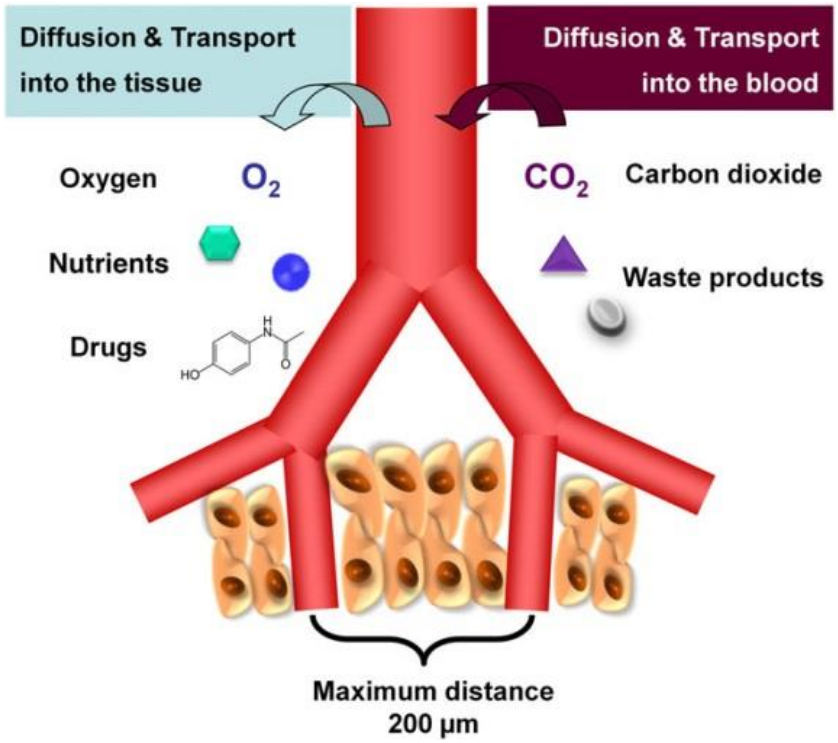


**Figure 4.1.1. Schematic description of diffusion and transport processes in vascularized tissues *in vivo*.** The surrounding tissue is supplied with oxygen, nutrients and drugs via the vasculature. Waste products and CO2 are removed from the tissue into the blood vessels. (Image adapted from Novosel et al.[4])

### 4.1.2 Vascular tissue engineering

The strategies that have been designed in tissue engineering in order to solve this issue are mainly divided in two groups: 1, promotion of rapid vascularization after transplantation by the host's own system and 2, pre-vascularization of the engineered construct *in vitro* [2] (Figure 4.1.2).

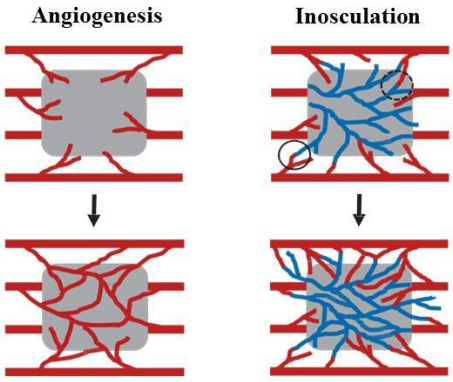


**Figure 4.1.2. Schematic drawing of angiogenesis and inosculation.** Angiogenesis is characterized by the ingrowth of newly formed blood vessels from the host tissue (red vessels). In the inosculation, the pre-formed blood vessels (blue vessels) develop interconnections to the host microvasculature within the construct or within the surrounding host tissue. (Image adapted from Laschke et al.[5])

In the first case, the ingrowth of newly formed blood vessels into an implanted tissue construct is a highly dynamic process. The initial step in this process is activation of host microvasculature at the implantation site by angiogenic growth factors, such as vascular endothelial growth factor (VEGF) or basic fibroblast growth factor (FGFβ) [6]. These factors can be produced by the host tissue itself or delivered by artificially designed systems. Then, upon angiogenic stimulation, endothelial cells degrade their surrounding basement membrane and migrate to form capillary sprouts and proliferate, elongating the newly blood vessels [3,7]. Several approaches have been developed to stimulate angiogenesis in the tissue construct focusing on scaffold bioactivation by the incorporation of deliverable growth factors (GF). Some examples reported their covalent immobilization to scaffolds, non-covalent bound to nanoparticles or entrapment in microspheres with defined degradation rates [6]. The main disadvantage of this strategy is that angiogenesis is a time-consuming process and when the vascularization is achieved most cells could be dead due to the absence of oxygen and nutrients during the initial days after implantation.

On the other hand, pre-vascularization or inosculation approaches use pre-formed microvascular networks within tissue constructs prior to their implantation in order to decrease the time of vascularization. The pre-vascularization can be obtained *in vitro* normally using endothelial cells. *In vivo* approaches include implantation of the scaffold in a well-vascularized area, and, after sufficient vascularization, the construct is explanted again and can be inserted into the

ischemic target site where it should rapidly develop interconnections with the host microvasculature [6]. The main disadvantage of the *in vivo* approach is the need of at least three surgeries: the implantation of the cell-free scaffold, the removal and the proximate insertion of the pre-vascularized biomaterial. Interestingly, inosculation was observed in nude mice within the first 4 days after implantation as compared to the 14 days that took the ingrowth of new blood vessels in the no pre-vascularized control [8]. However, experimental studies indicate that this approach does not ensure appropriate blood perfusion of grafted tissue constructs during the very first days after implantation [5]. Hence, many attempts have emerged to improve the existing approaches by tailoring scaffolds with growth factors combined with different types of cells.

### *Cells*

Independently of the strategy used, the source of cells used to create a vascular network is a critical issue. The generation of functional vessels has been reported using different mature endothelial cells (ECs) including human dermal microvascular ECs (HDMECs) or human umbilical vein ECs (HUVECs) [9]. Furthermore, the coculture of ECs with different cell types such as fibroblasts, adipocytes or osteoblasts is crucial to support angiogenic mechanisms [4,10,11]. However, ECs present some disadvantages such as low proliferation rates, heterogeneity in the genotype and phenotype, requirement of an invasive procedure to harvest. Alternatively, endothelial progenitor cells (EPCs) have been widely used in tissue engineering applications due to their ability to migrate and incorporate into ischemic tissue and promote neovascularization. Moreover, EPCs can be derived from bone marrow, fat tissue and peripheral blood. This type of cells has also been cocultured with different cell types such as fibroblasts or mesenchymal stem cells showing a modulation of the angiogenic process [9,12]. Finally, a wide spectrum of studies reported the use of different types of stem cells in vascular tissue engineering including bone marrow, adipose derived or mesenchymal stem cells [13].

### *Growth factors*

Angiogenic growth factors are used alone or in combination with cells and biomaterials as powerful initiators of neovascularization. They can activate endothelial or progenitor cells and promote migration towards the growth factor gradient. Moreover, they stimulate cell assembly, vessel formation and maturation. The main factors contributing to the initiation of angiogenesis, and induction of endothelial cell proliferation and migration are: vascular endothelial growth factor (VEGF), basic fibroblast growth factor (FGFβ) and hepatocyte growth factor (HGF) [4,14]. However, VEGF and its receptors constitute the key signaling system for angiogenic activity in tissue formation. In addition, different cytokines serve as indirect angiogenic factors and are involved in the regeneration of endothelial tube. Among them, platelet-derived growth factor (PDGF) and angiopoietines are agents that recruit pericytes and smooth muscle cells; and transforming growth factor beta (TGFβ) causes ECM deposition for stabilization of new vessels

[15]. The main issue when designing a new strategy is to properly deliver these signaling molecules locally and temporally to obtain the desired biological outcomes, while avoiding unfavorable side effects.

### *Scaffolds*

In the last years, different types of biomaterials have been developed as scaffolds for vascular tissue engineering which can be divided in natural and synthetic biomaterials. In the group of natural materials, the reuse of biological structures is a future promising approach for tissue engineering applications. This procedure consists on the decellularization of a mammalian section, and the repopulation of the matrix with desirable human primary cells. Some examples illustrate the extensive use of decellularized small pig intestine or vascular tissues like aorta [4,16,17]. However, the main problem associated with this approach is the rejection of allografts and xenografts. Besides, natural derived polymers such as collagen [18], gelatin [19] or hyaluronan [20,21] have been widely reported for vascular tissue engineering applications [22].

On the other hand, the use of synthetic polymers is increasing due to their controlled properties and composition, although improving their biocompatibility and bioactivity is a major concern in the field of biomaterials. Among others, some synthetic polymers reported for vascular tissue engineering applications are poly(vinylalcohol) [23], polycaprolactone [24,25] and polyethylene glycol [26,27]. As part of synthetic materials, self-assembling peptides are gaining importance in vascular tissue engineering due to their application as drug delivery systems for angiogenic growth factors. As it has been reviewed in Chapter 1, this class of peptides is characterized by self-assembling under physiological conditions into a network of interweaving nanofibers of around 10 nm diameter, forming a hydrogel scaffold with pores sizes of 50–200 nm and over 99% water content[28]. Other properties of self-assembling peptides are the ease of synthesis, modulation of mechanical properties, injectability, biocompatibility, biodegradability and options for the incorporation of bioactive motifs or molecules [29,30]. Some examples of their use in vascular tissue engineering exhibited the delivery of $VEGF_{165}$, or combined delivery of PDGF and FGFβ to promote cardiac regeneration after infarct using *in vivo* models[31–33]. Interestingly, intramyocardial injection of the self-assembling peptide RAD16-II combined with VEGF improved post-infarction neovascularization in rats and pigs[31]. Moreover, the delivery of VEGF from a tailored self-assembling peptide showed improved cardiac function, reduced scar size and collagen deposition in a rat model[32]. Finally, the dual delivery of PDGF and FGF lead to myocardial protection, stable vessel formation, and improvement in cardiac function also in a rat model [33]. Remarkably, in all cases there was recovery of damaged tissue thanks to the stimulation of angiogenesis. These results prove their potentiality as delivery systems for vascular tissue engineering.

### 4.1.3 Heparin as a strategy for growth factor delivery

Heparin has numerous important biological activities associated with its interaction with diverse proteins. It is a linear polydisperse sulphated polysaccharide consisting mainly of repeating units of 1→4-linked pyranosyluronic acid and 2-amino- 2-deoxyglucopyranose (glucosamine) residues. The presence and frequency of these saccharide units vary with the tissue source from which heparin is extracted (Figure 4.1.3). It possesses the highest negative charge density of all known biological macromolecules and has an average of 2.7 negative charges per disaccharide provided by sulfonic and carboxyl groups. Consequently, the most common binding between heparin and proteins is through ionic interactions and as a consequence most heparin-binding sites in proteins are characterized by the presence of clusters of positively charged basic amino acids. Non-electrostatic interactions such as hydrogen bonding and hydrophobic interactions can also contribute to the stability of heparin–protein complexes [34,35].

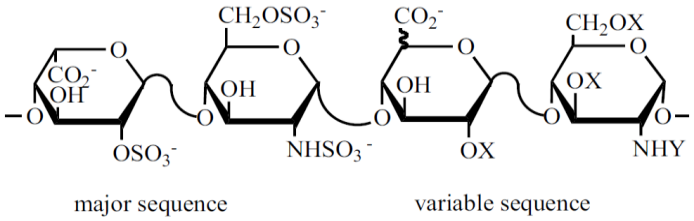


**Figure 4.1.3. Heparin structure.** Heparin is a linear polysaccharide with variable composition consisting on repeating units of disaccharides with its major sequence containing a containing an uronic acid residue and a glucosamine residue. Its composition varies depending on the tissue.(X= H or $SO_3^-$; Y= Ac or $SO_3^-$) (Image adapted from Murugesan et al. 2008 [34])

Heparin is widely used as anticoagulant due to its binding to the protease inhibitor antithrombin that accelerates its reaction with the protease thrombin and the formation of an active complex between protease and inhibitor [35]. Moreover, heparin can modulate various cellular functions such as cell growth, differentiation, morphology, and migration [36]. However, heparin has been used to develop new materials for GF delivery in tissue engineering approaches due to its growth factor binding affinity [1,32]. This binding is important in sequestering growth factors in the ECM to localize their activity, to protect them from degradation and in some cases to enhance their binding to cell surface receptors [37]. For this reason, polymeric growth factor delivery systems based on heparin are widely used because they can store growth factors similarly to the native ECM [38]. As an example of this strategy, a self-assembling peptide containing a heparin-binding domain have been designed to obtain a strong binding affinity to heparin. Interestingly, angiogenesis was promoted when this designed peptides was used in a rat corneal assay *in vivo* [1]. Similar strategies report the binding of heparin with other types of materials through covalent interaction to polymers such as alginate, polycaprolactone and collagen or entrapped within chitosan [1,24,39–41]. It is important to mention that the aim of all these strategies was to promote angiogenesis by releasing heparin binding growth factors.

## 4.2 Hypothesis and specific aims

Self-assembling peptides are ECM-mimetic, synthetic biomaterials traditionally used for the culture and maintenance of mammalian cells[42–45] . Nevertheless, nowadays they are also used as drug delivery hydrogels with different purposes [30,46]. Altogether, the growth factor binding affinity of heparin evidences the attractive properties to tailor new biomaterials for tissue engineering applications. Thus, we hypothesized that the combination of heparin and the self-assembling peptide RAD16-I could lead to the development of a new injectable nanofiber scaffold with drug binding and release capacities. Therefore, the aims for this chapter are the following:

(1) To develop a new biomaterial for tissue engineering applications composed by the self-assembling peptide RAD16-I and heparin.
(2) To characterize the new biomaterial in terms of nanofiber formation and growth factor delivery.
(3) To evaluate the behavior of human dermal microvascular endothelial cells (HDMVECs) within the new biomaterial and the control self-assembling peptide in terms of tubular-like structures development.

## 4.3 Materials and Methods

### 4.3.1 Culture of endothelial cells

Human Umbilical Vein Endothelial Cells (HUVECs) (CC-2519, Lonza) and Human Dermal Microvascular Endothelial cells (HDMECs) (C-12210, Promocell) (<10th passage) were cultured in 25-cm2 flasks, previously coated with 0.1% gelatin (G9391, Sigma), in Endothelial Basal Medium-2 (EBM-2) (CC-3156,Lonza) supplemented with Endothelial Cell Growth Media Single Quots kit (EGM-2) (4176,Lonza). Cultures were maintained in the incubator in humidified atmosphere at 37ºC and 5% CO2.

### 4.3.2 Culture of human Normal Dermal Fibroblasts

Human normal dermal fibroblasts (hNDF), isolated from the skin of anonymous adult patients, were kindly provided by Dr. Jesús Otero Hernández from "Hospital Universitario Central de Asturias". Cells were seeded in 75-cm2 flasks using Dulbecco's modified Eagle medium (DMEM; D5671, Sigma) supplemented with 10 % (v/v) fetal bovine serum (DE14-801F, Lonza), 100 U/mL Penicillin / 0.1 mg/mL Streptomycin (P11-010, PAA) and 2mM L-Glutamine (M11-004, PAA). Cultures were maintained in humidified atmosphere at 37ºC and 5% $CO_2$.

### 4.3.3 3D culture technique using endothelial cells

To obtain a 3D culture, a solution of commercial 1% (w/v) RAD16-I (BD PuraMatrix™,354250, Beckton Dickinson) was diluted in Sucrose 10% (w/w) (S1888, Sigma), to obtain a concentration of 0.1% (w/v). When using the composite RAD16-I-Heparin 95µl of RAD16-I 0.5% (w/v) and 5 µl of Heparin (H3149, Sigma) 0.01% (w/v) were combined and diluted to a final concentration of 0.1 (w/v) RAD16-I. This solution was mixed with an equal volume of a cell suspension (10 x $10^6$ cells/mL) in sucrose 10%, to obtain a final concentration of 5 x $10^6$ cells/mL in 0.05% (w/v) RAD16-I in sucrose 10%. 80µL of this mix were loaded into 9mm diameter cell culture inserts (PICM01250, Millipore), previously placed into a 6-well culture plate and equilibrated with culture media. Immediately, cell-peptide cultures were placed for 30 minutes in the incubator at 37°C and 5% $CO_2$, to allow the formation of the hydrogel by the action of a high ionic strength and the neutral pH of the medium. Elapsed this time washing steps, to dilute the content of sucrose, were performed by aspiration of the culture media in the well (outside of the insert), and the addition of the same amount (500µL) of fresh medium. The plate was placed again in the incubator for 10 minutes and this step was repeated 3 times, after which 2.5mL of fresh medium were added outside the insert and the plate placed in the incubator for 30 more minutes, to finally allow the construct to form, preventing its rupture. At this point, the addition of medium over the cell culture began, by adding 10µL in the inner wall of the insert letting it slowly slide to the gel, until a volume of 40µL is reached. The plate was placed once again in the incubator for 15 minutes and then the addition of fresh

medium over the cell construct continued, 20µL inside the insert, until a final volume of 200µL. 3D cell cultures were maintained in the incubator at 37°C and 5% $CO_2$. The medium was changed every second day by removing 500µL of medium from the well and the addition of 500µL of fresh medium inside the insert.

### 4.3.4 3D culture technique using fibroblasts

In this case RAD16-I and the composite RAD-Heparin were prepared at a final concentration of 0.30% (w/v) RAD16-I. Then, that solution was mixed with an equal volume of a cell suspension 4 x $10^6$ cells/mL in sucrose 10% (S0389, Sigma) to obtain a final concentration of 2 x $10^6$ cells/mL, 0.15% (w/v) of RAD16-I in 10% (w/v) sucrose. Then, the cell-peptide suspension was loaded into cell culture insert (PICM01250, Millipore) previously placed and equilibrated with FM inside 6-well culture plate. Once the mixture was loaded, the medium from the bottom membrane penetrates in the insert inducing the self-assembly of RAD16-I. Once the gel was formed, 40 µl of culture medium were added in the inner wall of the tissue culture insert and were let slide slowly to the top of the hydrogel, then the plate was placed in the incubator for 20 minutes. This step was repeated 3 times but adding 60µl of culture medium and placing the plate 10 minutes in the incubator. These steps favored the leaching of the sucrose. Finally, once aspirated the remaining medium in the well, 0.5 mL of fresh medium were added inside the tissue culture insert, and 2.5 mL were added in the well. 3D cell cultures were maintained in the incubator at 37°C and 5% $CO_2$. The medium was changed every second day by removing 500µL of medium from the well and the addition of 500µL of fresh medium inside the insert. Cultures were maintained for 8 days and then analyzed for viability.

### 4.3.5 2D culture on top of self-assembling peptide

RAD-Heparin composites were prepared combining 95µl of RAD16-I 0.5% (w/v) and 5 µl of Heparin (H3149, Sigma) 0.01% (w/v) and the mixture was diluted to a final concentration of 0.1%(w/v) RAD16-I. Control RAD16-I samples were also prepared with a final concentration of 0.1% (w/v). 80 µl of each type of sample were loaded into a cell culture insert (PICM-1250, Millipore) previously placed into a 6-well culture, and 500 µl of complete endothelial culture media were added under the insert to start the self-assembling process. Samples were let for 30 minutes at room temperature to allow the gel formation process. Once this time elapsed, 200 µl of endothelial culture media were added in the inner wall of the insert letting it slowly slide to the gel and 2.5mL of fresh medium were added outside the insert. Then, a suspension of 120.000 HUVECs in 200 µl of endothelial culture media was loaded over the gel. Cell cultures were maintained in the incubator at 37°C and 5% $CO_2$. The medium was changed every second day by removing 500µL of medium from the well and the addition of 500µL of fresh medium inside the insert.

### 4.3.6 Sample preparation for staining

RAD-Heparin composites were prepared combining 95µl of RAD16-I 0.5% (w/v) and 5 µl of heparin sodium salt solution (H3149, Sigma) in a concentration range between 0.01 and 1 % (w/v), control RAD16-I samples were prepared with a final concentration of 0.5% (w/v). 100 µl of each type of sample were loaded into a cell culture insert (PICM-1250, Millipore) previously placed into a 6-well culture plate, and 500 µl of PBS were added under the insert to star the self-assembling process. Samples were let for 30 minutes at room temperature to allow the gelification process. Once this time elapsed, 200 µl of PBS were added in the inner wall of the insert letting it slowly slide to the gel and 2.5mL of PBS were added outside the insert.

### 4.3.7 Toluidine Blue staining

Toludine Blue staining was performed to study the presence of highly negative charges provided by the heparin molecules. Samples were incubated with Toluidine Blue 0.05% (w/w) in water during 20 minutes and then washed several times with distilled water. Finally the samples were analyzed under a stereoscopic microscope (Nikon SMZ660).

### 4.3.8 Congo Red staining

Congo Red staining was performed to study the presence of the beta-sheet structure characteristic of the self-assembling peptide RAD16-I. Samples were incubated with 0.1% (w/v) Congo Red (75768, Sigma) in water for 5 minutes and washed several times with PBS. Finally the samples were analyzed under Stereoscopic microscope (Nikon SMZ660).

### 4.3.9 Scanning Electron Microscopy (SEM)

Briefly, samples were fixed in 5% (w/v) gluteraldehyde and dehydrated in successive ethanol washes. Dehydrated samples were dried using a CO2 critical point dryer and subsequently coated with gold. Finally, samples were examined under SEM (NovaNano SEM 230 model, FEI, The Netherlands).

### 4.3.10 Circular dichroism (CD)

Circular dichroism (CD) spectroscopy was performed on a JASCO-715 spectropolarimeter equipped with a Peltier system. RAD16-I samples were diluted from a peptide stock solution (1% (w/v), 5.38 mM) in deionized water to a final concentration of 100 µM. RAD-Heparin composites were prepared using different blending ratios and diluted in deionized water to a final concentration of 100µM RAD16-I. CD data were acquired in a range of 195-250 nm at a band width of 1 nm, scan speed of 20 nm/s and path length 1mm.

### 4.3.11 Growth factor release quantification by ELISA

RAD-Hep composite gels were prepared combining 95µl of RAD16-I 0.5% (w/v) and 5 µl of 0.01% (w/v) Heparin (H3149, Sigma); control RAD16-I samples were prepared with a final concentration of 0.5% (w/v). Both types of gels were prepared in triplicate and incubated with a solution of 500 ng/ml $VEGF_{165}$ or FGFβ in binding buffer (EBM-2 with 0.1%BSA and protease inhibitor) for 3 hours in the incubator at 37ºC and 5% $CO_2$. Then, the growth factor solution was removed and the gels were incubated with binding buffer to allow the release of $VEGF_{165}$ or FGFβ. Noncumulative studies were performed consisting on removing all the binding buffer with the growth factor released and adding fresh binding buffer to the gels. Samples were taken at 12, 24 and 36 hours and analyzed with ELISA kits for $VEGF_{165}$ (EHVEGF2, Themoscientific) and FGFβ (KHG0021, Invitrogen) following the manufacturer's protocol.

### 4.3.12 Statistics

All values were expressed as mean ± SD. Statistical differences were analyzed with GraphPad Prism 6 when samples were prepared in triplicate for the condition analyzed. When comparing two groups, unpaired student's t test was used to test for the significance level. When comparing three or more groups statistical analysis was carried out by 1-way or 2-way ANOVA, as appropriate, followed by Tukey post analysis.

## 4.4 Results

### 4.4.1 Development and characterization of a new bi-component material

The main objective of this chapter was to develop a new self-assembling nanofiber matrix containing heparin moieties with angiogenic capacity for tissue engineering applications (Figure 4.4.1). The first strategy envisaged the use of a self-assembling peptide with heparin binding domains (HBD) to allow the binding of heparin and as a consequence of growth factors containing HBD such as $VEGF_{165}$ or FGFβ..

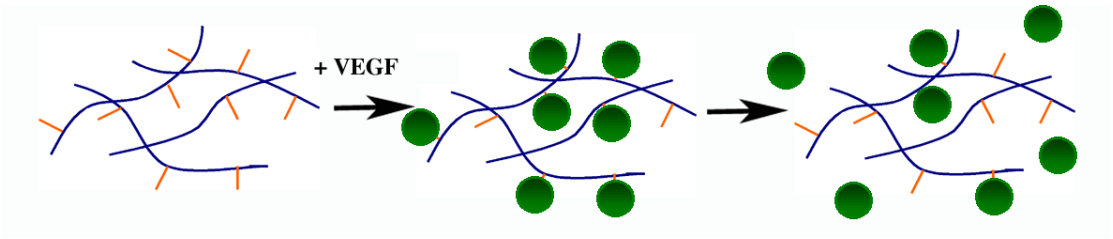


**Figure 4.4.1. Schematic process of VEGF binding and release to the self-assembling peptide with heparin moieties.**

In our laboratory, a functionalized peptide scaffold based on RAD16-I (AcN–RADARADARADARADA–CONH2) has been previously designed by direct solid phase synthesis extension at the amino terminal with the short-sequence motif TAGSCLRKFSTM. This peptide motif from the α1 chain of collagen type IV is known for its ability to specifically bind to heparin in a dose-dependent manner [29]. For this reason, it was used in combination with RAD16-I to obtain a self-assembling peptide with heparin binding capacity. In order to study the binding to glycosaminoglycans (GAGs), gels with blending ratio 95:5 (RAD16-I: RAD-TAG) and the control RAD16-I at a final concentration of 0.5% (w/v) were prepared and incubated with solutions of heparin and chondroitin sulphate (CS). Toluidine blue staining was performed to detect heparin and CS molecules thanks to its ability to form complexes with anionic glycoconjugates such as proteoglycans (PGs) and glycosaminoglycans (GAGs) [47]. This staining revealed that both molecules (heparin and CS) bound to the gels independently of the presence of the HBD, even at low heparin concentrations, suggesting an unspecific binding (Figure 4.4.2). Interestingly, when CS samples were stained presented an intense blue color; instead, heparin samples stained purple. This effect is due to the different interaction between the dye and the negative molecules as previously described [47].

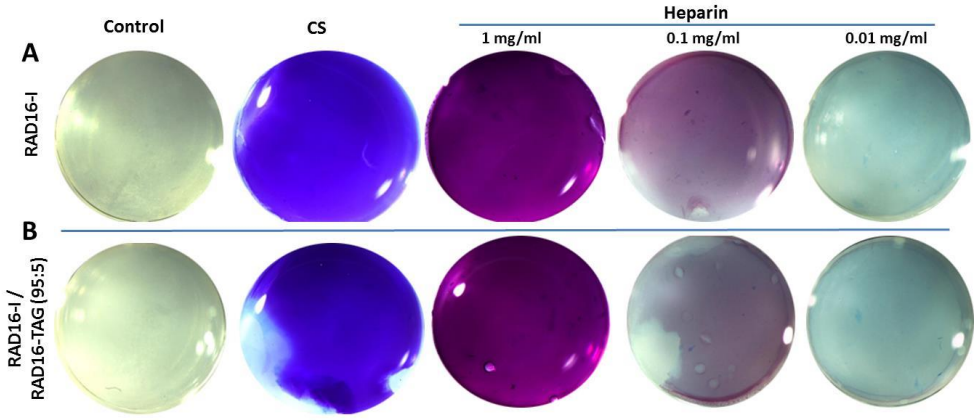


**Figure 4.4.2. Glycosaminoglycans binding to self-assembling peptides.** Toluidine blue staining of (A) RAD16-I and (B) RAD16-I:RAD-TAG (95:5) gels previously incubated overnight with solutions of 1mg/ml chondroitin sulphate (CS), and 1, 0.1 and 0.01 mg/ml heparin.

The next step was to evaluate the possibility of combine heparin and the self-assembling peptide with blending ratio 95:5 (RAD16-I: RAD-TAG) in order to assess the degree of interaction between both molecules. Different composites were prepared with blending ratios mg RAD16-I:RAD-TAG/mg Heparin ranging from 99,5/1 to 9,5/1. Interestingly, the combination was structurally very stable at physiological pH and developed a nanofiber composite self-assembling peptide-heparin. Toluidine Blue stained gels in a dose dependent manner (Figure 4.4.3, A). Moreover, Congo red staining showed the formation in all cases of β-sheet secondary structures and as a consequence of the nanofiber formation (Figure 4.4.3, B).

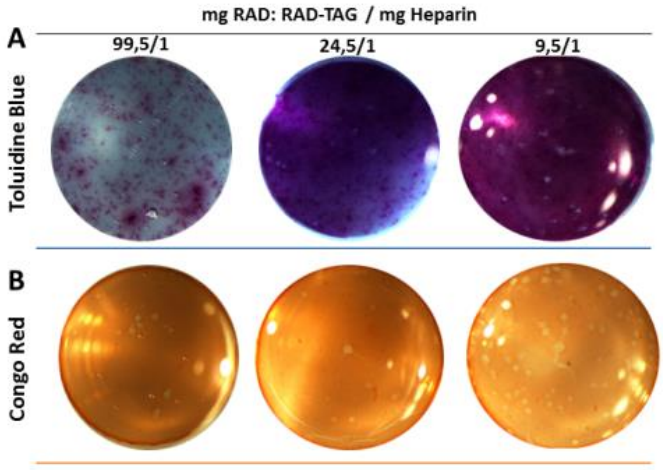


**Figure 4.4.3. Self-assembling peptide RAD-TAG behavior with increasing quantities of heparin**. (A) Toluidine blue staining, (B) Congo Red.

Thus, a similar behavior was observed when mixing RAD16-I directly with heparin which evidenced again the unspecific binding of heparin to the self-assembling peptide RAD16-I (Figure 4.4.4). For this reason, it was decided to simply combine RAD16-I and heparin, which eased the complexity of the protocol and reduced its cost due to the absence of the modified peptide synthesis.

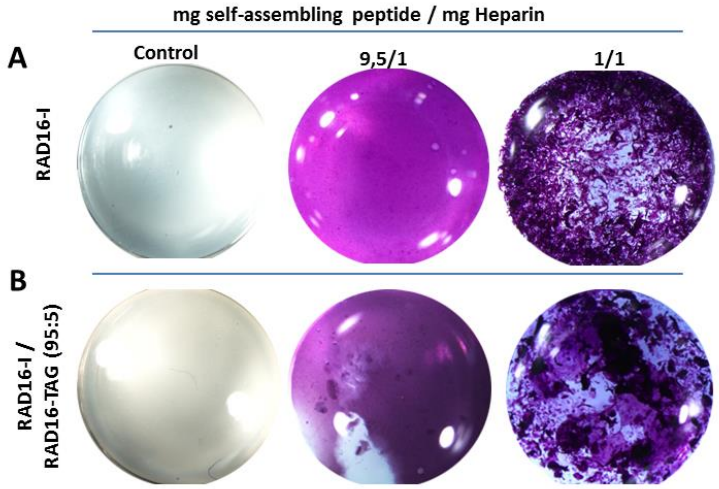


**Figure 4.4.4. Self-assembling peptides RAD16-I and RAD-TAG behavior with increasing quantities of heparin**. (A) RAD16-I, (B) RAD16-I:RAD-TAG (95:5).

Several RAD-heparin composites were prepared combining 95µl of RAD16-I 0.5% (w/v) and 5 µl of heparin in a concentration range between 0.01 and 1 % (w/v), which corresponded to a ratio mg RAD16-I/mg Heparin between 950/1 and 9,5/1. Control RAD16-I samples were also prepared at a final concentration of 0.5% (w/v). The permanent blue/purple color observed after the staining indicated the presence of highly negative charges provided by the heparin molecules associated with the self-assembling nanofiber network in a dose dependent manner (Figure 4.4.5, A) [48]. In addition, Congo Red, which stained β-sheet structures characteristic of the self-assembled RAD16-I [49] , showed that heparin was not interfering in the self-assembling process, independently of the heparin quantity (Figure 4.4.5, A).

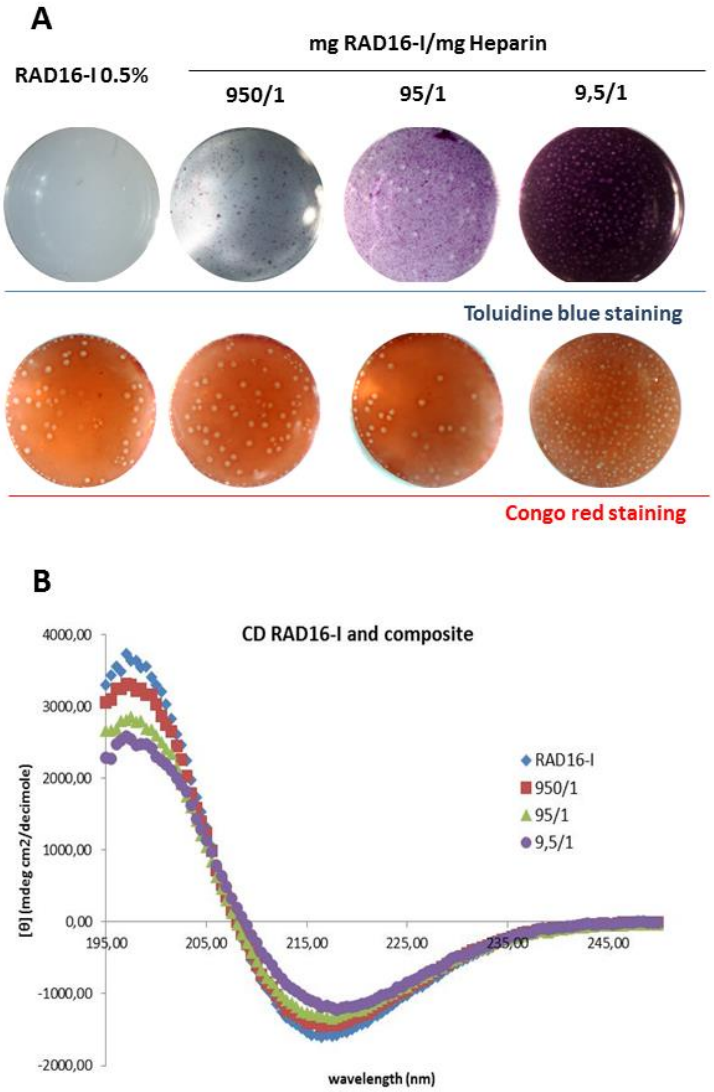


**Figure 4.4.5. Influence of heparin in the RAD16-I self-assembling process**. (A) Congo red and Toluidine blue staining of RAD16-I and composites with increasing quantities of heparin. Ratios mg RAD16-I/mg Heparin from 950/1 to 9,5/1. (B) CD of RAD16-I and composites with ratios mg RAD16-I/mg Heparin from 1000/1 to 10/1.

In addition, the effect of heparin in the β-sheet secondary structure characteristic of the peptide RAD16-I was studied by circular dichroism (CD) [50,51]. CD is a spectroscopy technique that refers to the differential absorption of the left and right circularly polarized components of plane-polarized radiation [51]. It is a useful tool for the structural characterization of proteins and peptides. A typical CD spectrum for a β-sheet structure shows a minimum molar ellipticity around 218 nm, which represents the β-sheet content and a maximum at 195 nm which corresponds to the backbone twist of the peptide in β-sheet configuration. The CD spectrum of an α-helix shows two minimums at 209 and 222 nm whereas random coil peptides or proteins are represented by a strong minimum in the 190-200 nm range (Figure 4.4.6) [52,53].

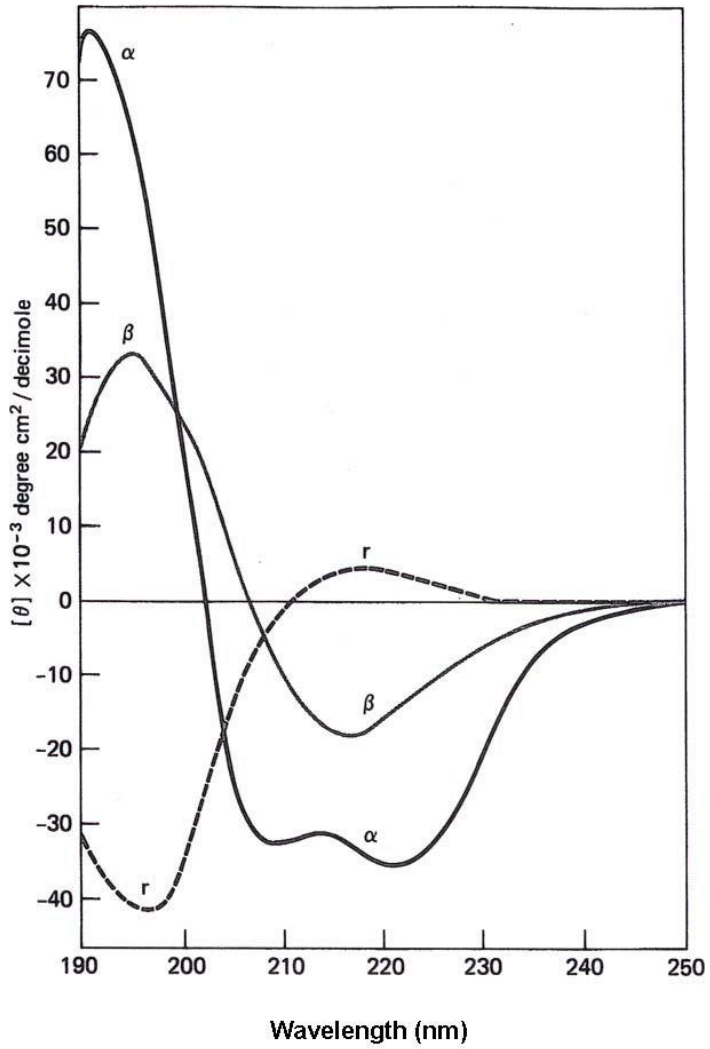


**Figure 4.4.6. CD spectra of poly(Lys) in the α-helical (α), β-sheet (β), and random coil (r) conformations.** (Greenfield and Fasman, 1969 [54])

First, RAD16-I was analyzed separately and as expected, it showed a typical CD spectrum for a β-sheet structure showing a minimum molar ellipticity (degcm$^2$/decimole) around 216 nm and a maximum at 195 nm (Figure 4.4.5, B). After that, the secondary structures of the composites were similarly studied to elucidate whether the addition of heparin was affecting the β-sheet secondary structure. Three types of composites were prepared with ratios mg RAD16-I/mg Heparin: 950/1, 95/1 and 9,5/1. The addition of heparin was translated into weaker β-sheet structures, represented with a decrease in the intensity of molar ellipticity in the minimum at 216 nm and the maximum at 198 nm. This effect was observed in a dose dependent trend : the higher the concentration of heparin, the weaker the β-sheet structure (Figure 4.4.5, B).

Then, Scanning Electron Microscopy (SEM) imaging was used to visualize and characterize the morphology of the nanofibers. As expected due to the CD analysis, a network of interweaving nanofibers was observed when the composite (950/1) and the control RAD16-I were analyzed. Although the diameter of the nanofibers was in the same range (around 20 nm), their length was shorter in the presence of heparin than in the control (Figure 4.4.7).

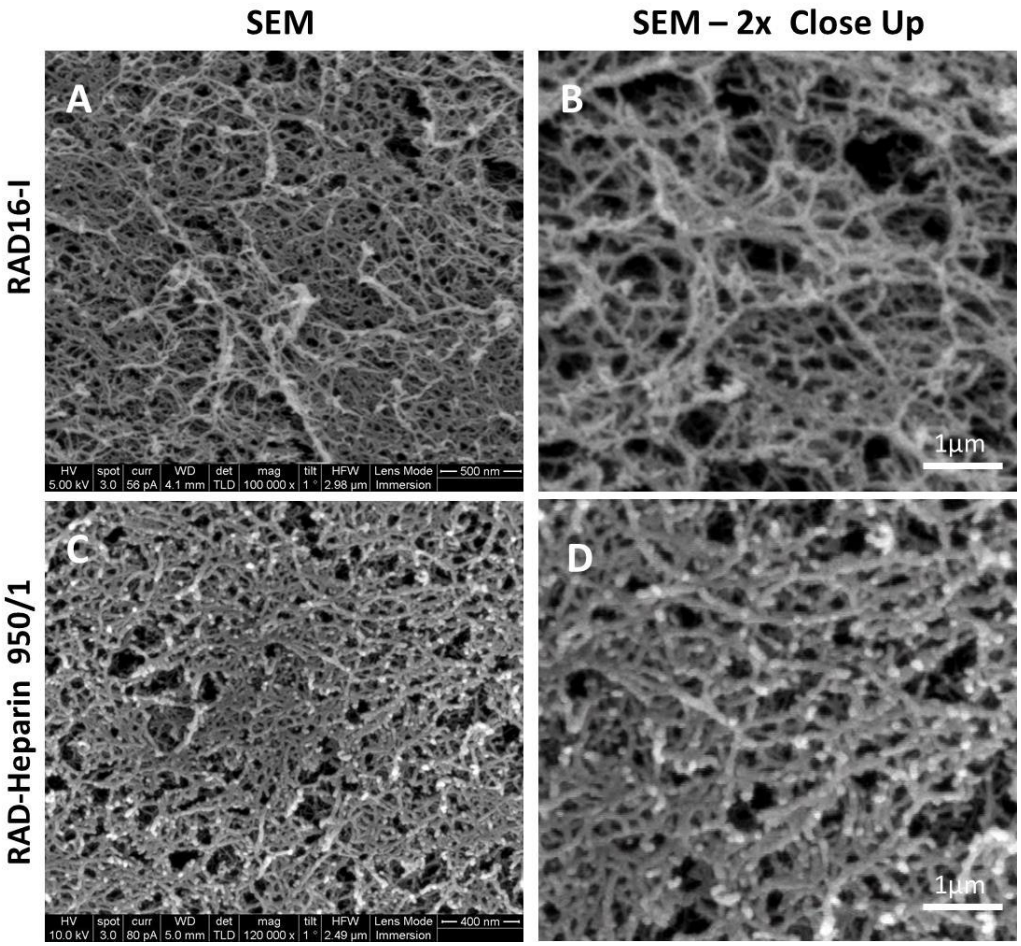


**Figure 4.4.7 . Scanning Electron Microscopy**. RAD16-I and the composite with ratios mg RAD16-I/mg Heparin 950/1 were prepared at a final concentration of 0.5% (w/w) RAD16-I. (A) SEM image of RAD16-I, (B) 2x close up from (A). (C) SEM image of composite, (D) 2x close up from (C).

Interestingly, areas with higher density of nanofibers, forming bundles but maintaining the nanofiber structure, were detected in a dose dependent manner in the composites with increasing quantities of heparin (Figure 4.4.8). We speculated that these areas were formed due to the strong ionic interaction between heparin, which is a highly sulfated anionic polysaccharide, and RAD16-I, which is an amphiphilic peptide consisting on repeating units of hydrophilic-hydrophobic aminoacids with alternating positive and negative charges in the hydrophilic phase. As a consequence, we also speculated that these nanofiber bundles corresponded to the areas stained with toluidine blue also observed in a dose dependent manner (Figure 4.4.8).

In view of these results, it was decided to use the lowest heparin concentration, ratio 950/1 for the subsequent analysis of growth factor delivery and cell cultures because its CD was slightly different from the control self-assembling peptide and it also maintained its structural properties as observed by SEM.

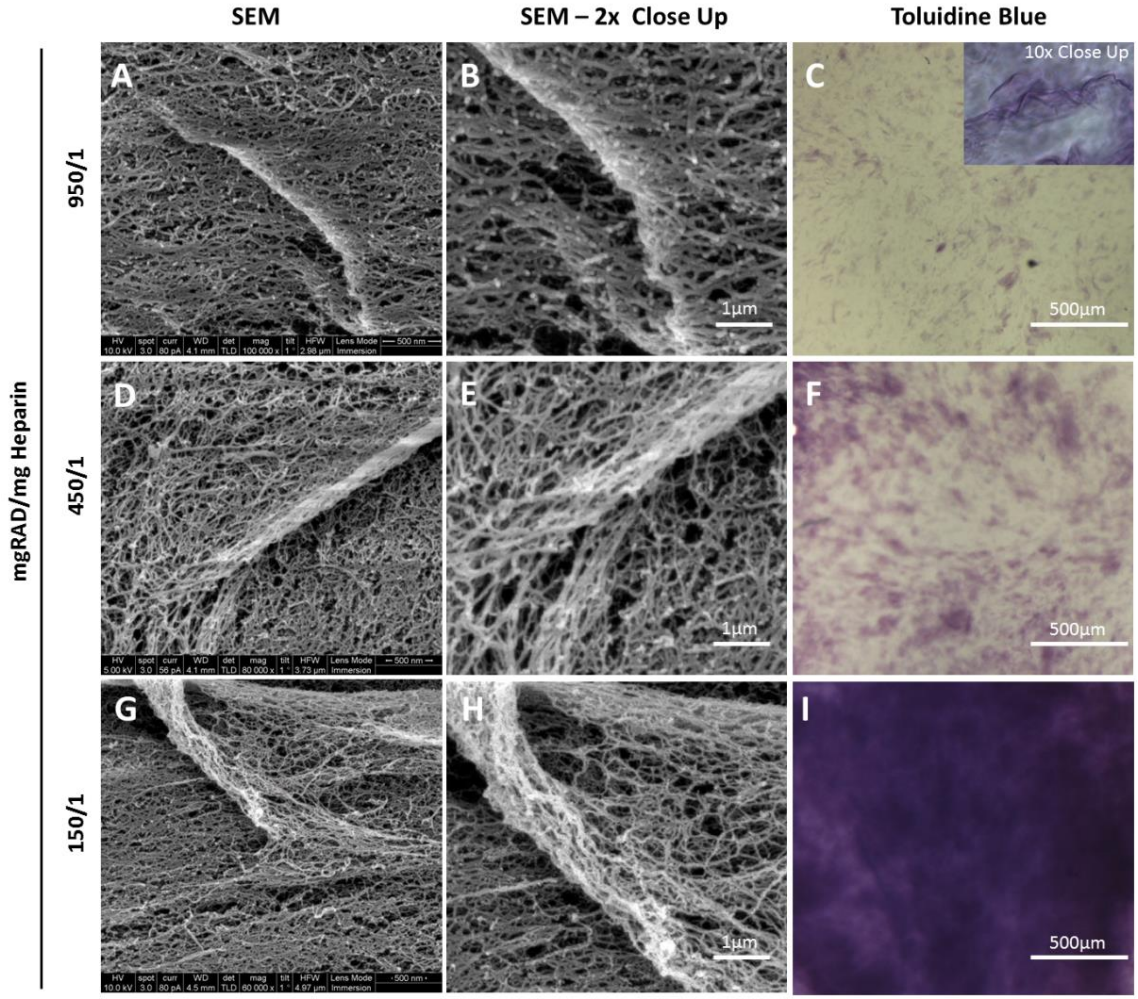


**Figure 4.4.8. Scanning Electron Microscopy of composites RAD-Heparin**. Composites were prepared with ratios mg RAD16-I/mg Heparin: 950/1, 450/1 and 150/1. (A,B) SEM images and (C) Toluidine Blue of 950/1 composite. (D, E) SEM images and (F) Toluidine Blue of 450/1 composite. (G ,H) SEM images and (I) Toluidine Blue of 150/1 composite.

### 4.4.2 Growth factor delivery

After analyzing the influence of heparin on the self-assembling process and the nanofiber formation, the suitability of the composite for drug delivery purposes was assessed. For this purpose, a non-cumulative quantification of the angiogenic factors $VEGF_{165}$ and FGFβ released by the composite and the control RAD16-I was performed. Interestingly, it was observed that the control scaffold released almost all the $VEGF_{165}$ in the first 12 hours and that the amount of GF after 24 hours nearly reached zero. Nevertheless, the peptide-heparin composite gradually released $VEGF_{165}$ over the course of the experiment (36 hours) (Figure 4.4.9, A). In the case of FGFβ, no significant differences in the release of GF were found between the control RAD16-I and the composite (Figure 4.4.9, B).

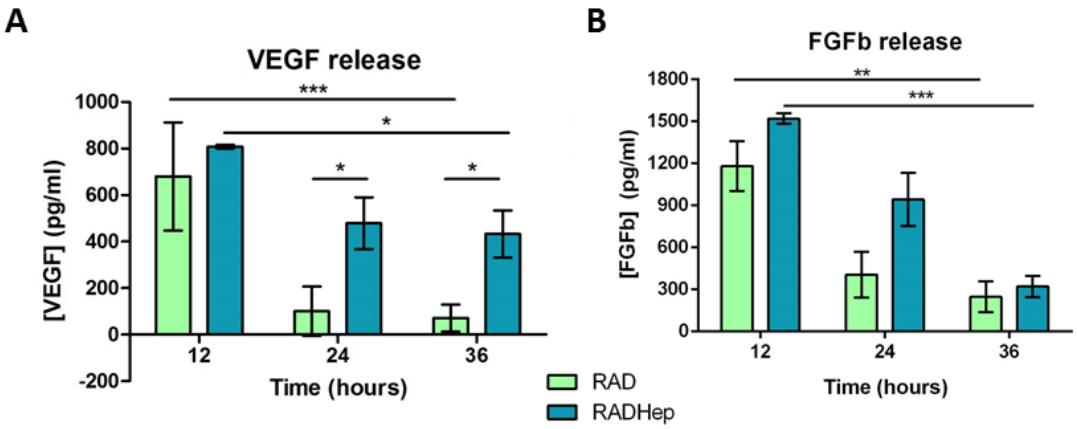


**Figure 4.4.9. Characterization of RAD16-I and the composite RAD-Hep as drug delivery hydrogels.** Non-cumulative quantification of (A) VEFG, and (B) FGFβ released by RAD16-I and the composite after 12, 24 and 36 hours of delivery. (Statistical differences are indicated as:* for $p<0.05$, ** for $p<0.01$, and *** for $p<0.001$, Two-way ANOVA, n=3)

In order to know if the released growth factor was biologically active, a functional study was performed, which consisted of adding the released growth factor to a 2D culture of HUVECs cultured in Endothelial Basal Media-2 without any additional growth factor. After 48 hours, cell cultures were stained with DAPI in order to count the cells of each type of culture: growth factor released from the control RAD16-I, growth factor released from the composite and the control without the addition of any growth factor (Figure 4.4.10, A). The results showed a clear effect of the released growth factors on HUVECs maintenance and proliferation with higher cell numbers in the cases were the growth factor was added to the culture media than the control where almost all cells were dead (Figure 4.4.10, B). These results elucidated that both, $VEGF_{165}$ and FGFβ, maintained their biological activity after being released by the hydrogels. No significant differences, in terms of cell number, were found between growth factors released from RAD16-I or the composite.

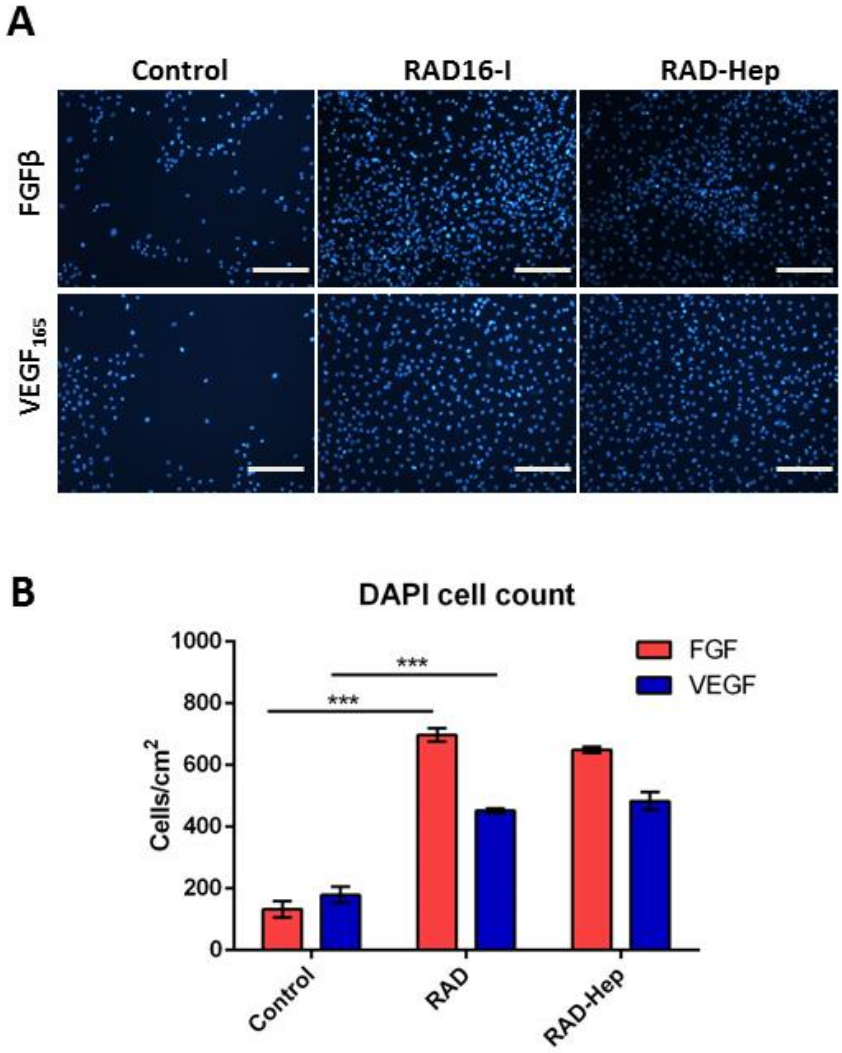


**Figure 4.4.10. Functional study of the released growth factor.** A) DAPI staining of 2D endothelial cells cultures after 48 hours of culture with the released growth factors from RAD and RAD-heparin composite and, B) Cell count of 2D cultures from A). (Statistical differences are indicated as *** for $p<0.001$, Two-way ANOVA, n=3)

### 4.4.3 Evaluation of the angiogenic capacity of the new bi-component material

Afterwards, the angiogenic capacity of both materials was tested using human dermal microvascular endothelial cells (HDMECs). First, cells were cultured in a 2D model (on top of both hydrogels) exhibiting a noticeable spatial re-arrangement in both materials after 1 day of culture (Figure 4.4.11, A, B). Then, the development of tubular-like structures was studied by encapsulating the endothelial cells in both materials. The hypothesis was that the lower the peptide concentration (the lower the matrix stiffness), the easier to develop tubular structures by the cells. [55,56]. Thus, cells cultured in 0.1% (w/v) RAD16-I presented rounded morphology compared to the cultures at low peptide concentration (0.05% (w/v) RAD16-I), which developed tubular structures independently of the presence of heparin after 2 days of culture. (Figure 4.4.11, C, D, E, F).

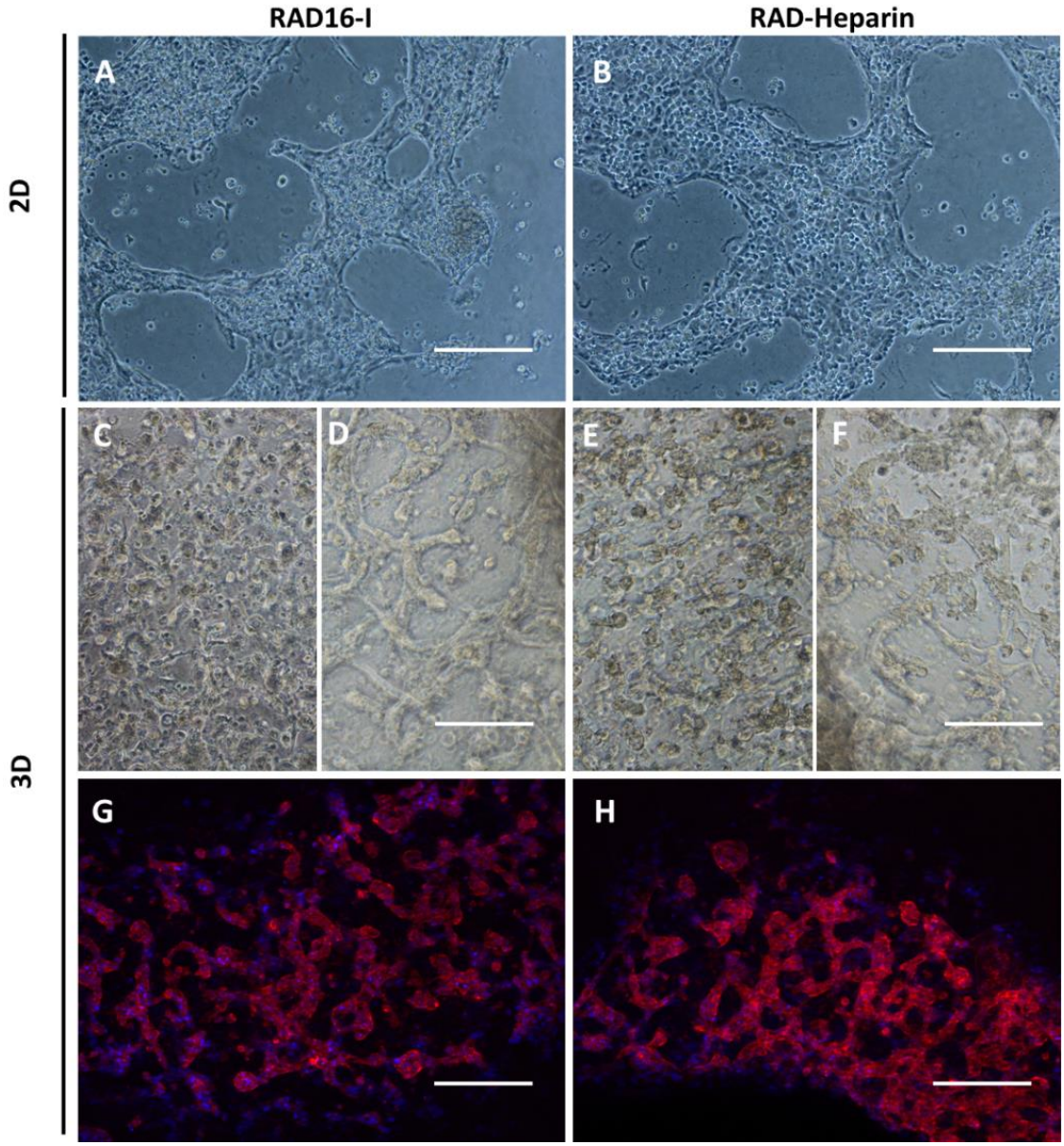


**Figure 4.4.11. 2D and 3D cultures of HDMECs using RAD16-I and RAD-Hep**. RAD16-I and the composite with ratios mg RAD16-I/mg Heparin 950/1 were prepared at a final concentration of 0.05% and 0.1% (w/w) RAD16-I. Phase contrast images show 2D soft cultures of HDMVECs after 1day of culture on top of (A) RAD16-I and (B) composite. When 3D cultures were prepared at final concentration 0.1% (w/w) RAD16-I cells looked rounded after 2 days (C, E) as compared to cultures at final concentration 0.05% (w/w) where cells were elongated creating tubular structures (D, F). These structures were clearly observed when cultures were stained with DAPI-Phalloidin in 3D cultures prepared with 0.05% (w/w) (G) RAD16-I and (H) composite. (Scale bars= 200 µM)

Remarkably, both materials (RAD16-I and the composite) supported robust capillary morphogenesis. Indeed, HDMVECs formed capillary-like networks when cultured at high protein concentration (10% (v/v) FBS) and this was in concordance with what had been previously demonstrated for HUVECs in RAD16-I [56] (Figure 4.4.11, G,H). However, this effect was not observed when cells were cultured in complete endothelial basal media with the regular protein concentration (2% (v/v) FBS). In this case, cells formed tubular-like structures in both biomaterials but only when cells were cultured with medium containing heparin (Figure 4.4.12,

A, C). Instead, when HDMECs were cultured in the medium without heparin, the formation of tubular-like structures was much higher in the composite than in RAD16-I where cells looked rounded (Figure 4.4.12 B, D). These results evidenced the biological activity of the heparin present in the scaffold, which promoted a positive effect on tubular-like structures formation and as a consequence it compensated the absence of heparin in the culture media.

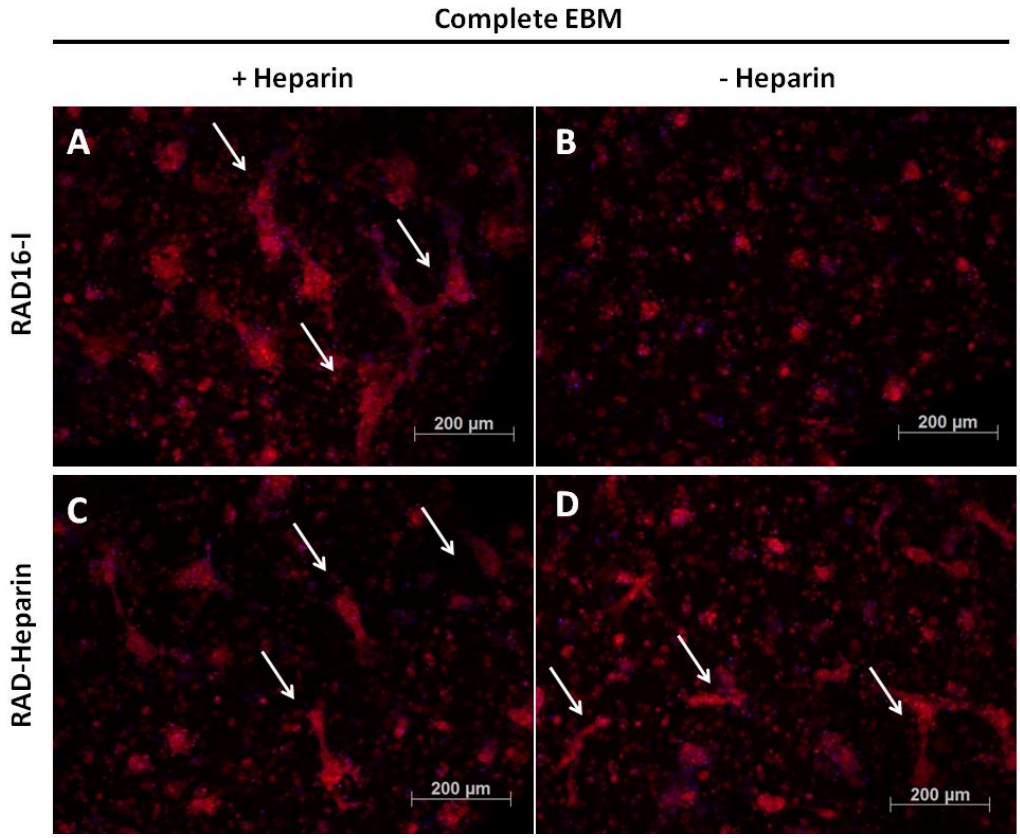


.

**Figure 4.4.12. HDMECs cultured in RAD16-I and RAD-Heparin composite maintained in EBM supplemented with 2%FBS.** RAD16-I and the composite with ratio mg RAD16-I/mg Heparin 950/1 were prepared at a final concentration of 0.05% (w/w) RAD16-I. HDMVECs were encapsulated in both materials and maintained for 2 days. DAPI-Phalloidin showed that when cells were cultured in media containing heparin there were not differences between capillary-like structures formation in (A) RAD16-I and (C) RAD-Hep. Instead when cells were cultured in the media without the addition of heparin (C) cells looked round in the control RAD16-I and the capillary-like structures were only observed in the (D) RAD-Heparin composite.

The effect of heparin on cell viability was evaluated using human normal dermal fibroblasts (hNDFs). Interestingly, cell viability was not affected by the presence of heparin compared to the control (RAD16-I) where almost all cells were alive (Figure 4.4.13, A, C). Moreover, a similar cell behavior was observed: cells elongated and developed a network as it was evidenced by the DAPI-Phalloidin staining (Figure 4.4.13, B, D).

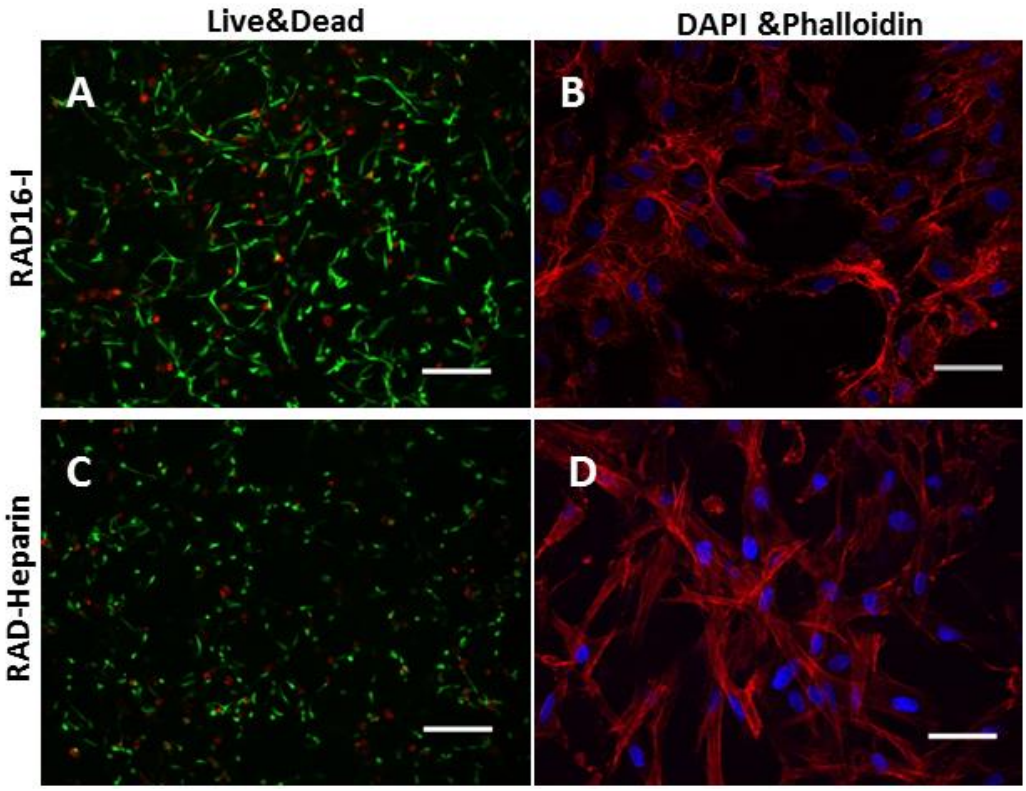


**Figure 4.4.13. hNDFs cell viability and network development in RAD16-I and the composite RAD-Hep.** RAD16-I and the composite with ratios mg RAD16-I/mg Heparin 950/1 were prepared at a final concentration of 0.15% (w/w) RAD16-I. hNDFs were encapsulated in both types of materials and maintained for 8 days. (A, C) Live and dead staining showed no differences in cell viability between different types of materials (Scale bars= 50 µM). (B, D) DAPI-Phalloidin staining showed similar cell behavior in all materials with cell elongation and development of a tight network. (Scale bars= 200 µM)

## 4.5 Discussion

In this chapter it was described the development of a new biomaterial for tissue engineering applications formed by simple combination of the self-assembling peptide RAD16-I and heparin sodium salt solution. Self-assembling peptides are ECM-mimetic, synthetic biomaterials traditionally used for the culture and maintenance of mammalian cells [42–45]; however, nowadays they are also used as drug delivery hydrogels with different purposes [30,46]. On the other hand, heparin is a class of glycosaminoglycan with growth factor binding affinity which is important in sequestering growth factors in the ECM to localize their activity protecting them from degradation and in some cases enhancing their binding to cell surface receptors [37]. Altogether it evidences the attractive qualities that motivated the combination of the self-assembling peptide RAD16-I and heparin to obtain a new scaffold for tissue engineering applications with drug delivery capacity. Interestingly, the combination of both materials exhibited structural stability at physiological pH, developing into a nanofiber composite. Further material characterization showed that the β-sheet structure characteristic of the self-assembling peptide RAD16-I and, as

a consequence, the subsequent self-assembling process and nanofiber formation was not interfered by the presence of heparin at chosen working concentration.

Remarkably, the composite could be used as a drug delivery system to bind and release physiologically significant quantities of $VEGF_{165}$ *in vitro* during the first 24-36h to promote a possible pro-angiogenic effect in an *in vivo* model. It is hypothesized that $VEGF_{165}$ associated to the matrix could be released by competing with free soluble heparin. Since heparin can be administrated and it is naturally present in the blood, the release of the $VEGF_{165}$ from the glycopeptidic matrix would be physiologically regulated promoting local angiogenesis by neighbor capillaries. Moreover, HDMVECs developed tubular-like structures in the composite scaffold when they were maintained in culture medium without heparin. These results suggested the biological activity of the heparin present in the scaffold and its possible use in vascular tissue engineering applications in combination with the growth factor delivery.

This material has been developed as part of the European project RECATABI (REgeneration of CArdiac Tissue Assisted by Bioactive Implant, EU $7^{th}$ frame Program) with the purpose to promote vascularization of ischemic areas after myocardial infarction. In addition to the assays with endothelial cells presented in this chapter, *in vitro* studies of cardiogenic differentiation with MSCs have been performed using the new composite in our laboratory. Interestingly, when MSCs were cultured in the composite hydrogel they presented an aligned growth characteristic of cardiogenic differentiation while control samples (RAD16-I) showed a disordered pattern. However, cardiogenic differentiation was analyzed and preliminary results showed that there were not differences in protein and gene expression due to the presence of heparin in the scaffold. Future approaches would include its use in *in vivo* models of angiogenesis such as the chick embryo chorioallantoic membrane (CAM), which is an extra embryonic membrane which serves as a gas exchange surface and its function is supported by a dense capillary network. Because of its extensive vascularization and easy accessibility has been broadly used to investigate mechanisms of angiogenesis [57]. The final approach of this material would be its use in an *in vivo* model of myocardial infarction to promote vascularization of ischemic areas which was the main purpose of the project.

Importantly, this new biomaterial could be used in other tissue engineering applications due to the ability of heparin to bind different growth factors including TGFβ, which is a well-known chondrogenic inductor with heparin binding affinity. According to the literature, heparinized scaffolds seem to induce and enhance chondrogenic differentiation. This effect could be explained due to the unique bioactivities of heparin moieties that can hold various growth factors safely and protect them from denaturation [58]. In addition, it was also speculated that heparin could deposit GAGs produced by cells via heparin-binding affinity [58]. Taking all this

into account, the new biomaterial developed in this thesis is actually being used in our laboratory as a scaffold to support *in vitro* chondrogenic differentiation as part of the project BIOCART (BIOactive and biomimetic scaffolds for CARTtilage regeneration, AO Fundation Switzerland). This project aims to develop potential injectable scaffolds that mimic the natural extracellular matrix of cartilage for their use in clinical applications of cartilage repair. Up to now, promising results have been obtained which showed enhanced MSCs viability in the presence of heparin as compared to the controls. Moreover, preliminary results showed that heparin promoted higher expression of chondrogenic markers than the controls in the self-assembling peptide RAD16-I. It was speculated that heparin could be sequestering growth factors, such as TGFβ, in the ECM and localizing their activity as compared to the control cultures in RAD16-I. Ongoing experiments are focused on studying the influence of heparin in the chondrogenic differentiation process. Afterwards, future approaches would include its use in an *in vivo* model of cartilage defect in order to obtain cartilage recovery.

Stupp and coworkers reported the development of a self-assembling peptide with similar characteristics to the composite developed in this thesis [1]. It contains a heparin binding domain that self-assembles into nanofiber gels when mixed with heparin and activates heparin-binding angiogenic growth factors. It was demonstrated that the presentation of growth factors (VEGF and FGFβ) via the heparinized gel enhanced their angiogenic bioactivity *in vitro* and induced an extensive angiogenic response in an *in vivo* rat corneal assay [1,59]. Afterwards, it was used for the delivery of angiogenic factors into pancreatic islets evidencing the versatility of the heparinized self-assembling peptide [60]. However, the advantage of our composite is the commercial availability of both components which facilitates its use and reduces its cost due to the absence of peptide synthesis.

Altogether the results presented in this chapter indicate that the new composite is a promising "easy to prepare" material for different tissue engineering applications. It is made by simple combination of two commercial products: self-assembling peptide RAD16-I (PuraMatrix™) and heparin sodium salt solution. Remarkably, the commercial availability of clinical grade PuraMatrix™ and heparin enables its future use for *in vivo* studies.

## 4.6 Concluding Remarks

- A new biomaterial for tissue engineering applications has been developed by simple combination of self-assembling peptide RAD16-I and heparin sodium salt. The availability of clinical grade RAD16-I and heparin enables its future use in *in vivo* applications, including human trials.

- This new biomaterial could be used as a drug delivery system to bind and release physiologically significant quantities of $VEGF_{165}$ *in vitro* during the first 24-36h to promote pro-angiogenesis in an *in vivo* model.

- The composite material presented promising results for its use in vascular tissue engineering applications; however, it could be used for other tissue engineering applications including cartilage and cardiac regeneration.

## 4.7 References


1. Rajangam, K. *et al.* Heparin binding nanostructures to promote growth of blood vessels. *Nano Lett.* **6,** 2086–90 (2006).

2. Auger, F. a, Gibot, L. & Lacroix, D. The Pivotal Role of Vascularization in Tissue Engineering. *Annu. Rev. Biomed. Eng.* 177–200 (2013). doi:10.1146/annurev-bioeng-071812-152428

3. Castells-sala, C. *et al.* Current Applications of Tissue Engineering in Biomedicine. *Biochips & Tissue chips* **S2:004,** (2013).

4. Novosel, E. C., Kleinhans, C. & Kluger, P. J. Vascularization is the key challenge in tissue engineering. *Adv. Drug Deliv. Rev.* **63,** 300–11 (2011).

5. Laschke, M. W., Vollmar, B. & Menger, M. D. Inosculation: connecting the life-sustaining pipelines. *Tissue Eng. Part B. Rev.* **15,** 455–65 (2009).

6. Laschke, M. W. & Menger, M. D. Vascularization in tissue engineering: angiogenesis versus inosculation. *Eur. Surg. Res.* **48,** 85–92 (2012).

7. Carmeliet, P. & Jain, R. K. Molecular mechanisms and clinical applications of angiogenesis. *Nature* **473,** 298–307 (2011).

8. Tremblay, P.-L., Hudon, V., Berthod, F., Germain, L. & Auger, F. a. Inosculation of tissue-engineered capillaries with the host's vasculature in a reconstructed skin transplanted on mice. *Am. J. Transplant* **5,** 1002–10 (2005).

9. Chen, X. *et al.* Rapid anastomosis of endothelial progenitor cell-derived vessels with host vasculature is promoted by a high density of cotransplanted fibroblasts. *Tissue Eng. Part A* **16,** 585–94 (2010).

10. Unger, R. *et al.* The rapid anastomosis between prevascularized networks on silk fibroin scaffolds generated in vitro with cocultures of human microvascular endothelial and osteoblast cells and the host vasculature. *Biomaterials* **31,** 6959–67 (2010).

11. Borges, J., Müller, M., Momeni, A., Stark, G. & Torio-Padron, N. In vitro analysis of the interactions between preadipocytes and endothelial cells in a 3D fibrin matrix. *Minim Invasive Ther Allied Technol* **17,** 141–8 (2007).

12. Aguirre, A., Planell, J. & Engel, E. Dynamics of bone marrow-derived endothelial progenitor cell/mesenchymal stem cell interaction in co-culture and its implications in angiogenesis. *Biochem. Biophys. Res. Commun.* **400,** 284–91 (2010).

13. Nemeno-Guanzon, J. G. *et al.* Trends in tissue engineering for blood vessels. *J. Biomed. Biotechnol.* **2012,** 956345 (2012).

14. Naderi, H., Matin, M. M. & Bahrami, A. R. Review paper: critical issues in tissue engineering: biomaterials, cell sources, angiogenesis, and drug delivery systems. *J. Biomater. Appl.* **26,** 383–417 (2011).

15. Karamysheva, a F. Mechanisms of angiogenesis. *Biochem. Biokhimiia* **73,** 751–62 (2008).

16. Nowocin, A. K. *et al.* The development and implantation of a biologically derived allograft scaffold. *J. Tissue Eng. Regen. Med.* (2013). doi:10.1002/term

17. Andrée, B., Bär, A., Haverich, A. & Hilfiker, A. Small Intestinal Submucosa Segments as Matrix for Tissue Engineering : Review. *Tissue Eng Part B* **19,** 279–292 (2013).

18. Miyagi, Y. *et al.* Biodegradable collagen patch with covalently immobilized VEGF for myocardial repair. *Biomaterials* **32,** 1280–90 (2011).

19. Patel, Z. S., Ueda, H., Yamamoto, M., Tabata, Y. & Mikos, A. G. In vitro and in vivo release of vascular endothelial growth factor from gelatin microparticles and biodegradable composite scaffolds. *Pharm. Res.* **25,** 2370–8 (2008).

20. Hanjaya-Putra, D. *et al.* Controlled activation of morphogenesis to generate a functional human microvasculature in a synthetic matrix. *Blood* **118,** 804–15 (2011).

21. Hanjaya-Putra, D. *et al.* Spatial control of cell-mediated degradation to regulate vasculogenesis and angiogenesis in hyaluronan hydrogels. *Biomaterials* **33,** 6123–31 (2012).

22. Camci-unal, G. *et al.* Hydrogel surfaces to promote attachment and spreading of endothelial progenitor cells. 337–347 (2013). doi:10.1002/term

23. Yokoyama, T. *et al.* In vivo engineering of metabolically active hepatic tissues in a neovascularized subcutaneous cavity. *Am. J. Transplant* **6,** 50–9 (2006).

24. Singh, S., Wu, B. M. & Dunn, J. C. Y. The enhancement of VEGF-mediated angiogenesis by polycaprolactone scaffolds with surface cross-linked heparin. *Biomaterials* **32,** 2059–69 (2011).

25. Singh, S., Wu, B. M. & Dunn, J. C. Y. Delivery of VEGF using Collagen-coated Polycaprolactone Scaffolds Stimulate Angiogenesis. **100,** 720–727 (2012).

26. Salimath, A. S. *et al.* Dual delivery of hepatocyte and vascular endothelial growth factors via a protease-degradable hydrogel improves cardiac function in rats. *PLoS One* **7,** e50980 (2012).

27. Oliviero, O., Ventre, M. & Netti, P. a. Functional porous hydrogels to study angiogenesis under the effect of controlled release of vascular endothelial growth factor. *Acta Biomater.* **8,** 3294–301 (2012).

28. Semino, C. E. Self-assembling Peptides: From Bio-inspired Materials to Bone Regeneration. *J. Dent. Res.* **87,** 606–616 (2008).

29. Genové, E., Shen, C., Zhang, S. & Semino, C. E. The effect of functionalized self-assembling peptide scaffolds on human aortic endothelial cell function. *Biomaterials* **26,** 3341–51 (2005).

30. Puig-Sanvicens, V. A. C. & Semino, C. E. Self-assembling peptide scaffolds as innovative platforms for drug and cell delivery systems in cardiac regeneration. *Drug Deliv. Transl. Res.* **3,** 330–335 (2013).

31. Lin, Y.-D. *et al.* Instructive nanofiber scaffolds with VEGF create a microenvironment for arteriogenesis and cardiac repair. *Sci. Transl. Med.* **4,** 146ra109 (2012).

32. Guo, H. *et al.* Sustained delivery of VEGF from designer self-assembling peptides improves cardiac function after myocardial infarction. *Biochem. Biophys. Res. Commun.* **424,** 105–11 (2012).

33. Kim, J. *et al.* The enhancement of mature vessel formation and cardiac function in infarcted hearts using dual growth factor delivery with self-assembling peptides. *Biomaterials* **32,** 6080–8 (2011).

34. Murugesan, S., Xie, J. & Linhardt, R. J. Immobilization of heparin: approaches and applications. *Curr. Top. Med. Chem.* **8,** 80–100 (2008).

35. Muñoz, E. M. & Linhardt, R. J. Heparin-binding domains in vascular biology. *Arterioscler. Thromb. Vasc. Biol.* **24,** 1549–57 (2004).

36. Ono, K., Hattori, H., Takeshita, S., Kurita, A. & Ishihara, M. Structural features in heparin that interact with VEGF165 and modulate its biological activity. *Glycobiology* **9,** 705–711 (1999).

37. Sakiyama-Elbert, S. E. & Hubbell, J. a. Development of fibrin derivatives for controlled release of heparin-binding growth factors. *J. Control. Release* **65,** 389–402 (2000).

38. Benoit, D. S. W. & Anseth, K. S. Heparin functionalized PEG gels that modulate protein adsorption for hMSC adhesion and differentiation. *Acta Biomater.* **1,** 461–70 (2005).

39. Wissink, M. J. *et al.* Binding and release of basic fibroblast growth factor from heparinized collagen matrices. *Biomaterials* **22,** 2291–9 (2001).

40. Tanihara, M., Suzuki, Y., Yamamoto, E., Noguchi, a & Mizushima, Y. Sustained release of basic fibroblast growth factor and angiogenesis in a novel covalently crosslinked gel of heparin and alginate. *J. Biomed. Mater. Res.* **56,** 216–21 (2001).

41. Lee, K. W. *et al.* Sustained release of vascular endothelial growth factor from calcium-induced alginate hydrogels reinforced by heparin and chitosan. *Transplant. Proc.* **36,** 2464–5 (2004).

42. Quintana, L. *et al.* Early tissue patterning recreated by mouse embryonic fibroblasts in a three-dimensional environment. *Tissue Eng Part A* **15,** 45–54 (2009).

43. Genové, E. *et al.* Functionalized self-assembling peptide hydrogel enhance maintenance of hepatocyte activity in vitro. *J. Cell. Mol. Med.* **13,** 3387–97 (2009).

44. Scaffold, T. P. N., Semino, C. E., Kasahara, J. & Hayashi, Y. Entrapment of Migrating Hippocampal Neural Cells in. *Tissue Eng Part* **10,** (2004).

45. Kopesky, P., Vanderploeg, E., Kurz, B. & Grodzinsky, A. J. Self-assembling peptide hydrogels modulate in vitro chondrogenesis of bovine bone marrow stromal cells. *Tissue Eng Part A* **16,** (2009).

46. Miller, R. E., Kopesky, P. W. & Grodzinsky, A. J. Growth factor delivery through self-assembling peptide scaffolds. *Clin. Orthop. Relat. Res.* **469,** 2716–24 (2011).

47. Macintosh, F. C. A colorimetric method for the standardization of heparin preparations. *Biochem. J.* **35,** 776–82 (1941).

48. Terry, D. E., Chopra, R. K., Ovenden, J. & Anastassiades, T. P. Differential Use of Alcian Blue and Toluidine Blue Dyes for the Quantification and Isolation of Anionic Glycoconjugates from Cell Cultures : Application to Proteoglycans and a High-Molecular-Weight Glycoprotein Synthesized by Articular Chondrocytes. *Anal Biochem* **285,** 211–219 (2000).

49. Klunk, W. E., Pettegrew, J. W. & Abraham, D. J. Quantitative evaluation of congo red binding to amyloid-like proteins with a beta-pleated sheet conformation. *J. Histochem. Cytochem.* **37,** 1273–1281 (1989).

50. Daura, X. *et al.* Circular dichroism spectra of beta-peptides: sensitivity to molecular structure and effects of motional averaging. *Eur. Biophys. J.* **32,** 661–70 (2003).

51. Kelly, S. M. & Price, N. C. The use of circular dichroism in the investigation of protein structure and function. *Curr. Protein Pept. Sci.* **1,** 349–84 (2000).

52. Havel, H. A. *Spectroscopic Methods for Determining Protein Structure in Solution*. (1996).

53. Greenfield, N. J. Using circular dichroism spectra to estimate protein secondary structure. *Nat. Protoc.* **1,** 2876–2890 (2006).

54. Greenfield, N. & Fasman, G. D. Computed circular dichroism spectra for the evaluation of protein conformation. *Biochemistry* **8,** 4108–16 (1969).

55. Sieminski, a. L., Was, a. S., Kim, G., Gong, H. & Kamm, R. D. The Stiffness of Three-dimensional Ionic Self-assembling Peptide Gels Affects the Extent of Capillary-like Network Formation. *Cell Biochem. Biophys.* **49,** 73–83 (2007).

56. Sieminski, a L., Semino, C. E., Gong, H. & Kamm, R. D. Primary sequence of ionic self-assembling peptide gels affects endothelial cell adhesion and capillary morphogenesis. *J. Biomed. Mater. Res. A* **87,** 494–504 (2008).

57. Ribatti, D. in *Cardiovasc. Dev. Methods Protoc.* (Peng, X. & Antonyak, M.) **843,** 47–57 (Humana Press, 2012).

58. Kim, M., Kim, S. E., Kang, S. S., Kim, Y. H. & Tae, G. The use of de-differentiated chondrocytes delivered by a heparin-based hydrogel to regenerate cartilage in partial-thickness defects. *Biomaterials* **32,** 7883–96 (2011).

59. Rajangam, K., Arnold, M. S., Rocco, M. a & Stupp, S. I. Peptide amphiphile nanostructure-heparin interactions and their relationship to bioactivity. *Biomaterials* **29,** 3298–305 (2008).

60. Chow, L., Wang, L., Dixon, B., Kaufman, D. & Stupp, S. I. Self-assembling Nanostructures to Deliver Angiogenic Factors to Pancreatic Islets. *Biomaterials* **31,** 6154–6161 (2011).

# CONCLUSIONS

Design of tissue engineering strategies for cartilage tissue engineering using the self-assembling peptide RAD16-I:

- MEFs cultured under certain biomechanical conditions (G' around 0.1 kPa), were able to develop a rich interconnected cellular network which promoted increase of several basic parameters including cell density, cell-cell contact and matrix storage modulus. This process created a unique environment, which favored the system to engage in a spontaneous chondrogenesis differentiation evidenced by the expression of the chondrogenic markers Sox9, Coll II and proteoglycans.

- MEFs developed an isolated spontaneous adipogenic differentiation in RAD16-I which was favored by the formation of a tight cell network. Interestingly, it was described for the first time the adipogenic differentiation of MEFs in 2D and 3D cultures by the addition of the growth factor PDGF to the culture media.

- Matrix instruction played an important role in the multipotent commitment acquired by MEF in the self-assembling peptide RAD16-I since cultures in collagen type I did not engage neither in the spontaneous chondrogenic nor adipogenic differentiation.

- The balance Noggin/BMP4 was found to play a critical role in the observed chondrogenic differentiation of MEFs cultured in RAD16-I. Remarkably, the chondrogenic inductor BMP4 was only expressed under mechanical conditions where the spontaneous chondrogenic differentiation was observed.

- The observed spontaneous chondrogenic differentiation of MEFs in the self-assembling peptide together with the partial redifferentiation of dedifferenitiated bovine chondrocytes evidenced the potential of this scaffold for its use in cartilage tissue engineering applications.

Evaluation of the biologically induced osteogenic differentiation of MEFs in the self-assembling peptide RAD16-I:

- MEFs undergoing chondrogenesis in the self-assembling peptide RAD16-I switched to osteogenic-like commitment due the biological induction of ECs in a coculture system. This is the first description of the osteogenic differentiation of fibroblast due to the crosstalk with endothelial cells.

- The osteogenic commitment of MEFs was evidenced by the expression of collagen type X and matrix mineralization. Additionally, other factors expressed by the mentioned cocultures were Runx2 and VEGF-A, which could promote the possible formation of new blood vessels, necessary for the endochondral ossification.

- Von Kossa staining showed matrix mineralization in areas of direct interaction between MEFs and ECs, which suggested an effective cross talk between MEFs and HUVECs that could be studied more in detail in future research projects.

- Preliminary results of osteogenic differentiation suggest that future *in vivo* implantation of the MEFs 3D-constructs in an *in vivo* mouse model of ectopic bone formation or in a fracture site would promote the formation of a vascularized bone graft.

Development of a new biomaterial for tissue engineering applications based on the self-assembling peptide RAD16-I:

- A new biomaterial for tissue engineering applications has been developed by simple combination of self-assembling peptide RAD16-I and heparin sodium salt. The availability of clinical grade RAD16-I and heparin enables its future use in *in vivo* applications, including human trials.

- This new biomaterial could be used as a drug delivery system to bind and release physiologically significant quantities of $VEGF_{165}$ *in vitro* during the first 24-36h to promote pro-angiogenesis in an *in vivo* model.

- The composite material presented promising results for its use in vascular tissue engineering applications; however, it could be used for other tissue engineering applications including cartilage and cardiac regeneration.

# CONCLUSIONES

Diseño de estrategias de ingeniería de tejidos para la reparación de cartílago usando el péptido de auto-ensamblaje RAD16-I:

- Los MEFs cultivados en el péptido de auto-ensamblaje RAD16-I en ciertas condiciones mecánicas (G' alrededor de 0.1 kPa), desarrollaron una densa red celular que promovió el aumento de diferentes parámetros incluyendo densidad celular, contactos célula-célula y el módulo de almacenamiento de la matriz. Este proceso creó un ambiente que favoreció que el sistema iniciara un proceso espontáneo de diferenciación condrogénica caracterizado por la expresión de los marcadores condrogénicos Sox9, Colágeno II y proteoglicanos.

- Los MEFs iniciaron un proceso aislado de diferenciación adipogénica espontánea en el péptido de auto-ensamblaje RAD16-I el cual fue favorecido por la formación de una densa red celular. De forma interesante, se describió por primera vez la diferenciación adipogénica de los MEFs en cultivos 2D y 3D mediante la suplementación del medio de cultivo con el factor de crecimiento PDGF.

- La instrucción de la matriz jugó un papel muy importante en la capacidad de diferenciación multipontencial adquirida por los MEFs en el péptido RAD16-I ya que los cultivos de MEFs en colágeno tipo I no iniciaron los procesos espontáneos de diferenciación condrogénica y adipogénica descritos en la matriz peptídica.

- El balance Noggin/BMP4 tuvo un papel muy importante en la diferenciación condrogénica observada cuando los MEFs se cultivaron en el péptido RAD16-I. Notablemente, los MEFs solo expresaron el inductor condrogénico BMP4 bajo ciertas condiciones mecánicas en las cuales se observó la diferenciación condrogénica espontánea.

- La diferenciación condrogénica espontánea de los MEFs y la rediferenciación parcial de los condrocitos bovinos desdiferenciados cuando se cultivaron en la matriz peptídica RAD16-I prueban la potencialidad de este material para ser usado en estrategias de ingeniería de tejidos de reparación de cartílago.

Evaluación de la diferenciación osteogénica inducida biológicamente de los MEFs en el péptido de auto-ensamblaje RAD16-I:

- Los MEFs experimentando diferenciación condrogénica en el péptido RAD16-I se redirigieron hacia una diferenciación osteogénica debido a la inducción biológica de las células endoteliales. Esta es la primera vez que se describe la diferenciación osteogénica de los fibroblastos debido a un "diálogo" con células endoteliales.

- La diferenciación osteogénica de los MEFs fue probada por la expresión del marcador hipertrófico colágeno tipo X y la mineralización de la matriz. Además, otros factores expresados por los cocultivos fueron el marcador hipertrófico Runx2 y el factor de crecimiento vascular VEGF, lo que podría inducir la formación de nuevos capilares los cuales son necesarios para el proceso de osificación endocondral.

- La tinción de Von Kossa mostró la mineralización de la matriz en las zonas de interacción entre los MEFs y las células endoteliales lo que sugiere un diálogo entre los MEFs y las HUVECs que podría ser estudiado con más detalle en futuros proyectos.

- Los resultados preliminares diferenciación osteogénica sugieren que la futura implantación de los cultivos tridimensionales de MEFs en un modelo *in vivo* de formación de hueso ectópico, o en una fractura, promoverían la formación de un implante de hueso vascularizado.

<u>Desarrollo de un nuevo biomaterial basado en el péptido de auto-ensamblaje RAD16.I para aplicaciones de ingeniería de tejidos:</u>

- Un nuevo biomaterial para aplicaciones de ingeniería de tejidos se ha desarrollado mediante la simple combinación del péptido de auto-ensamblaje RAD16-I y la sal sódica de heparina. La disponibilidad de RAD16-I y heparina de grado clínico permite su futuro uso en aplicaciones *in vivo*, incluyendo ensayos en humanos.

- El nuevo biomaterial se podría usar como un sistema de la unión y liberación de cantidades fisiológicas del factor de crecimiento $VEGF_{165}$ durante las primeras 24-36 horas para así promover un posible efecto pro-angiogénico en un modelo *in vivo*.

- El material compuesto de heparina y RAD16-I presentó resultados prometedores para su uso en aplicaciones de ingeniería de tejido vascular; sin embargo, podría ser usado en otras aplicaciones de ingeniería de tejidos como la reparación de cartílago o cardíaca.

# APPENDICES

# Appendix I

## Supplementary Video. Attached CD.

MEFs behavior in soft 3D peptide scaffolds. MEFs were seeded in low elastic modulus 3D self-assembling peptide scaffolds (G' around 0.1kPa). Interestingly, their behavior denotes multiple cellular activities including migration, cell network formation, proliferation and matrix contraction. The scaffold was placed in an incubation chamber associated with an inverted microscope. The 30 seconds video represents series of pictures taken during the first 12 hours of culture.

# Appendix II

**The data presented in this Thesis has been published or is under process of publication. The state of publication is the following:**

**Chapter 2 and Chapter 3:**

**Fernández-Muiños, T**., Suárez-Muñoz, M., Sanmartí-Espinal, M., Semino, C.E., *Matrix dimensions, stiffness and structural properties modulate spontaneous chondrogenic commitment of mouse embryonic fibroblasts.* Tissue Engineering.Part A. (Accepted October 15th 2013)

**Chapter 4:**

**Fernández-Muiños, T**.*, Recha-Sancho, L.*, López-Chicón, P., Castells-Sala, C., Semino, C.E., *Bimolecular based self-assembling hidrogel for tissue engineering applications.* (In preparation) *Equal contribution

**Other papers published in collaboration with members of the laboratory:**

Castells-Sala, C.*, Alemany-Ribes, M.*, **Fernández-Muiños, T.**, Recha-Sancho, L., López-Chicón, P., Aloy-Reverté, C., Caballero-Camino, J., Márquez-Gil, A., Semino, C.E., *Current applications of tissue engineering in biomedicine.* Biochips and Tissue Chips, S2: 004. (2013) doi: 10.4172/2153-0777.S2-004 (Review article) *Equal contribution

Wu, J., Marí-Buyé, N., Lopez, L., **Fernández Muiños, M. T**., Borrós, S., Favia, P., Semino, C. E., *Nanometric self-assembling peptide layers enhance CYP3A2 expression of primary rat hepatocyte sandwich cultures*. Journal of Nanobiotechnology, 8, 29 (2010).

Quintana Ll., **Fernández Muiños T**., Genove.E., Olmos M., Borros S., Semino C.E. *Early tissue patterning is recreated by mouse embryonic fibroblasts in a three-dimensional environment*. Tissue Engineering.Part A. Volume 15, 1, (2009)

**Book chapters:**

**Fernández Muiños, M.T.,** Semino, C.E., *Self-assembling peptides as a synthetic extracellular matrix.* Polymer concepts in regenerative medicine. From nano- to macro-structures. Series editors: Monleón,M and Vicent,MJ *WILEY & SONS* (Under edition)

Marí-Buyé, N., **Fernández Muiños, M. T**., Semino, C. E., *Three-dimensional cultures in soft selfassembling nanofibers*. In Methods in Bioengineering: 3D Tissue Engineering (2010). Series editors: Berthiaume, F. and Morgan, *J. Artech House*. ISBN: 978-1-59693-458-0